COOPERATIVE CONTROL OF TWO ACTIVE SPACECRAFT DURING PROXIMITY OPERATIONS

by

Robert J. Polutchko

S.B., Massachusetts Institute of Technology, (1985)

SUBMITTED IN PARTIAL FULFILLMENT

OF THE REQUIREMENTS FOR THE DEGREE OF

MASTER OF SCIENCE

IN AERONAUTICS AND ASTRONAUTICS

AT THE

MASSACHUSETTS INSTITUTE OF TECHNOLOGY

AUGUST 1989

© Robert J. Polutchko, 1989

Signature of Author_____

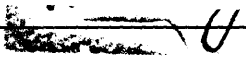Department of Aeronautics and Astronautics
August 1, 1989

Certified by _____   _____

Professor Walter M. Hollister, Thesis Supervisor
Professor of Aeronautics and Astronautics

Certified by _____

Edward V. Bergmann, Technical Supervisor
Charles Stark Draper Laboratory

Accepted by _____

Professor Harold Y. Wachman
Chairman, Department Graduate Committee

COOPERATIVE CONTROL OF TWO ACTIVE
SPACECRAFT DURING PROXIMITY OPERATIONS

by

Robert J. Polutchko

ABSTRACT

A cooperative autopilot is developed for the control of the relative attitude, relative position, and absolute attitude of two maneuvering spacecraft during on orbit proximity operations. The autopilot consists of a open-loop trajectory solver which computes a nine dimensional linearized nominal state trajectory at the beginning of each maneuver and a phase space regulator which maintains the two spacecraft on the nominal trajectory during coast phases of the maneuver. A linear programming algorithm is used to perform jet selection. Simulation tests using a system of two space shuttle vehicles are performed to verify the performance of the cooperative controller and comparisons are made to a traditional "passive target / active pursuit vehicle" approach to proximity operations. The cooperative autopilot is shown to be able to control the two vehicle system when both the would be pursuit vehicle and the target vehicle are not completely controllable in six degrees of freedom. The cooperative controller is also shown to use as much as 37% less fuel and 57% fewer jet firings than a single pursuit vehicle during a simple docking approach maneuver.

Thesis Supervisor: Professor Walter M. Hollister
Title: Professor of Aeronautics and Astronautics, M.I.T

Technical Supervisor: Edward V. Bergmann
Title: Section Chief, Flight Systems Section
                                   Charles Stark Draper Laboratory

ACKNOWLEDGEMENTS

TABLE OF CONTENTS

4

CHAPTER 1

INTRODUCTION TO PROXIMITY OPERATIONS

1.0 Introduction

As the frequency and complexity of space missions increase, the scope of the tasks to be performed on orbit will grow beyond the capabilities of single spacecraft and will necessitate collaboration among multiple specialized vehicles. The safe and efficient operation of multiple spacecraft in close proximity to one another will place new demands on both pilots and flight control systems in the near future. Inflight construction of the space station and other complex on orbit tasks will require a flexibility and spontaneity beyond current proximity operation techniques. Operations between the space station, orbital maneuvering vehicles, free flyers, and the shuttle will continue to depend on the ability to routinely perform complex rendezvous, formationkeeping, and docking maneuvers.[10] Though shuttle crews can perform many of these tasks manually, extended duration formationkeeping requirements and the introduction of highly maneuverable unmanned vehicles will cause crew workloads to increase and will necessitate the development of automatic systems to handle standard proximity operations.

The proximity operations problem has usually been solved using an 'active' pursuit spacecraft to establish a desired position and attitude relative to a 'passive' target vehicle.[12] This pursuit vehicle approach neglects both the ability of the 'passive' vehicle to perform complementary attitude and translation maneuvers and the superior fault tolerance of a system employing two active vehicles. Consequently, the pursuit vehicle maneuver sequences are less efficient and more constrained than those generated using the control authority available from both vehicles.

This paper presents a cooperative autopilot approach to the control of joint maneuvers of two spacecraft during proximity operations. The cooperative approach considers the two spacecraft as a single system and exploits the rotational and translational capabilities of each spacecraft in order to control the state of this system. The efficiency and robustness to jet failures of this new autopilot design is demonstrated.

1.1 Background

Previous treatments of spacecraft proximity operations have focussed on the control of the motion of a single maneuvering vehicle in a reference frame fixed to a target vehicle.[18,21,22] This pursuit vehicle initiates rendezvous and docking, performs formationkeeping activities, and implements collision avoidance maneuvers. Though the target vehicle may perform some independent attitude control during the approach phases of the rendezvous, the commanded attitude of the target vehicle is pre-determined and is not updated to account for the actual state of the pursuit vehicle. The closed-loop control used in this approach to proximity operations formulates reaction control jet firing commands for the pursuit vehicle in order to minimize the fuel consumed, the time to reach the target state, and/or the final state error.

Single vehicle control was successfully applied to terminal phase proximity operations and docking during the Apollo and Skylab missions. On these missions the target spacecraft remained essentially passive while the pursuit vehicle performed simple, manually controlled approach maneuvers. During the shuttle era, the target spacecraft have been science platforms or communication and observation satellites which have not been designed for extensive orbital maneuvering. Consequently the space shuttle performs most of the proximity operations maneuvers even though it is more massive than most of its rendezvous partners. The use of single vehicle control avoids the complexity of the cooperative maneuvering problem and in current space shuttle operations does not significantly impact the performance of the two vehicle system due to the imbalance of control authority between the vehicles.

The introduction of the next generation of advanced spacecraft will add a new dimension to proximity operations. Spacecraft like the Orbital Maneuvering Vehicle (OMV) will be unmanned, maneuverable, and designed specifically for the rendezvous mission. Future enhancements to the shuttle autopilot will make the shuttle a more agile and more efficient proximity operations vehicle. Artificially constraining one of these advanced vehicles to remain passive during proximity operations eliminates the natural synergism that exists between two agile spacecraft. Conversely, employing the control authority of both spacecraft to perform coordinated maneuvers will provide an increased level of flexibility and a greater margin of safety during proximity operations.

In many mission scenarios spacecraft will be required to operate at a range of only a few vehicle lengths. Control of the relative attitude and position of two spacecraft in this

operating regime is especially difficult due to stringent plume impingement constraints and "fail-safe" collision avoidance rules.[14]

Many spacecraft rely on hot gas reaction control jets to perform on orbit maneuvers. The space shuttle reaction control system utilizes bipropellent (nitrogen tetraoxide and monomethyl hydrazine) hypergolic jets.[4] These jets expel a plume of high velocity gas when fired that could damage or disrupt a neighboring vehicle during close proximity operations. While vehicles with delicate optical instruments or solar panels are particularly sensitive to the chemical effects of the jet plume, spacecraft with flexible or articulated appendages may experience adverse perturbations due to the force of the plume impingement. Vehicles operating in close proximity to the space station will be required to orchestrate maneuvers such that the thruster exhaust does not impinge on the station.[10]

When operating in close proximity to a spacecraft which is sensitive to jet plume effects, the space shuttle crew manually disallows jet firings which may impinge upon the target spacecraft. For example, if the shuttle passes beneath such a vehicle all upwardly firing jets are disallowed.[14] In each situation where a jet or set of jets is to be disallowed the controllability of the maneuvering vehicle must be re-evaluated. During single active vehicle proximity operations, the pursuit vehicle must be capable of avoiding a collision with the passive target vehicle under a variety of limited failure modes. The types of maneuvers a pursuit vehicle may perform become extremely limited under collision avoidance and plume impingement constraints as the spacecraft get very close. If a large number of jets on the pursuit vehicle are deselected or have failed, the maneuvers available to the crew will probably be fairly fuel inefficient and in the extreme case, the pursuit vehicle may become unable to control the relative states of the two vehicles.

The cooperative control scheme developed in this thesis exploits the natural redundancy provided by the actuators on the target vehicle in order to make the two vehicle system more robust to jet unavailabilities.

1.2 Application

The cooperative autopilot approach to the control of two vehicle proximity operations is applicable to any two spacecraft. This thesis develops the concept for a system of two shuttle vehicles. As the principle support vehicle for construction of the

8

space station, deployment and retrieval of advanced spacecraft, and other maintenance and resupply operations, the shuttle will continue to conduct rendezvous missions well into the next century. In addition, the shuttle's asymmetrical mass distribution and complicated configuration of forty-four reaction control jets make it a fine example of a general class of complex, highly maneuverable spacecraft. Two identical spacecraft are employed to ensure that the difference in performance between the standard single vehicle control architecture and the new cooperative control architecture is not a consequence of introducing a more efficient or otherwise superior spacecraft in place of the non-maneuvering target vehicle. Specifically, the use of two shuttle vehicles will facilitate direct comparisons between cooperative control and traditional 'shuttle as a pursuit vehicle' proximity operations solutions.

The general scenario to be considered in this thesis is a joint maneuver by two space shuttles operating in low earth orbit (LEO). The shuttles are in nearly identical 90 min (300 nm) circular orbits at a relative range of less than 3000 ft. The maneuver will typically last less than one orbit. The initial attitude of each vehicle is unconstrained. The two spacecraft are idealized as three dimensional rigid bodies; the mass (m), inertia (I), and center of mass location (r_{cm}), of each vehicle is constant and known in the vehicle's body fixed coordinate frame. Similarly, the locations (r_j), and the thrust vectors (f_j), of the 44 reaction control jets on each orbiter are known in the body fixed frames. The attitude and position of each vehicle in an earth centered inertial coordinate frame is available from onboard navigation devices. The relative states of the vehicles are assumed to be available either as a direct measurement (by a laser ranger for instance) or as the difference of the inertial states. These sensor and estimator requirements are not unique to a cooperative control architecture and have already been proposed for use during traditional proximity operations.[22]

The cooperative autopilot resides on the 'master' vehicle; the other vehicle is designated the 'slave'. A communication link similar to those proposed for use by remotely piloted spacecraft such as the OMV is assumed to exist between the two spacecraft. The slave vehicle provides mass property parameters, jet status data as well as current position and attitude information to the master vehicle. The master vehicle passes the numbers of the jets to be fired and the corresponding firing times to the slave vehicle.

1.3 Overview of the Cooperative Controller

The cooperative controller is a two tiered system consisting of an open-loop maneuver planner block and a closed-loop regulator block. The maneuver planner employs a linearized model of the vehicles to plan an open-loop trajectory consisting of an acceleration burn, a coast period, and a deceleration burn. During the coast phase of the maneuver the regulator monitors the state errors and computes any necessary corrective jet firings in order to keep the system following the pre-planned trajectory. Figure 1.1 is a block diagram of the cooperative controller.

The **trajectory solver** (chapter 5) accepts a state command form a guidance algorithm or pilot interface module and computes a trajectory consisting of an acceleration burn, a coast, and a deceleration burn which carries the system from the current state to the commanded final state. The acceleration and deceleration jet firing commands are determined by a **simplex jet selection algorithm** (chapter 4) which minimizes a cost function based on total jet firing time. The trajectory itself is optimized to minimize the final state error.

Once a satisfactory trajectory has been determined the trajectory solver passes the acceleration jet firing commands, the desired value of the system state at the beginning of the coast phase of the trajectory, and the deceleration jet firing commands to the trajectory sequencer. The trajectory sequencer initiates the planned maneuver by passing the jet firing commands to the jet sequencer which actually implements them. At the end of the acceleration burn the trajectory sequencer initializes the **nominal trajectory state generator** (section 5.3) with the pre-computed value of the system state at the beginning of the coast phase and activates the **phase space regulator** (chapter 6).

During the coast phase of the maneuver the nominal trajectory generator updates the target value of the system state at 12.5 hz using a linearized model of the two vehicle system. The state error is then computed as the difference between the current state and the target state. The phase space regulator compares the state error to a set of predetermined thresholds and determines when a corrective jet firing is required. To implement a corrective jet firing a velocity impulse request is passed to the simplex jet selection algorithm which computes an optimum set of jet firing commands. These feedback initiated jet firing commands are immediately passed to the jet sequencer and implemented.
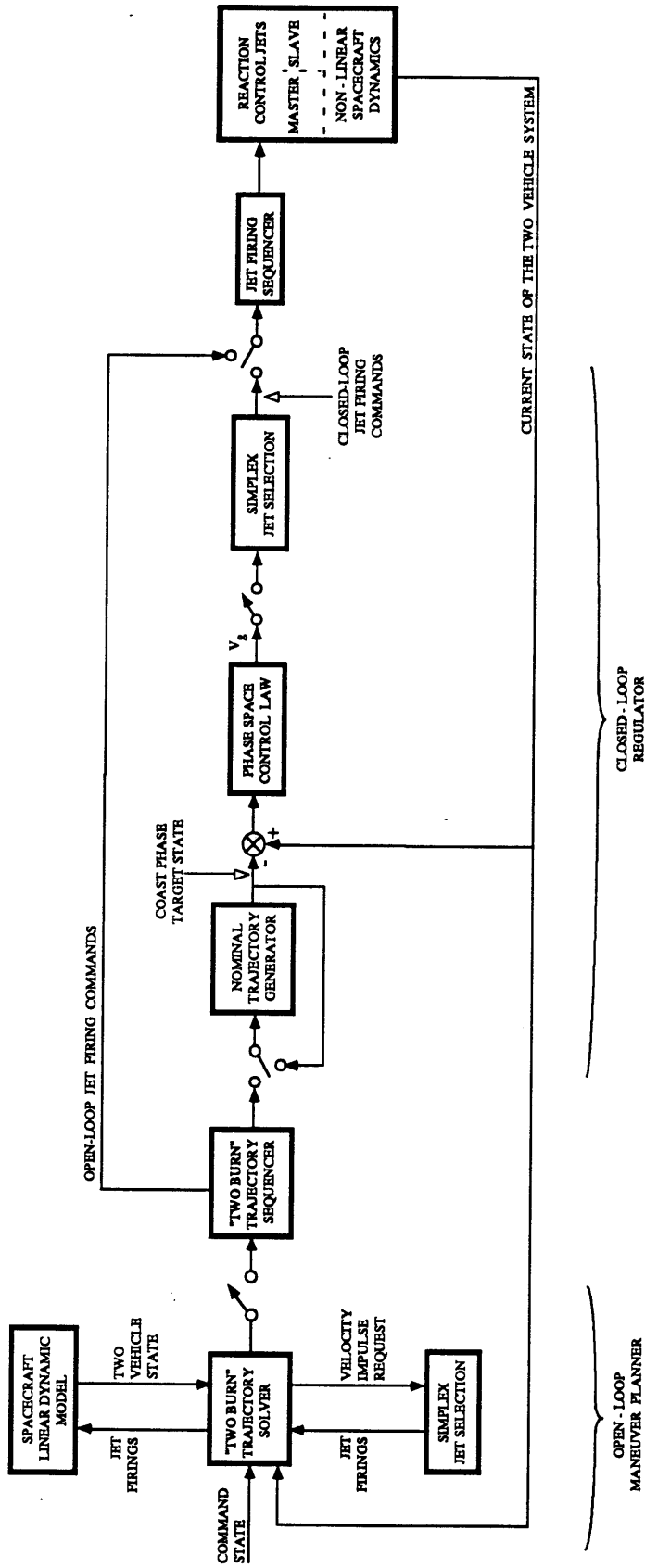
Figure 1.1
Cooperative Controller Block Diagram.

At the end of the coast phase of the maneuver the pre-computed deceleration jet firings are implemented. At the end of the deceleration jet firing sequence the two burn maneuver is complete. A new maneuver is then commanded or the coast phase feedback loop is reactivated to maintain the two vehicle system at the commanded state. In the latter case the output of the trajectory state generator is the commanded state and is constant.

1.4 Outline of this Thesis

Chapter 2 develops the rotational equations of motion for a body in space and derives an expression for the relative motion of two rigid bodies.

Chapter 3 presents a derivation of the Clohessy - Wiltshire equations for the translational motion of a body with respect to a neighboring circular orbit. These equations are then used to develop an expression for the relative motion of two maneuvering spacecraft.

Chapter 4 develops the cooperative control jet selection algorithm. The two vehicle jet selection problem is first formulated as a linear programming problem. The properties of linear programming problems are then presented and the revised simplex algorithm introduced as a solution technique. Finally the practical aspects of the application of the revised simplex algorithm to the jet selection problem are discussed.

Chapter 5 develops the two vehicle trajectory solver which determines the open-loop trajectory for the two burn maneuver. First, the linearized algebraic equations describing the final state of the system in terms of the initial state and the coast velocity parameters are derived. An iterative method for determining the values of the coast velocity parameters which minimize the final state error is then presented. The coast phase nominal state trajectory generator is formulated.

Chapter 6 formulates the phase space regulator for the two spacecraft cooperative control problem. The velocity to be gained algorithm and the concept of the phase sphere are introduced as the basis for general phase space control. The application of phase space control to the cooperative control problem is then discussed.

12

Chapter 7 contains a description of the tests used to verify the operation of the cooperative controller for the two space shuttle example. A detailed analysis of the results of the tests is presented and comparisons are made between the pursuit vehicle approach and the cooperative control approach to proximity operations.

Chapter 8 contains a summary of this investigation and outlines some key areas for further research which should be addressed prior to an actual flight test of this system.

CHAPTER 2

ROTATIONAL MOTION DURING PROXIMITY OPERATIONS

2.0 Introduction

The rotational motion of a spacecraft is based primarily on rigid body angular momentum principles. This section provides a derivation of Euler's Momentum Equations. Though a general closed form solution of Euler's equations does not exist, in certain cases good approximations may be made and accurate solutions formulated. The essential approximations to be employed during the development of the cooperative autopilot are introduced and the linearized rotational equations of motion formulated. Quaternions will be employed to express the angular displacements between reference frames and are briefly introduced.

2.1 Kinematics of a Rigid Body [7,8]

Consider a rigid body of mass m as a collection of particles with individual mass m_i (figure 2.1). The ith particle has instantaneous position $\mathbf{R_i}$ and instantaneous velocity $\dot{\mathbf{R}}_i$ with respect to an inertial reference frame. The linear momentum of this particle is given by Newton's Second Law:

$$\mathbf{p_i} = m_i\, \dot{\mathbf{R}}_i \tag{2-1}$$

The moment of this momentum about an arbitrary point O located at $\mathbf{R_o}$ is defined as

$$\mathbf{h_{o_i}} = \mathbf{r_i} \times m_i\, \dot{\mathbf{R}}_i \tag{2-2}$$

where $\mathbf{r_i}$ is the instantaneous position of the ith particle with respect to an intermediate coordinate frame centered at the point O. Since $\mathbf{R_i} = \mathbf{R_o} + \mathbf{r_i}$, the first derivative of $\mathbf{R_i}$ is $\dot{\mathbf{R}}_i = \dot{\mathbf{R}}_o + \dot{\mathbf{r}}_i$ and the moment of momentum becomes

$$\mathbf{h_{o_i}} = \mathbf{r_i} \times m_i\, \dot{\mathbf{r}}_i + \mathbf{r_i} \times m_i\, \dot{\mathbf{R}}_o \tag{2-3}$$

14
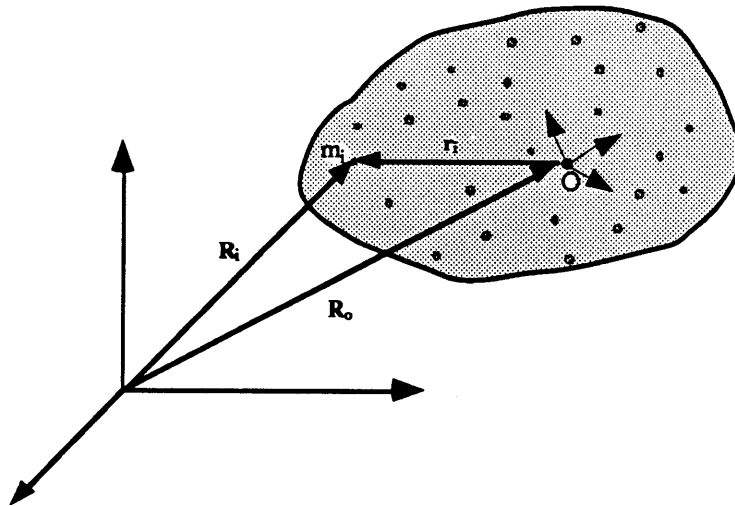
Figure 2.1

Position of particle m_i in an
inertial and a rotating reference frame.

The first term in this expression is the angular momentum of the particle observed in the intermediate coordinate frame and the second term is the correction due to the motion of the point O.

The total angular momentum of the body about point O is the vector sum of the angular momenta of the i particles.

$$H_o = \sum_i h_{o_i} = \sum_i r_i \times m_i \dot{r}_i - \dot{R}_o \times \sum_i r_i m_i \qquad (2\text{-}4)$$

If the point O is constrained to correspond to the center of mass of the rigid body, then by definition

$$\sum_i r_i m_i = 0 \qquad (2\text{-}5)$$

and the angular momentum equation becomes

$$H_o = \sum_i r_i \times m_i \dot{r}_i \qquad (2\text{-}6)$$

The time derivative of the position of the ith particle in the intermediate frame with respect to the inertial reference frame is

15

$$\dot{r}_i = \dot{r}_i^* + \omega \times r_i \qquad (2\text{-}7)$$

where $\dot{r}_i^*$ indicates differentiation of r_i with respect to time in the intermediate coordinate frame and ω is the angular velocity of the body with respect to the inertial frame. Since the body is rigid and the intermediate reference frame is fixed in the body, $\dot{r}_i^* = 0$ and

$$\dot{r}_i = \omega \times r_i \qquad (2\text{-}8)$$

Substituting this expression into the expression for H_o yields

$$H_o = \sum_i r_i \times m_i (\omega \times r_i) \qquad (2\text{-}9)$$

As the number of particles in the body is allowed to increase while the individual m_i decrease such that $m = \Sigma\, m_i$ remains constant, the particle model of the body approaches a continuum model. In the limit, this summation over the particle mass elements becomes an integration over the differential elements of mass, dm.

$$H_o = \int r \times (\omega \times r)\, dm \qquad (2\text{-}10)$$

The argument of this integral is evaluated by expressing the vector products in component form along the body fixed coordinate directions.

$$
\begin{aligned}
r \times (\omega \times r) = &\left(\omega_x (y^2+z^2) - \omega_y (xy) - \omega_z (xz) \right) \hat{i} \\
&+ \left(-\omega_x (xy) + \omega_y (x^2+z^2) - \omega_z (yz) \right) \hat{j} \\
&+ \left(-\omega_x (xz) - \omega_y (yz) + \omega_z (x^2+y^2) \right) \hat{k}
\end{aligned}
\qquad (2\text{-}11)
$$

The components of the angular momentum along the body axes are then

$$H_x = \omega_x \int (y^2+z^2)\, dm - \omega_y \int (xy)\, dm - \omega_z \int (xz)\, dm$$

$$H_y = -\omega_x \int (xy)\, dm + \omega_y \int (x^2+z^2)\, dm - \omega_z \int (yz)\, dm \qquad (2\text{-}12)$$

$$H_z = -\omega_x \int (xz)\, dm - \omega_y \int (yz)\, dm + \omega_z \int (x^2+y^2)\, dm$$

The integrals in the above equations are constant in any coordinate frame fixed to the rigid body. By convention,

16

$$I_{xx} = \int (y^2+z^2)\, dm \qquad I_{yy} = \int (x^2+z^2)\, dm \qquad I_{zz} = \int (x^2+y^2)\, dm \quad (2\text{-}13)$$

are defined as the **moments of inertia** and

$$I_{xy} = \int (xy)\, dm \qquad I_{xz} = \int (xz)\, dm \qquad I_{yz} = \int (yz)\, dm \qquad (2\text{-}14)$$

as the **products of inertia.** The components of the angular momentum may be rewritten in terms of these constants.

$$
\begin{aligned}
H_x &= I_{xx}\omega_x - I_{xy}\omega_y - I_{xz}\omega_z \\
H_y &= -I_{xy}\omega_x + I_{yy}\omega_y - I_{yz}\omega_z \\
H_z &= -I_{xz}\omega_x - I_{yz}\omega_y + I_{zz}\omega_z
\end{aligned}
\qquad (2\text{-}15)
$$

Matrix notation is often the most convenient way to write an expression for the total angular momentum.

$$\mathbf{H_o = I}\,\omega \qquad (2\text{-}16)$$

The matrix **I** is the **inertia tensor**

$$
\mathbf{I} = \begin{bmatrix}
I_{xx} & -I_{xy} & -I_{xz} \\
-I_{xy} & I_{yy} & -I_{yz} \\
-I_{xz} & -I_{yz} & I_{zz}
\end{bmatrix}
\qquad (2\text{-}17)
$$

The rate of change of the angular momentum is calculated by taking the derivative of this last expression for $\mathbf{H_o}$ with respect to time.

$$\dot{\mathbf{H}}_o = \dot{\mathbf{I}}\omega + \mathbf{I}\dot{\omega} = \mathbf{I}^*\omega + \omega \times \mathbf{I}\,\omega + \mathbf{I}\omega^* + \mathbf{I}(\omega \times \omega) \qquad (2\text{-}18)$$

Here $\mathbf{I}^*$ and ω^* are the derivatives of $\mathbf{I}$ and ω in the body fixed reference frame. Since the inertia tensor of a rigid body is constant in a frame fixed in the body, $\mathbf{I}^* = 0$ and hence the first term on the right hand side of this equation is zero. Since $\omega \times \omega = 0$, the last term on the right is also zero. The rate of change of the angular momentum is then expressed

$$\dot{\mathbf{H}}_o = \mathbf{I}\dot{\omega} + \omega \times \mathbf{I}\,\omega \qquad (2\text{-}19)$$

2.2 Euler's Moment Equation [7,8]

Newton's second law relates the force on a particle, F_i, to the linear momentum of the particle, p_i.

$$F_i = \dot{p}_i \qquad (2\text{-}20)$$

where

$$p_i \equiv m_i \dot{R}_i \qquad (2\text{-}21)$$

Since the mass of a particle is constant, Newton's second law may be written

$$F_i = m_i \ddot{R}_i \qquad (2\text{-}22)$$

From equation 2-6, the total angular momentum of the body can be written in terms of the of the momenta of the individual particles

$$H_o = \sum_i r_i \times m_i \dot{r}_i \qquad (2\text{-}23)$$

Differentiating this expression for the angular momentum with respect to time and noting that $\dot{r}_i \times \dot{r}_i = 0$

$$\dot{H}_o = \sum_i r_i \times m_i \ddot{r}_i \qquad (2\text{-}24)$$

Since $r_i = R_i - R_o$

$$\dot{H}_o = \sum_i r_i \times m_i \ddot{R}_i + \ddot{R}_o \times \sum_i m_i r_i \qquad (2\text{-}25)$$

The origin of the body coordinate frame has been constrained to be the center of mass of the rigid body. Thus by definition of the center of mass

$$\sum_i m_i r_i = 0 \qquad (2\text{-}26)$$

and the rate of change of the angular momentum is

$$\dot{H}_o = \sum_i r_i \times m_i \ddot{R}_i \qquad (2\text{-}27)$$

18

The factor $m_i\ddot{R}_i$ is the time rate of change of the linear momentum of the ith particle and may be replaced using the above expression for Newton's second law

$$\dot{H}_o = \sum_i r_i \times F_i \qquad (2\text{-}28)$$

If the external force on the ith particle is defined as E_i and the force exerted on the ith particle by the jth particle is defined as f_{ij}, then the total force exerted on the ith particle is

$$F_i = E_i + \sum_j f_{ij} \qquad (2\text{-}29)$$

Substituting this expression for the total force into equation 2-28

$$\dot{H}_o = \sum_i r_i \times E_i + \sum_i \sum_j r_i \times f_{ij} \qquad (2\text{-}30)$$

The double summation in this equation is composed of pairs of terms of the form

$$\left(r_i \times f_{ij}\right) + \left(r_j \times f_{ji}\right) \qquad (2\text{-}31)$$

From Newton's third law

$$f_{ij} = -f_{ji} \qquad (2\text{-}32)$$

so that the double sum may be rewritten

$$\sum_i \sum_j (r_i - r_j) \times f_{ij} \qquad (2\text{-}33)$$

In an ideal rigid body, (no particle deformation), the mutual forces between particles act through the particle centers. Consequently, the direction of the f_{ij} force vectors correspond with the direction of the the relative position vectors ($r_i - r_j$) and each cross product in the double summation is zero. The rate of change of the angular momentum vector of a rigid body is

$$\dot{H}_o = \sum_i r_i \times E_i \qquad (2\text{-}34)$$

E_i is the total external force vector applied to the ith particle. The corresponding moment applied to the rigid body by this force is given by

$$r_i \times E_i \qquad (2\text{-}35)$$

19

and the total external moment applied to the rigid body is

$$\mathbf{M_o} = \sum_i \mathbf{r_i} \times \mathbf{E_i} \tag{2-36}$$

Finally, combining equation 2-34 and 2-36 we arrive at the familiar governing equation for the rotational motion of a rigid body

$$\dot{\mathbf{H}}_o = \mathbf{M_o} \tag{2-37}$$

When the total external moment applied to the body is zero, this equation is merely a statement of the principle of the conservation of angular momentum. In addition, if the kinematic expression for the rate of change of the angular momentum (equation 2-19) is substituted for $\dot{\mathbf{H}}_o$, this equation becomes

$$\mathbf{M_o} = \mathbf{I}\dot{\omega} + \omega \times \mathbf{I}\,\omega \tag{2-38}$$

This is the matrix form of **Euler's Moment Equations**. These three coupled, non-linear differential equations completely describe the rotational motion of a rigid body about its center of mass. Though a general closed form solution of Euler's equations does not exist, in special cases when the body is axisymmetrical, the angular velocity is small, or the applied moments are large, good approximations can be made and simple closed form solutions to the resulting linear differential equations derived.

Euler's equations may be written in component form as

$$M_x = \frac{d}{dt}\left(I_{xx}\omega_x - I_{xy}\omega_y - I_{xz}\omega_z\right)$$

$$- I_{xz}\omega_x\omega_y - I_{yz}\omega_y^2 + I_{zz}\omega_y\omega_z$$

$$+ I_{xy}\omega_x\omega_z - I_{yy}\omega_y\omega_z + I_{yz}\omega_z^2$$

$$M_y = \frac{d}{dt}\left(-I_{xy}\omega_x + I_{yy}\omega_y - I_{yz}\omega_z\right)$$

$$+ I_{xx}\omega_x\omega_z - I_{xy}\omega_y\omega_z - I_{xz}\omega_z^2 \tag{2-39}$$

$$+ I_{xz}\omega_x^2 + I_{yz}\omega_x\omega_y - I_{zz}\omega_x\omega_z$$

$$M_z = \frac{d}{dt}\left(- I_{xz}\omega_x - I_{yz}\omega_y + I_{zz}\omega_z\right)$$

$$- I_{xy}\omega_x^2 + I_{yy}\omega_x\omega_y - I_{xz}\omega_x\omega_z$$

$$- I_{xx}\omega_x\omega_y + I_{xy}\omega_y^2 + I_{xz}\omega_y\omega_z$$

If the angular rates ω_x, ω_y, ω_z are small, the second order terms may be neglected and these equations reduced to

$$M_x = I_{xx}\dot{\omega}_x - I_{xy}\dot{\omega}_y - I_{xz}\dot{\omega}_z$$

$$M_y = - I_{xy}\dot{\omega}_x + I_{yy}\dot{\omega}_y - I_{yz}\dot{\omega}_z \qquad (2\text{-}40)$$

$$M_z = - I_{xz}\dot{\omega}_x - I_{yz}\dot{\omega}_y + I_{zz}\dot{\omega}_z$$

Which may be re-written in matrix form as

$$\mathbf{M} = \mathbf{I}\,\dot{\omega} \qquad (2\text{-}41)$$

so that the rate of change of the angular velocity is

$$\dot{\omega} = \mathbf{I}^{-1}\mathbf{M} \qquad (2\text{-}42)$$

If in addition, the external moment applied to the vehicle is zero, then the spacecraft equations of motion become

$$\omega = constant \qquad (2\text{-}43)$$

Many spacecraft employ reaction control jets to perform attitude and position control. Each reaction control jet on a spacecraft is described by its location (r_j) and its force vector (f_j). The moment applied about the spacecraft center of mass (r_{cm}) by the jth jet is

$$\mathbf{M}_j = (\mathbf{r}_j - \mathbf{r}_{cm}) \times \mathbf{f}_j \qquad (2\text{-}44)$$

Define α_j, the angular acceleration due to the jth jet, as

$$\alpha_j = \mathbf{I}^{-1}\mathbf{M}_j \qquad (2\text{-}45)$$

If a *control vector* u is defined such that

$$u_j = \begin{cases} 1 & \text{when the } j^{th} \text{ jet is firing} \\ 0 & \text{otherwise} \end{cases}$$

(2-46)

then the equation 2-42 governing the rotational motion of the spacecraft may be written

$$\dot{\omega} = \sum_{j=1}^{N} \alpha_j u_j$$

(2-47)

where N is the number of reaction control jets on the spacecraft.

2.3 Attitude Displacements [17,20]

Consider a coordinate frame rotating with a constant angular velocity ω with respect to a reference coordinate frame. The angular velocity vector may be written as

$$\omega = \frac{d\theta}{dt} \hat{i}_\omega = \frac{d\theta}{dt} \left(l \hat{i}_x + m \hat{i}_y + n \hat{i}_z \right)$$

(2-48)

Integrating this constant angular velocity over the period $\Delta t = t_1 - t_0$

$$\int_{t_0}^{t_1} \omega \, dt = \frac{d\theta}{dt} \hat{i}_\omega \int_{t_0}^{t_1} dt = \frac{d\theta}{dt} (\Delta t) \hat{i}_\omega$$

(2-49)

This angular displacement vector represents a rotation by an angle $\Delta\theta = \frac{d\theta}{dt} (\Delta t)$ about an axis $\hat{i}_\omega$. A more convenient representation of this rotation is Hamilton's four element *quaternion*.

$$\tilde{q} = \begin{bmatrix} \delta \\ q \end{bmatrix} = \begin{bmatrix} \delta \\ \alpha \\ \beta \\ \gamma \end{bmatrix}$$

(2-50)

$\delta, \alpha, \beta, \gamma$ are the **Euler Parameters** and are defined as

22

$$\delta = \cos\frac{1}{2}\Delta\theta \quad \alpha = l\,\sin\frac{1}{2}\Delta\theta \quad \beta = m\,\sin\frac{1}{2}\Delta\theta \quad \gamma = n\,\sin\frac{1}{2}\Delta\theta \quad (2\text{-}51)$$

From this definition it is clear that

$$\mathbf{q} = \alpha\,\hat{\mathbf{i}}_x + \beta\,\hat{\mathbf{i}}_y + \gamma\,\hat{\mathbf{i}}_z = \left(\sin\frac{1}{2}\Delta\theta\right)\hat{\mathbf{i}}_\omega \qquad (2\text{-}52)$$

and that

$$\alpha^2 + \beta^2 + \gamma^2 + \delta^2 = 1 \qquad (2\text{-}53)$$

The new orientation of a reference frame following a rotational displacement θ about an axis $\hat{\mathbf{i}}_\omega$ is given by

$$\tilde{\mathbf{q}}_f = \tilde{\mathbf{q}}_o\,\tilde{\mathbf{q}}_\theta \qquad (2\text{-}54)$$

where $\tilde{\mathbf{q}}_o$ is the quaternion representation of the original orientation of the reference frame and quaternion multiplication is defined by

$$\tilde{\mathbf{q}}_1\,\tilde{\mathbf{q}}_2 = \delta_1\delta_2 - \mathbf{q}_1^T\mathbf{q}_2 + \delta_1\mathbf{q}_2 + \delta_2\mathbf{q}_1 + \mathbf{q}_1 \times \mathbf{q}_2$$

$$= \begin{bmatrix} \delta_1 & -\alpha_1 & -\beta_1 & -\gamma_1 \\ \alpha_1 & \delta_1 & -\gamma_1 & \beta_1 \\ \beta_1 & \gamma_1 & \delta_1 & -\alpha_1 \\ \gamma_1 & -\beta_1 & \alpha_1 & \delta_1 \end{bmatrix} \begin{bmatrix} \delta_2 \\ \alpha_2 \\ \beta_2 \\ \gamma_2 \end{bmatrix} \qquad (2\text{-}55)$$

$$= \mathbf{S}(\tilde{\mathbf{q}}_1)\,\tilde{\mathbf{q}}_2$$

A vector may be rotated thru an angle represented by the quaternion $\tilde{\mathbf{q}}$ in the following manner. Define the four element vector $\tilde{\mathbf{r}}_o$ as

$$\tilde{\mathbf{r}}_o = \begin{bmatrix} 0 \\ \mathbf{r}_o \end{bmatrix} \qquad (2\text{-}56)$$

then the rotated vector is

$$\tilde{\mathbf{r}} = \tilde{\mathbf{q}}\,\tilde{\mathbf{r}}_o\,\tilde{\mathbf{q}}^{-1} \qquad (2\text{-}57)$$

2.4 Relative Rotational Motion of Two Spacecraft

Consider the rotational motion of two rigid spacecraft. Define the relative angular velocity as

$$\omega_R = \omega_2 - \omega_1 \tag{2-58}$$

where ω_1 and ω_2 are the angular velocity of vehicle #1 and vehicle #2. The rate of change of the relative angular velocity is the derivative of this equation in an inertial reference frame

$$\dot{\omega}_R = \dot{\omega}_2 - \dot{\omega}_1 \tag{2-59}$$

Euler's Moment equation provides an expression for the angular acceleration experienced by each vehicle in terms of the external moment applied to the vehicle. Thus $\dot{\omega}_R$ may be re-written

$$\dot{\omega}_R = I_2^{-1}\left(M_2 - \omega_2 \times I_2\, \omega_2\right) - I_1^{-1}\left(M_1 - \omega_1 \times I_1\, \omega_1\right) \tag{2-60}$$

As before, if the angular velocity of each vehicle is small, the second order rate terms may be neglected. Since the external moments experienced by each spacecraft are primarily due to reaction control jet activity, the moments M_1 and M_2 may be expanded as the sum of the moments applied by the individual jets.

$$\dot{\omega}_R = I_2^{-1}\left(\sum_{j=1}^{N_2} (r_{2j} - r_{2cm}) \times f_{2j}\right) - I_1^{-1}\left(\sum_{j=1}^{N_1} (r_{1j} - r_{1cm}) \times f_{1j}\right) \tag{2-61}$$

The additional subscript has been added in this expression to indicate the vehicle referenced. As before, if the angular acceleration of the spacecraft due to firing the jth jet is α_j the this equation may be re-written as

$$\dot{\omega}_R = \left(\sum_{j=1}^{N_2} \alpha_{2j}\, u_{2j}\right) - \left(\sum_{j=1}^{N_1} \alpha_{1j}\, u_{1j}\right) \tag{2-62}$$

where u_1, u_2 are the control vectors for the two vehicles. When none of the jets in the two vehicle system are active, the angular momentum of the system is conserved and the governing equation for the relative attitude of the vehicles becomes

$$\dot{\omega}_R = 0 \qquad \rightarrow \qquad \omega_R = constant \tag{2-63}$$

24

CHAPTER 3

SPACECRAFT TRANSLATION DYNAMICS

3.0 Introduction

The translational motion of a spacecraft is based upon the linear momentum of an equivalent mass particle under the influence of external forces. This section derives the equations of motion for a rigid body undergoing pure translation. The predominant external force on a spacecraft is the gravitational force of the planet it is orbiting. A formulation of the general two-body problem is presented. Though a treatment of the methods generally employed to solve the resulting non-linear second order differential equations is beyond the scope of this thesis, these equations serve as the basis of a derivation of the Clohessy - Wiltshire[18] (Euler-Hill) equations for motion relative to reference point travelling in an unperturbed circular orbit. The primary interest of this thesis is the control of the relative motion of two active spacecraft. The equations of relative motion are derived in a "local vertical local horizontal" reference frame.

3.1 Translational Motion of a Rigid Body [7]

Consider a rigid body of mass m as a collection of particles with individual mass m_i. The ith particle has an instantaneous position R_i and instantaneous velocity $\dot{R}_i$ with respect to an inertial reference frame. The linear momentum of this particle is defined as

$$p_i = m_i \dot{R}_i \qquad (3\text{-}1)$$

Define r_i as the instantaneous position of the ith particle with respect to an intermediate coordinate frame centered at the point O such that $R_i = R_o + r_i$, where R_o is the instantaneous position of the point O in the inertial frame. The linear momentum of the ith particle is then

$$p_i = m_i \dot{R}_o + m_i \dot{r}_i \qquad (3\text{-}2)$$

The total linear momentum of the body is the sum of the linear momenta of the i particles

$$p = \sum_i m_i \dot{R}_o + \sum_i m_i \dot{r}_i \qquad (3-3)$$

Since the mass of the ith particle is constant,

$$\sum_i m_i \dot{r}_i = \frac{d}{dt}\left(\sum_i m_i r_i\right) \qquad (3-4)$$

If the point O is constrained to correspond to the center of mass of the rigid body, then by definition

$$\sum_i r_i \, m_i = 0 \qquad (3-5)$$

and the linear momentum equation becomes

$$p = \sum_i m_i \dot{R}_o = \dot{R}_o \sum_i m_i \qquad (3-6)$$

By definition $m = \sum_i m_i$ so that the total linear momentum of a rigid body reduces to

$$p = m\dot{R}_o \qquad (3-7)$$

which is just the linear momentum of a point mass m located at the center of mass of the body. The rate of change of the total linear momentum is the derivative of this expression with respect to time

$$\dot{p} = m\ddot{R}_o \qquad (3-8)$$

If the external force on the ith particle is defined as E_i and the force exerted on the ith particle by the jth particle is defined as f_{ij}, then the total force exerted on the ith particle is

$$F_i = E_i + \sum_j f_{ij} \qquad (3-9)$$

The total force on the body is the sum of the total force acting on each particle

$$F = \sum_i F_i = \sum_i E_i + \sum_i \sum_j f_{ij} \qquad (3-10)$$

From Newton's third law it is clear that

$$f_{ij} = -f_{ji} \qquad (3-11)$$

26

and thus that the double summation over the internal force vectors in the total force expression is zero. The total force is then the sum of the external forces applied to the particles in the body.

$$F = \sum_i E_i \tag{3-12}$$

Applying Newton's second law ($F_i = \dot{p}_i$) permits $\dot{p}$ to be eliminated between equation 3-8 and equation 3-12 and yields the governing equation for translational motion of a rigid body .

$$m\ddot{R}_o = \sum_i E_i \tag{3-13}$$

As expected, the pure tanslational motion of a rigid body in the presence of external forces is equivalent to the motion of a single particle of equivalent mass located at the center of mass of the body translating under the influence of a single force equivalent to the vector sum of all the external forces.

3.2 Two Body Problem [17]

Consider two bodies with instantaneous positions R_1 and R_2 with respect to an inertial reference frame. If the bodies are far enough apart, of have sufficiently spherical mass distributions and are not in contact with each other, then their mutual gravitational attraction will act through their mass centers and they may be treated as particle masses m_1 and m_2. Newton's law of gravitation states that any two particles attract one another with a force of magnitude

$$F = \frac{Gm_1m_2}{R_{12}^2} \tag{3-14}$$

acting along the line joining them. Here G is the universal gravitational constant and R_{12} is the distance between the particles.

$$R_{12} = R_{21} = \sqrt{(R_2 - R_1)^T (R_2 - R_1)} \tag{3-15}$$

The vector representation of the gravitational force experienced by each body is

$$F_1 = \frac{Gm_1m_2}{R_{12}^3}(R_2 - R_1) \qquad\qquad F_2 = \frac{Gm_1m_2}{R_{21}^3}(R_1 - R_2) \qquad (3\text{-}16)$$

Newton's second law states

$$F = m\ddot{R} \qquad (3\text{-}17)$$

and may be applied to the gravitational force equation for each vehicle to yield two differential equations describing the motion of the two bodies in the inertial reference frame.

$$\ddot{R}_1 = \frac{Gm_2}{R_{12}^3}(R_2 - R_1) \qquad\qquad \ddot{R}_2 = \frac{Gm_1}{R_{21}^3}(R_1 - R_2) \qquad (3\text{-}18)$$

The motion of m_2 relative to m_1 is obtained by differencing these equations

$$\left(\ddot{R}_2 - \ddot{R}_1\right) = \frac{-G(m_1 + m_2)}{R_{21}^3}(R_2 - R_1) \qquad (3\text{-}19)$$

Thus the basic differential equations of relative motion for the two body system is

$$\ddot{R} + \frac{\mu}{R^3}R = 0 \qquad (3\text{-}20)$$

where $\mu = G(m_1 + m_2)$.

In this thesis, the primary interest is the motion of a rigid body about the earth. In this case, the center of mass of the two body system very nearly corresponds with the center of mass of the earth. Thus the relative motion differential equations (3-20) may be interpreted as a description of the motion of a rigid body about a center of attraction.

3.3 Translational Motion with Respect to a Nominal Circular Orbit [18, 7, 11]

Consider a reference point travelling in an unperturbed circular orbit about the earth. The motion of the point in an earth centered inertial reference frame is given by

$$\ddot{R}_o + \frac{\mu}{R_o^3}R_o = 0 \qquad (3\text{-}21)$$

28

Define a "local vertical - local horizontal" reference frame centered on and moving with this reference point. The LVLH unit vectors are defined as:

$$\hat{i_z} = -\frac{R_o}{R_o} \qquad \hat{i_y} = -\frac{R_o \times \dot{R}_o}{R_o \dot{R}_o} \qquad \hat{i_x} = \hat{i_y} \times \hat{i_z} \qquad (3\text{-}22)$$

In other terms, $\hat{i_z}$ is defined opposite the instantaneous orbital radius vector, $\hat{i_y}$ is defined opposite the angular momentum vector of the orbit, and $\hat{i_x}$ is defined to complete the right handed coordinate system.

Consider a spacecraft travelling in a separate orbit and experiencing an external perturbation force such as drag from the upper atmosphere, gravitational anomalies, or reaction control jet activity. The motion of this vehicle in an earth centered inertial reference frame is governed by

$$\ddot{R}_1 + \frac{\mu}{R_1^3} R_1 = a_1 \qquad (3\text{-}23)$$

where a_1 is the force per unit mass of the perturbation force. The motion of the spacecraft relative to the reference point is described by the difference of the second order equations describing the individual motions in inertial space.

$$\ddot{r}_1 = \left(\ddot{R}_1 - \ddot{R}_o \right) = \frac{\mu}{R_o^3} \left(R_o - \frac{R_o^3}{R_1^3} R_1 \right) + a_1 \qquad (3\text{-}24)$$

Here r_1 is defined as the instantaneous position of the spacecraft relative to the reference point O.

The position of the reference point, R_o, and the relative position vector, r_1, are easily expressed in the LVLH coordinate frame as

$$R_o = [\ 0 \quad 0 \quad -R_o]^T \qquad (3\text{-}25)$$

$$r_1 = [\ x \quad y \quad z\ ]^T \qquad (3\text{-}26)$$

Since $R_1 = R_o + r_1$, the inertial position of the spacecraft may also be expressed in the LVLH coordinate frame

$$R_1 = [\ x \quad y \quad (z - R_o)\ ]^T \qquad (3\text{-}27)$$

29

The ratio

$$\frac{R_o^3}{R_1^3} = \left(R_o^T R_o\right)^{3/2} \left(R_1^T R_1\right)^{-3/2}$$

(3-28)

may be expressed in terms of the LVLH coordinate variables by substituting the expression in equation 3-25 for R_0 and the expression in equation 3-27 for R_1.

$$\frac{R_o^3}{R_1^3} = R_o^3 \left(x^2 + y^2 + (z - R_o)^2\right)^{-3/2}$$

(3-29)

During proximity operations $r_1 \ll R_0$ and therefore $x, y, z \ll R_0$. Under this condition, the second factor in equation 3-29 may be expanded as a binomial series and the equation re-written as

$$\frac{R_o^3}{R_1^3} = R_o^3 \left\{ (R_o - z)^{-3} - \frac{3}{2}(R_o - z)^{-5}\left(x^2 + y^2\right) + H.O.T. \right\}$$

(3-30)

Expanding the (R_0-z) terms as binomial series and collecting similar terms yields

$$\frac{R_o^3}{R_1^3} = 1 + 3\frac{z}{R_o} - \frac{3}{2}\left(x^2 + y^2\right)\left(\frac{1}{R_o^2} + 5\frac{z}{R_o^3}\right) + H.O.T.$$

(3-31)

Since $\frac{x}{R_o}, \frac{y}{R_o}, \frac{z}{R_o} \ll 1$ second order terms involving these ratios are neglected leaving

$$\frac{R_o^3}{R_1^3} \approx 1 + 3\frac{z}{R_o}$$

(3-32)

Substituting this expression into equation 3-24

$$\ddot{r}_1 = \frac{\mu}{R_o^3}\left(R_o - \left(1 + 3\frac{z}{R_o}\right)R_1\right) + a_1$$

(3-33)

and noting again that $R_1 = R_o + r_1$

$$\ddot{r}_1 = \frac{\mu}{R_o^3}\left(-r_1 - 3\frac{z}{R_o}R_o - 3\frac{z}{R_o}r_1\right) + a_1$$

(3-34)

Since $\frac{z}{R_o} \ll 1$, the last term in the brackets represents a small fraction of the LVLH coordinate displacements and may be neglected without introducing significant errors.

30

With these simplifications the linearized differential equation governing the motion of a spacecraft relative to a unperturbed reference orbit becomes

$$\ddot{r}_1 = \frac{\mu}{R_o^3} \begin{bmatrix} -x_1 \\ -y_1 \\ 2z_1 \end{bmatrix} + a_1 \qquad (3\text{-}35)$$

The complete derivative of the position of the spacecraft relative to the orbiting reference point may be written as

$$\dot{r}_1 = r_1^* + \omega \times r_1 \qquad (3\text{-}36)$$

where r_1^* is the derivative with respect to the LVLH coordinate system and ω is the angular velocity of the LVLH frame relative to the earth centered inertial frame. The complete derivative of this relative velocity is the relative acceleration.

$$\ddot{r}_1 = r_1^{**} + 2\left(\omega \times r_1^*\right) + \dot{\omega} \times r_1 + \omega \times \left(\omega \times r_1\right) \qquad (3\text{-}37)$$

Since the LVLH coordinate frame is aligned with the instantaneous radius vector of the reference orbit, the angular velocity of the LVLH frame is equal to the instantaneous angular velocity of the reference point about the center of the earth. For a general unperturbed reference, this angular velocity is time varying and equal to

$$\omega = \frac{d\theta}{dt} \hat{i}_h = \frac{h}{R_o^2} \qquad (3\text{-}38)$$

where h is the *massless angular momentum* of the orbit.

When the reference orbit is defined to be an unperturbed circular orbit, R_o is a constant and equal to the semi-major axis of the orbit. From Kepler's Second Law (equal areas in equal time) the angular velocity of the circular orbit is constant and equal to the *mean motion of the orbit*

$$\omega = \sqrt{\frac{\mu}{R_o^3}} \hat{i}_h = -\eta_o \hat{i}_y \qquad (3\text{-}39)$$

Here η_o is the mean motion and $\hat{i}_y$ is the cross-plane unit vector of the LVLH frame. Thus for a circular reference orbit the complete derivative of the relative position vector may be written

$$
\ddot{\mathbf{r}}_1 = \begin{bmatrix} x_1^{**} \\ y_1^{**} \\ z_1^{**} \end{bmatrix} + 2\eta_0 \begin{bmatrix} -z_1^{*} \\ 0 \\ x_1^{*} \end{bmatrix} - 2\eta_0^2 \begin{bmatrix} x_1^{*} \\ 0 \\ z_1^{*} \end{bmatrix} \tag{3-40}
$$

Eliminating $\ddot{\mathbf{r}}_1$ between this kinematic expression and equation 3-35 yields the set of three second order linear differential equations for the relative motion of a spacecraft in the LVLH reference frame.

$$
x_1^{**} = 2\eta_0\, z_1^{*} + a_x
$$

$$
y_1^{**} = -\eta_0^2 y_1 + a_y \tag{3-41}
$$

$$
z_1^{**} = -2\eta_0\, x_1^{*} + 3\eta_0^2 z_1 + a_z
$$

These equations are known as the Clohessy - Wiltshire (Euler - Hill) equations and are often expressed is state space form ($\dot{\mathbf{X}} = \mathbf{A}\mathbf{X} + \mathbf{B}\mathbf{f}$) as

$$
\begin{bmatrix} \dot{x}_1 \\ \dot{y}_1 \\ \dot{z}_1 \\ \ddot{x}_1 \\ \ddot{y}_1 \\ \ddot{z}_1 \end{bmatrix} = \begin{bmatrix} 0 & 0 & 0 & 1 & 0 & 0 \\ 0 & 0 & 0 & 0 & 1 & 0 \\ 0 & 0 & 0 & 0 & 0 & 1 \\ 0 & 0 & 0 & 0 & 0 & 2\eta \\ 0 & -\eta^2 & 0 & 0 & 0 & 0 \\ 0 & 0 & 3\eta^2 & -2\eta & 0 & 0 \end{bmatrix} \begin{bmatrix} x_1 \\ y_1 \\ z_1 \\ \dot{x}_1 \\ \dot{y}_1 \\ \dot{z}_1 \end{bmatrix} + \begin{bmatrix} 0 & 0 & 0 \\ 0 & 0 & 0 \\ 0 & 0 & 0 \\ m_i^{-1} & 0 & 0 \\ 0 & m_i^{-1} & 0 \\ 0 & 0 & m_i^{-1} \end{bmatrix} \begin{bmatrix} f_x \\ f_y \\ f_z \end{bmatrix} \tag{3-42}
$$

where a_1 has been replaced by $m_i^{-1}f$.

The character of the motion of an unpowered satellite may be ascertained by inspection of equations 3-41 or equation 3-42. The motion of the satellite in the direction perpendicular to the orbital plane ($\hat{\mathbf{i}}_y$) is uncoupled from the motion along the other LVLH directions and is a simple harmonic oscillation with a period equal to the orbital period of the reference point, $\frac{2\pi}{\eta_0}$. Qualitatively, this motion is the consequence of a slight difference in the inclination of the spacecraft and reference orbits.

The motion along the x and z axes is a coupled oscillation. Note however, that when the vehicle is positioned on the LVLH x axis ($z_1 = 0$) with zero inplane velocity ($\dot{x}_1, \dot{z}_1 = 0$) the second derivatives of x and z are also zero and the vehicle is at an

equilibrium point. Consequently, positions along the x axis are efficient points at which to stationkeep and are commonly exploited during many types of proximity maneuvers.

The complete solution of the Clohessy-Wiltshire (C.W.) equations is the sum of their homogeneous and particular solutions. Equations 3-41 may be written as a set of unforced differential equations

$$\ddot{x} = 2\eta_o \dot{z}$$

$$\ddot{y} = -\eta_o^2 y \qquad (3\text{-}43)$$

$$\ddot{z} = -2\eta_o \dot{x} + 3\eta_o^2 z$$

For simplicity the subscript 1 has been dropped and the '*' replaced with '" though the derivative is still to be carried out in the LVLH frame. As noted above, the second equation represents a simple harmonic oscillation and thus the equation governing the motion in the cross-plane direction is

$$y = y_0 \cos \eta_o t + \frac{\dot{y}_0}{\eta_o} \sin \eta_o t \qquad (3\text{-}44)$$

with first derivative

$$\dot{y} = \dot{y}_0 \cos \eta_o t - y_0 \eta_o \sin \eta_o t \qquad (3\text{-}45)$$

y_0 and $\dot{y}_0$ are respectively the initial out-of-plane position and the initial out-of-plane velocity.

To solve the remaining two coupled differential equations describing the in plane motion, integrate the first equation and evaluate the resulting integration constant at the initial condition (t=0, x=x$_0$, z=z$_0$, etc.)

$$\dot{x} = 2\eta_o z + \left(\dot{x}_0 - 2\eta_o z_0\right) \qquad (3\text{-}46)$$

Substitute this expression for $\dot{x}$ into the third equation and collect common terms.

$$\ddot{z} = -\eta_o^2 z + \left(4\eta_o^2 z_0 - 2\eta_o \dot{x}_0\right) \qquad (3\text{-}47)$$

The solution to this equation will take the form $z = A\cos\eta t + B\sin\eta t + C$, where A, B, and C are constants to be determined from initial conditions. The solution is

$$z = \left(\frac{2\dot{x}_0}{\eta_o} - 3z_0\right)\cos\eta_o t + \frac{\dot{z}_0}{\eta_o}\sin\eta_o t + \left(4z_0 - 2\frac{\dot{x}_0}{\eta_o}\right) \tag{3-48}$$

and has first derivative

$$\dot{z} = \dot{z}_0\cos\eta_o t - \left(2\dot{x}_0 - 3\eta_o z_0\right)\sin\eta_o t \tag{3-49}$$

Substitution of this expression for z into the above equation for $\dot{x}$ yields

$$\dot{x} = \left(4\dot{x}_0 - 6\eta_o z_0\right)\cos\eta_o t + 2\dot{z}_0\sin\eta_o t + \left(6\eta_o z_0 - 3\dot{x}_0\right) \tag{3-50}$$

Since each of the coefficients in this equation is constant, the governing equation for x may be obtained by direct integration. The resulting integration constant is again evaluated at the initial condition, t = 0.

$$x = \left(\frac{4\dot{x}_0}{\eta_o} - 6z_0\right)\sin\eta_o t - \frac{2\dot{z}_0}{\eta_o}\cos\eta_o t + \left(6\eta_o z_0 - 3\dot{x}_0\right)t + \left(x_0 + 2\frac{\dot{z}_0}{\eta_o}\right) \tag{3-51}$$

Unlike the other equations, this equation contains the secular term $\left(6\eta_o z_0 - 3\dot{x}_0\right)t$. This term drives the spacecraft in the positive x direction if $z_0 > 0$ (spacecraft is below the reference point) and in the negative x direction if $z_0 < 0$ (spacecraft is above the reference point). This characteristic of the relative motion is primarily due to the small difference in the semi-major axis (and thus the period) of the two orbits.

These six equations for x, y, z, $\dot{x}$, $\dot{y}$, $\dot{z}$ in terms of their initial values may be organized in a matrix structure and written as

$$\begin{bmatrix} x \\ y \\ z \\ \dot{x} \\ \dot{y} \\ \dot{z} \end{bmatrix} = \begin{bmatrix} 1 & 0 & 6\eta_o t - 6S & \frac{4}{\eta_o}S - 3t & 0 & \frac{2}{\eta_o}(1-C) \\ 0 & C & 0 & 0 & \frac{1}{\eta_o}S & 0 \\ 0 & 0 & 4-3C & -\frac{2}{\eta_o}(1-C) & 0 & \frac{1}{\eta_o}S \\ 0 & 0 & 6\eta_o(1-C) & 4C-3 & 0 & 2S \\ 0 & -\eta_o S & 0 & 0 & C & 0 \\ 0 & 0 & 3\eta_o S & -2S & 0 & C \end{bmatrix} \begin{bmatrix} x_0 \\ y_0 \\ z_0 \\ \dot{x}_0 \\ \dot{y}_0 \\ \dot{z}_0 \end{bmatrix} \tag{3-52}$$

where 'C' and 'S' have been substituted for the expressions 'cos $\eta_o t$' and 'sin $\eta_o t$'. This homogeneous solution is in state transition matrix form,

$$x_h(t) = \Phi(t) x(t_0) \tag{3-53}$$

34

The complete solution may be evaluated using the sum of the particular and the homogeneous solutions.

$$x(t) = \Phi(t) \, x(t_0) + \int_{t_0}^{t_f} \Phi(\tau) \, B(\tau) \, f(\tau) \, d\tau \tag{3-54}$$

The matrix $B(\tau)$ is the control weighting matrix identified in equation 3-42. Since B is constant for a fixed vehicle configuration, the integral in equation 3-54 may be evaluated for periods of constant thrust ($f(\tau) = f$).

$$\int_{t_0}^{t_f} \Phi(\tau) \, B(\tau) \, f(\tau) \, d\tau = \left\{ \int_{t_0}^{t_f} \Phi(\tau) \, d\tau \right\} B \, f = \Gamma(t) \, m_i^1 f \tag{3-55}$$

$\Gamma(t)$ is a matrix and is dependent only on the length of the period of constant thrust and the mean motion of the reference orbit.

$$\Gamma(t) = \begin{bmatrix} \dfrac{4}{\eta_o^2}(1-C) - 3t^2 & 0 & \dfrac{2}{\eta_o}\left(t - \dfrac{S}{\eta_o}\right) \\[2mm] 0 & \dfrac{1}{\eta_o^2}(1-C) & 0 \\[2mm] \dfrac{-2}{\eta_o}\left(t - \dfrac{S}{\eta_o}\right) & 0 & \dfrac{1}{\eta_o^2}(1-C) \\[2mm] \dfrac{4}{\eta_o}S - 3t & 0 & \dfrac{2}{\eta_o}(1-C) \\[2mm] 0 & \dfrac{1}{\eta_o}S & 0 \\[2mm] \dfrac{-2}{\eta_o}(1-C) & 0 & \dfrac{1}{\eta_o}S \end{bmatrix} \tag{3-56}$$

The complete solution of the Clohessy Wiltshire equations for a period of constant thrust in matrix can be expressed using matrix notation as

$$x(t) = \Phi(t) \, x(t_0) + \Gamma(t) \, m_i^1 f \tag{3-57}$$

3.4 Relative Translational Motion of Two Active Spacecraft

Consider two spacecraft travelling in very similar near circular orbits. In addition define an LVLH coordinate system attached to a reference point travelling in a neighboring

unperturbed circular orbit. The motion of each spacecraft with respect to the reference point is described by equation 3-57. The relative position of the two spacecraft is

$$x_R(t) = x_2(t) - x_1(t) \tag{3-58}$$

which may be expanded as

$$x_R(t) = \Phi(t) x_R(t_0) + \Gamma(t) \left(m_2^{-1} f_2 - m_1^{-1} f_1 \right) \tag{3-59}$$

Since the perturbation forces are primarily due to reaction control jets the external forces f_1 and f_2 may be expanded in terms of the contributions of the individual jets. The equation for the relative position of the two spacecraft becomes

$$x_R(t) = \Phi(t) x_R(t_0) + \Gamma(t) \left(m_2^{-1} \sum_{j=1}^{N_2} f_{2j} - m_1^{-1} \sum_{j=1}^{N_1} f_{1j} \right) \tag{3-60}$$

CHAPTER 4

JET SELECTION FOR COOPERATIVE CONTROL

4.0 Introduction

The cooperative jet selection algorithm must select an appropriate set of reaction control jets on each spacecraft and compute the corresponding firing times in order to simultaneously implement the rate change requested by the control system and minimize a linear fuel expenditure function. A linear programming solution to the single vehicle jet selection problem was incorporated into the shuttle OEX autopilot and successfully flight-tested on missions STS 51G and STS 61B in 1985. The extension of this algorithm to a two spacecraft system was first performed by B. Persson at the C.S. Draper Laboratory[16]. This section presents a discussion of this extended linear programming solution to the multi-vehicle jet selection problem.

4.1 The Two vehicle Jet Selection Problem.

The cooperative autopilot developed in this thesis controls the attitude of the master vehicle with respect to an external reference frame, the attitude of the slave vehicle with respect to the master, and the position of the slave vehicle with respect to the master. Define an *activity vector*, A_j, to be the second derivative of the control variables in response to a firing of the jth jet.

$$
A_j = \begin{bmatrix} \dot{\omega}_a \\ --- \\ \dot{\omega}_R \\ --- \\ \dot{v}_R \end{bmatrix}_j
$$

(4-1)

where $\dot{\omega}_{aj}$ is the rate of change of the angular velocity of the master vehicle, $\dot{\omega}_{Rj}$ is the rate of change of the relative angular velocity vector, and $\dot{v}_{Rj}$ is the rate of change of the relative linear velocity. Expressions for each sub-vector in this nine dimensional activity vector may be derived from the treatment of rotational and translational motion provided in chapter 2 and chapter 3.

The rate of change of the relative angular velocity is the difference of the angular accelerations experienced by the individual spacecraft.

$$\dot{\omega}_R = \dot{\omega}_2 - \dot{\omega}_1 \tag{4-2}$$

Similarly, the rate of change of the relative linear velocity is

$$\dot{v}_R = \dot{v}_2 - \dot{v}_1 \tag{4-3}$$

Each reaction control jet on a spacecraft applies a linear force and a moment about the spacecraft center of mass when fired. The linear and angular acceleration of the spacecraft in response to a firing of the jth reaction control jet are

$$\dot{v}_j = m^{-1} f_j \tag{4-4}$$

$$\dot{\omega}_j = I^{-1} \left((r_j - r_{cm}) \times f_j \right) \tag{4-5}$$

Here I is the vehicle inertia matrix, m is the vehicle mass, r_j is the location of the jth jet, $\dot{r}_{cm}$ is the location of the center of mass of the vehicle, and f_j is the jet force vector.

The jets on the master vehicle have a direct effect on the angular velocity of the master, but as seen in equations 2-62 and 3-60 an opposite effect on the relative angular velocity and relative linear velocity. The nine dimensional activity vector for a master vehicle jet is defined to be

$$A_{1j} = \begin{bmatrix} \dot{\omega}_a \\ \hline \dot{\omega}_R \\ \hline \dot{v}_R \end{bmatrix}_{1j} = \begin{bmatrix} I_1^{-1} \left((r_{1j} - r_{1cm}) \times f_{1j} \right) \\ -I_1^{-1} \left((r_{1j} - r_{1cm}) \times f_{1j} \right) \\ -m_1^{-1} f_{1j} \end{bmatrix} \tag{4-6}$$

The jets on the slave vehicle have a direct effect on the relative angular velocity and the relative linear velocity of the system, but have no effect on the angular velocity of the master vehicle. The nine dimensional activity vector for a slave vehicle jet is

$$A_{2j} = \begin{bmatrix} \dot{\omega}_a \\ \hline \dot{\omega}_R \\ \hline \dot{v}_R \end{bmatrix}_{2j} = \begin{bmatrix} 0 \\ I_2^{-1} \left((r_{2j} - r_{2cm}) \times f_{2j} \right) \\ m_2^{-1} f_{2j} \end{bmatrix} \tag{4-7}$$

38

The impulse provided to the system by a master vehicle jet firing is the integral over time of the rate of change of the velocities effected by the jet.

$$
\Delta W_{1j} = \begin{bmatrix} \Delta\omega_a \\ --- \\ \Delta\omega_R \\ --- \\ \Delta v_R \end{bmatrix}_{1j} = \int_{t_0}^{t_1} A_{1j}dt = \begin{bmatrix} \int_{t_0}^{t_1} I_1^{-1}\left((r_{1j} - r_{1cm}) \times f_{1j}\right)dt \\ \int_{t_0}^{t_1} -I_1^{-1}\left((r_{1j} - r_{1cm}) \times f_{1j}\right)dt \\ \int_{t_0}^{t_1} -m_1^{-1}\, f_{1j}\, dt \end{bmatrix}
\qquad (4\text{-}8)
$$

Similarly, the impulse provided to the system by a slave vehicle jet firing is

$$
\Delta W_{2j} = \begin{bmatrix} \Delta\omega_a \\ --- \\ \Delta\omega_R \\ --- \\ \Delta v_R \end{bmatrix}_{2j} = \int_{t_0}^{t_1} A_{2j}dt = \begin{bmatrix} 0 \\ \int_{t_0}^{t_1} I_2^{-1}\left((r_{2j} - r_{2cm}) \times f_{2j}\right)dt \\ \int_{t_0}^{t_1} m_2^{-1}\, f_{2j}\, dt \end{bmatrix}
\qquad (4\text{-}9)
$$

If each vehicle may be accurately modelled as a rigid body with constant mass, the parameters r_j, r_{cm}, I, and m will remain constant during the integration if it is performed in the respective body fixed frame. For a non-throttleable reaction control jet f_j is also constant. Under these assumptions the nine dimensional impulse provided by the jth master vehicle jet and the jth slave vehicle jet reduce to

$$
\Delta W_{1j} = \begin{bmatrix} I_1^{-1}\left((r_{1j} - r_{1cm}) \times f_{1j}\right) \\ -I_1^{-1}\left((r_{1j} - r_{1cm}) \times f_{1j}\right) \\ -m_1^{-1}\, f_{1j} \end{bmatrix} (t_1 - t_0) = A_{1j}\,\Delta t_{1j}
\qquad (4\text{-}10)
$$

$$
\Delta W_{2j} = \begin{bmatrix} 0 \\ I_2^{-1}\left((r_{2j} - r_{2cm}) \times f_{2j}\right) \\ m_2^{-1}\, f_{2j} \end{bmatrix} (t_1 - t_0) = A_{2j}\,\Delta t_{2j}
\qquad (4\text{-}11)
$$

The total impulse provided by firing a group of jets on both vehicles is the sum of the impulses provided by the individual jets.

$$\Delta W = \Delta W_1 + \Delta W_2 = \sum_{j=1}^{N_1} A_{1j} \Delta t_{1j} + \sum_{j=1}^{N_2} A_{2j} \Delta t_{2j} \qquad (4\text{-}12)$$

Here N_1 and N_2 are respectively the number of jets on the master and the number of jets on the slave vehicle. For those jets not fired during the sequence, $\Delta t_j = 0$.

The components of the activity vectors defined in equation 4-10 and equation 4-11 are expressed using body fixed parameters of the two spacecraft. Combining these vectors as suggested in equation 4-12 requires that the elements of the activity vectors be expressed in a common coordinate frame. Define a general activity vector

$$A_j = \begin{bmatrix} \alpha_a \\ \hline \alpha_R \\ \hline a_R \end{bmatrix}_j \qquad (4\text{-}13)$$

where α_a is the angular acceleration of the master vehicle expressed in the master vehicle body frame, α_R is the rate of change of the relative angular velocity expressed in the master vehicle body frame, and a_R is the rate of change of the relative linear velocity expressed in the reference LVLH frame. In terms of the components of the body frame activity vectors and the appropriate rotation quaternions this general activity vector is written

$$A_j = \begin{cases} \begin{bmatrix} \dot{\omega}_a \\ \hline \dot{\omega}_R \\ \hline \tilde{q}_{1L} \dot{v}_R \tilde{q}_{1L}^{-1} \end{bmatrix}_{1j} = \begin{bmatrix} I_1^{-1}\left((r_{1j} - r_{1cm}) \times f_{1j} \right) \\ -I_1^{-1}\left((r_{1j} - r_{1cm}) \times f_{1j} \right) \\ -m_1^{-1} \tilde{q}_{1L} f_{1j} \tilde{q}_{1L}^{-1} \end{bmatrix} & \text{for } 1 \le j \le N_1 \\[4em] \begin{bmatrix} \dot{\omega}_a \\ \hline \tilde{q}_{21} \dot{\omega}_R \tilde{q}_{21}^{-1} \\ \hline \tilde{q}_{2L} \dot{v}_R \tilde{q}_{2L}^{-1} \end{bmatrix}_{2j} = \begin{bmatrix} 0 \\ \tilde{q}_{21} I_2^{-1}\left((r_{2j} - r_{2cm}) \times f_{2j} \right) \tilde{q}_{21}^{-1} \\ m_2^{-1} \tilde{q}_{2L} f_{2j} \tilde{q}_{2L}^{-1} \end{bmatrix} & \text{for } N_1+1 \le j \le N_1+N_2 \end{cases} \qquad (4\text{-}14)$$

Here $\tilde{q}_{1L}$ is the quaternion representation of a rotation from the master vehicle body frame to the reference LVLH frame. Similarly, $\tilde{q}_{2L}$ is the rotation from the slave vehicle body frame to the reference LVLH frame, and $\tilde{q}_{21}$ is the rotation from the slave vehicle body

frame to the master vehicle body frame. $\tilde{q}_{1L}$, $\tilde{q}_{2L}$, and $\tilde{q}_{21}$ are assumed to be known and constant during the jet firing sequence. This approximation is appropriate whenever the vehicles have small angular velocities and the jet firing duration is short.

Equation 4-12 for the total impulse applied to the two spacecraft system can be now be written

$$\Delta W = \sum_{j=1}^{N_1+N_2} A_j \, \Delta t_j \qquad (4\text{-}15)$$

or in matrix notation as

$$\Delta W = A \, t \qquad (4\text{-}16)$$

where A is the $9 \times (N_1+N_2)$ matrix of activity vectors

$$A = \begin{bmatrix} \alpha_{a(1)} & \alpha_{a(2)} & \cdots & \alpha_{a(N_1)} & \alpha_{a(N_1+1)} & \cdots & \alpha_{a(N_1+N_2)} \\ \alpha_{R(1)} & \alpha_{R(2)} & \cdots & \alpha_{R(N_1)} & \alpha_{R(N_1+1)} & \cdots & \alpha_{R(N_1+N_2)} \\ a_{R(1)} & a_{R(2)} & \cdots & a_{R(N_1)} & a_{R(N_1+1)} & \cdots & a_{R(N_1+N_2)} \end{bmatrix} \qquad (4\text{-}17)$$

and t is the (N_1+N_2) dimensional firing time vector

$$t = \begin{bmatrix} t_1 & t_2 & \cdots & t_{N_1} & t_{N_1+1} & \cdots & t_{N_1+N_2} \end{bmatrix}^T \qquad (4\text{-}18)$$

If the total impulse ΔW to be delivered to the system of two vehicles by a jet firing sequence is specified by the cooperative autopilot as ΔW_c , then the jet select algorithm must determine an appropriate set of jet firing times t to satisfy

$$\Delta W_c = A \, t \qquad (4\text{-}19)$$

If the rank of matrix A is nine (*full rank*) then there exists at least one subset (*basis*) of nine linearly independent activity vectors which span nine dimensional space. Since any other nine dimensional vector may be expressed as a linear combination of a set of basis vectors, the structural constraint equation has at least one solution. If the rank is nine and $N_1+N_2 > 9$ then the system of equations is under-constrained, the basis set is not unique, and an infinite number of solutions are possible. Of these possible solutions, only those solutions where $t_j > 0$ for $j=1$ to N_1+N_2 need to be considered since negative jet firings are not feasible. The objective of the jet selection algorithm is to select the *optimum* solution from this "smaller" infinite set.

The optimum solution will satisfy the constraints in equation 4-19, be non-negative, and minimize a linear fuel expenditure function (cost function)

$$F(t) = c_1 t_1 + c_2 t_2 + \cdots + c_{N-1} t_{N-1} + c_N t_N \qquad (4\text{-}20)$$

where c_j is the cost coefficient for the jth jet and is determined based on fuel usage, the lifetime of the jet, and vehicle geometry heuristics. In this equation N (= $N_1 + N_2$) is the total number of jets on the two spacecraft. It is no longer necessary to differentiate between jets on the master vehicle and those on the slave vehicle.

The jet selection problem as stated in equations 4-19 and 4-20 is formulated as a linear programming problem. The characteristics of linear programming problems and their solutions are discussed in the following sections.

4.2 Linear Programming [6]

The general linear programming problem is to determine the values for the unknowns t_1, t_2, ...t_N which minimize a linear objective function

$$F(t) = C^T t \qquad (4\text{-}21)$$

subject to the m linear structural constraints

$$A t \leq P \qquad (4\text{-}22)$$

and the N non-negativity constraints

$$t_i \geq 0 \quad \text{for } i = 1,2,\cdots N \qquad (4\text{-}23)$$

Two important characteristics of linear programming problems are utilized in most solution algorithms:

- The solutions to the set of m+N constraint equations form a *convex* set

- The optimal solution lies at an *extreme point* of this set

A convex set is defined as a set of points defined such that a line segment joining any two of the points in the set lies entirely within the set. Figure 4.1(a) shows a two

dimensional convex set where the line segments joining any two points x_1 and x_2 lies completely within the set. In figure 4.1(b) it is possible to define a line segment $\overline{x_1 x_2}$ such that a portion of the segment lies outside the set. This set is not convex.

Figure 4.1(a)
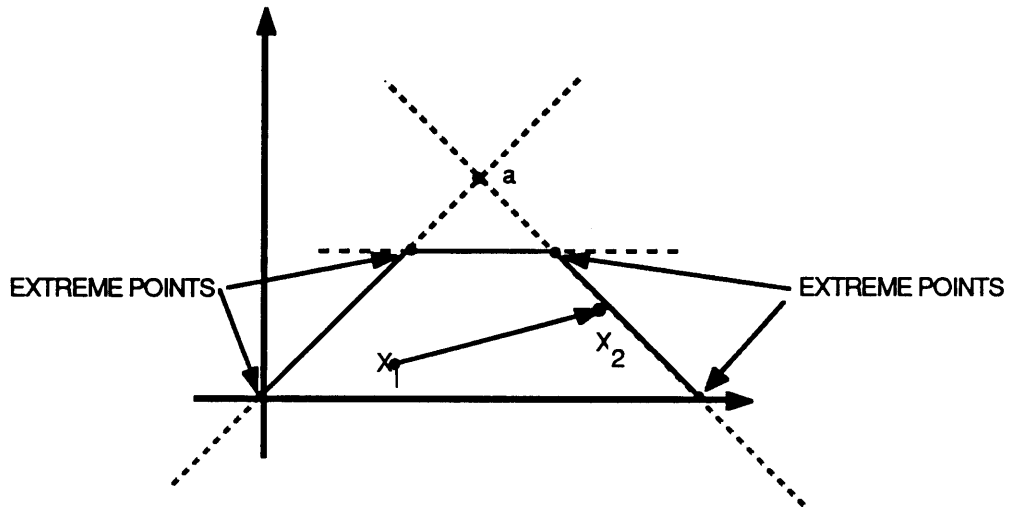
A convex set.
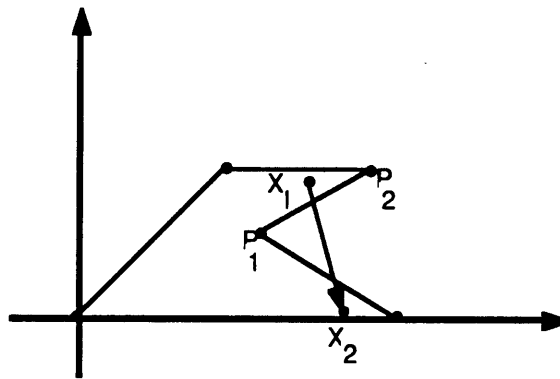

Figure 4.1(b)

A non-convex set.

Each of the m+N inequality constraints in equations 4-22 and 4-23 describes a *halfspace* on and below a *hyperplane* which partitions the m-dimensional space in two. The hyperplane is the constraint boundary and is described by the equation formed by replacing the inequality with an equality. The intersection of these halfspaces is by

43

definition a polygonal convex set and represents the solution space of the set of inequalities. In two dimensions a hyperplane is a line and the halfspace defined by a $\leq$ inequality is the halfplane below the line. The trapezoidal region in figure 4.1(a) is the intersection of four such halfplanes and represents the set of feasible solutions to a set of linear equality constraints. In contrast, the notch region in figure 4.1(b) cannot be constructed as the intersection of a set of halfplanes. Note that points x_1 and x_2 are on opposite sides of the perimeter segment $\overline{p_1 p_2}$ and thus cannot both satisfy an inequality formulated about the line containing the $\overline{p_1 p_2}$ segment. This region cannot represent the solution set for a set of linear equality constraints.

An extreme point is a point in the convex set which does not lie on any line segment connecting any two other points in the set. For a convex set defined in N dimensional space, all the extreme point solutions lie at the intersections of N of the m+N hyperplanes. Note that not all such intersections are extreme points of the convex solution set. In two dimensions the extreme points lie at the intersections of the constraint lines. In figure 4.1(a) the corners of the trapezoidal region are the extreme points but the point 'a' is not.

While any point in the convex set described by the m structural and N non-negativity constraints is a "feasible" solution to the linear programming problem, extreme point solutions are "basic feasible solutions", (i.e. only m of the t_j are non-zero). To demonstrate this, note that the structural inequality constraints may be re-written as equalities by introducing m "slack" variables to preserve this solution space.

$$A t + s = P \qquad where \qquad s = \begin{bmatrix} s_1 \\ s_2 \\ \vdots \\ s_m \end{bmatrix} \qquad (4-24)$$

The values taken by the slack variables indicate the location of the solution with respect to each inequality constraint. If $s_i > 0$ then the left side of the inequality is less than the right side and the constraint is satisfied; if $s_i = 0$ then the two sides are equal and the solution point lies on the constraint boundary; if $s_i < 0$ then the left side is larger than the right and the constraint has been violated. Obviously $s_i \geq 0$ for all feasible solutions.

The extreme points of a convex set lie at the intersections of N of the constraint boundaries and thus simultaneously satisfy N of the m+N constraints in their equality form. If k of these N satisfied constraints are structural constraints then the corresponding k slack variables are zero. The other N-k boundary equations satisfied at the extreme

point correspond to non-negativity constraints and thus N-k of the t_j are also zero. Since there are N+m total variables, k + (N-k) of which are zero, the extreme point solution has at most m non-zero values and is thus a basic feasible solution.

Since a extreme point solution has at most m nonzero t_j, equations 4-21 and 4-22 may be written in terms of a vector $\tilde{t}$ containing the m non-zero t_j, a square matrix **B** containing the corresponding m columns of the structural constraint matrix **A**, and the vector $\tilde{C}$ containing the m corresponding cost coefficients.

$$\mathbf{B}\,\tilde{t} = \mathbf{P} \tag{4-25}$$

$$F(t) = \tilde{C}^T \tilde{t} \tag{4-26}$$

In addition, an extreme point of the convex set is defined as a point that does not lie on a segment between any two other points in the set and therefore may not be expressed as a combination of any two other solutions. Consequently, $\tilde{t}$ is a unique solution to equation 4-25. From linear algebra, if **B** is not full rank then an infinite number of $\tilde{t}$ will satisfy equation 4-26. Therefore the m columns of **B** must be linearly independent and form a vector basis for m dimensional space.

The optimal solution to the linear programming problem is the member of the convex set of solutions to the inequality constraints that also minimizes the objective function. To demonstrate that the optimal solution is an extreme point of the convex solution set, define the gradient of the object function as

$$\mathbf{G} = -\left[\frac{dF(t)}{t_1} \cdots \frac{dF(t)}{t_N}\right] = -\mathbf{C}^T \tag{4-27}$$

Since the objective function is linear, **G** is constant and specifies the direction of maximum decrease of the objective function. The point on the convex set which extends furthest in this direction is the optimum solution and will be an extreme point of the set. In the unusual case that the gradient vector is perpendicular to a hyperplane segment between two extreme points, every point on the segment is optimal and all have equal cost.

In figure 4.2 a gradient line representing the direction of maximum decrease of an objective function has been superimposed on the two dimensional convex solution set of figure 4.1(a). Point 'a' extends the furthest in the specified direction and is therefore the minimum cost solution.
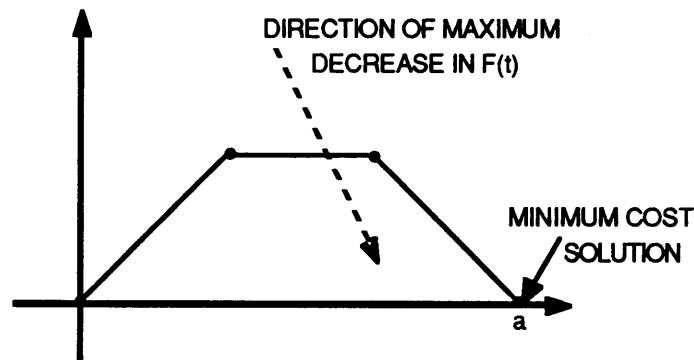
Figure 4.2

Gradient method for finding the optimal extreme point solution.

In a two or three dimensional system involving a small number of inequality constraints, it may be acceptable to simply evaluate the objective function at each extreme point and select the solution that corresponds to the minimum result. If the dimension of the system is large, a more efficient method of selecting the optimal solution point from the numerous (but finite) set of extreme points is required. The **Revised Simplex** algorithm is an efficient method for systematically evaluating the extreme point solutions to the constraint equation and determining the optimal solution. The next section discusses the theoretical basis for the simplex method and presents as overview of the algorithm itself.

4.3 The Revised Simplex Algorithm [6,2]

The previous section established two important facts:

(1) The optimal solution of the linear programming problem lies at an extreme point of the convex set of feasible solutions.

(2) Each extreme point is a basic solution ($\tilde{t}$) and is associated with a set of m basis vectors (**B**) and a value of the objective function ($F(\tilde{t})$).

The Simplex algorithm provides a systematic method to move from the current extreme point solution to one with a lower objective function value by replacing a basis vector with a column of the structural constraint matrix **A**. The incoming column vector is chosen based on its effect on the value of the objective function. The outgoing basis vector

46

is selected to insure the feasibility of the new solution. Simplex iterates on this vector by vector replacement process until either the optimal solution has been found or it has been established that no feasible solution exists. The Revised Simplex algorithm actually implemented in this research operates in the same manner but is computationally more efficient than the standard Simplex method.

From equation 4-25 an extreme point solution is described by the matrix of basis vectors **B** and the basis solution vector $\tilde{t}$

$$\mathbf{B}\,\tilde{t} = \mathbf{P} \tag{4-28}$$

Since **B** is a basis set, every column of the structural constraint matrix **A** may be expressed as a combination of the columns of **B**

$$\mathbf{A}_j = \mathbf{B}\,\mathbf{Y}_j \tag{4-29}$$

This equation defines the combination coefficients for the non-basis vector $\mathbf{A}_j$ as

$$\mathbf{Y}_j = \mathbf{B}^{-1}\mathbf{A}_j \;\rightarrow\; \mathbf{Y}_j = \begin{bmatrix} y_{1j} \\ y_{2j} \\ \vdots \\ y_{mj} \end{bmatrix} \tag{4-30}$$

Using equation 4-29 to both add and subtract β units of the the non-basis vector $\mathbf{A}_j$ from the left hand side of the extreme point solution in equation 4-28 yields

$$\mathbf{B}\left(\tilde{t} - \beta\mathbf{Y}_j\right) + \beta\mathbf{A}_j = \mathbf{P} \tag{4-31}$$

Thus the addition of β units of $\mathbf{A}_j$ requires a reduction of each $\tilde{t}_i$ by βy_{ij} in order to preserve the equality. As β increases the coefficient of the ith basis vector will decrease if the corresponding combination coefficient element y_{ij} is positive. (If none of the y_{ij} are positive then the optimal solution corresponds to the current extreme point.) Eventually the coefficient of one of the basis vectors (say b_k) will become zero; effectively removing it from the basis solution. This occurs when

$$\tilde{t}_k = \beta y_{ij} \quad \text{i.e. at} \quad \beta = \frac{\tilde{t}_k}{y_{ij}} \tag{4-32}$$

At this point the coefficients of the other m-1 basis vectors may be calculated according to

$$\tilde{t}_i' = \tilde{t}_i - \beta y_{ij} = \tilde{t}_i - \tilde{t}_k \frac{y_{ij}}{y_{kj}}$$

(4-33)

and equation 4-31 re-written as

$$b_1 \tilde{t}_1' + b_2 \tilde{t}_2' + \cdots + b_k (0) + \cdots + b_m \tilde{t}_m' + \beta A_j = P$$

(4-34)

Since the coefficient of b_k is 0 the left side of this equation is still the weighted sum of only m column vectors. The new basic solution and objective function value may be expressed in matrix notation by replacing the outgoing basis vector b_k with the incoming non-basis vector A_j, setting the corresponding element $\tilde{t}_k' = \beta$ and the corresponding cost coefficient $\tilde{c}_k = c_j$

$$B' \tilde{t}' = P$$

(4-35)

$$F(\tilde{t}') = \tilde{C}'^T \tilde{t}'$$

(4-36)

The feasibility of the solution has been preserved by selecting the outgoing basis vector to be the vector corresponding to the minimum positive $\frac{t_i}{y_{ij}}$ ratio.

In terms of the objective function, the reduction per unit of A_j of the $\tilde{t}_i$ by y_{ij} corresponds to an improvement of $\tilde{C}^T Y_j$, however, the addition of a unit of A_j into the solution represents an increase in the objective function of c_j. The net decrease in the objective function per unit of A_j is

$$\Delta F = \tilde{C}^T Y_j - c_j$$

(4-37)

Substituting the expression for Y_j from equation 4-30 this becomes

$$\Delta F = \tilde{C}^T B^{-1} A_j - c_j$$

(4-38)

The net decrease of the objective function is calculated for each non-basis vector in the constraint matrix A . A row vector may be defined as

$$\Delta F = \begin{bmatrix} \Delta F_1 & \Delta F_2 & \cdots & \Delta F_N \end{bmatrix}$$

$$= \begin{bmatrix} \tilde{C}^T B^{-1} A_1 - c_1 & \tilde{C}^T B^{-1} A_2 - c_2 & \cdots & \tilde{C}^T B^{-1} A_N - c_N \end{bmatrix}$$

$$= \tilde{C}^T B^{-1} \begin{bmatrix} A_1 & A_2 & \cdots & A_N \end{bmatrix} - \begin{bmatrix} c_1 & c_2 \cdots c_N \end{bmatrix}$$

(4-39)

48

$$= \tilde{C}^T B^{-1} A - C$$

The member of the constraint matrix **A** selected to be included into the basis is the vector corresponding to the maximum positive element of the vector ΔF. The value of the objective function at each extreme point is (equation 4-26)

$$F(\tilde{t}) = \tilde{C}^T \tilde{t} \tag{4-40}$$

From equation 4-25

$$\tilde{t} = B^{-1} P \tag{4-41}$$

So that the value of the objective function may be expressed for any basic solution as

$$F(\tilde{t}) = \tilde{C}^T B^{-1} P \tag{4-42}$$

Note that in order to select the incoming vector, the combination coefficients for each column of **A** must be computed and ΔF formed using equation 4-30. These operations are computationally very intensive. A more direct manner performing the basis update is required.

It is useful to define a partitioned matrix **T** representative of the "simplex tableau" described in much of the literature on linear programming.

$$T = \begin{bmatrix} Y & \vline & \tilde{t} \\ - - - - & \vline & - - \\ \Delta F(\tilde{t}) & \vline & F(\tilde{t}) \end{bmatrix} \tag{4-43}$$

Here **Y** is the matrix of combination coefficient vectors corresponding to the columns of the constraint matrix **A** and is calculated using the current extreme point basis **B**.

$$Y = \begin{bmatrix} Y_1 & Y_2 & \cdots & Y_N \end{bmatrix}$$

$$= \begin{bmatrix} B^{-1}A_1 & B^{-1}A_2 & \cdots & B^{-1}A_N \end{bmatrix} \tag{4-44}$$

$$= B^{-1}A$$

Substituting equations 4-30, 4-39, 4-41, and 4-42 into this partitioned matrix yields

$$T = \begin{bmatrix} B^{-1}A & \vdots & B^{-1}P \\ --- & \vdots & --- \\ \tilde{C}B^{-1}A-C & \vdots & \tilde{C}B^{-1}P \end{bmatrix} \qquad (4\text{-}45)$$

which may be factored as

$$T = \begin{bmatrix} B^{-1} & 0 \\ \tilde{C}B^{-1} & 1 \end{bmatrix} \begin{bmatrix} A & P \\ -C & 0 \end{bmatrix}$$

$$= \begin{bmatrix} B & 0 \\ -\tilde{C} & 1 \end{bmatrix}^{-1} \begin{bmatrix} A & P \\ -C & 0 \end{bmatrix} \qquad (4\text{-}46)$$

$$= \widehat{B}^{-1}\widehat{A}$$

Note that the ΔF vector may now be computed as an inner product of the successive columns of $\widehat{A}$ with the last row of $\widehat{B}^{-1}$. The combination coefficients need only be computed after the incoming basis vector has been selected from the columns of the constraint coefficient matrix. In addition, the $(m+1)\times(N+1)$ matrix $\widehat{A}$ is not affected by a change of basis and remains constant during the Simplex iterations. The $\widehat{B}^{-1}$ matrix however, must be updated each time a new vector is swapped into the basis.

An efficient method of performing the update of the $\widehat{B}^{-1}$ matrix may be developed as follows. Each column of the augmented basis $\widehat{B}$ is

$$\widehat{b}_j = \begin{bmatrix} b_j \\ --- \\ \tilde{c}_j \end{bmatrix} \quad \text{for } j = 1 \text{ to } m \quad ; \quad \widehat{b}_{m+1} = \begin{bmatrix} 0 \\ --- \\ \tilde{c}_j \end{bmatrix} \qquad (4\text{-}47)$$

The incoming constraint matrix column A_k corresponds to the kth column of $\widehat{A}$ which is

$$\widehat{A}_k = \begin{bmatrix} A_k \\ --- \\ c_k \end{bmatrix} \qquad (4\text{-}48)$$

and may be expressed as a linear combination of the columns of the augmented basis $\widehat{B}$

$$\widehat{A}_k = \widehat{B} Y_k \qquad (4\text{-}49)$$

50

If the lth basis vector $(\widehat{b}_l)$ is replaced by $\widehat{A_k}$ then the new basis $(\widehat{B}\,')$ may be written as

$$\widehat{B}\,' = \widehat{B}\,E \qquad (4\text{-}50)$$

where E is an "elementary matrix"

$$E = \begin{bmatrix} 1 & 0 & \cdots & y_{1k} & \cdots & 0 \\ 0 & 1 & \cdots & y_{2k} & \cdots & 0 \\ \vdots & \vdots & \ddots & \vdots & & \vdots \\ 0 & 0 & \cdots & y_{lk} & \cdots & 0 \\ \vdots & \vdots & & \vdots & \ddots & \vdots \\ 0 & 0 & \cdots & y_{(m+1)k} & \cdots & 1 \end{bmatrix} \qquad (4\text{-}51)$$

Taking the inverse of each side of equation 4-50

$$\left(\widehat{B}\,'\right)^{-1} = E^{-1}\,\widehat{B}^{\,-1} \qquad (4\text{-}52)$$

$$E^{-1} = \begin{bmatrix} 1 & 0 & \cdots & \dfrac{-y_{1k}}{y_{lk}} & \cdots & 0 \\[2mm] 0 & 1 & \cdots & \dfrac{-y_{2k}}{y_{lk}} & \cdots & 0 \\[2mm] \vdots & \vdots & \ddots & \vdots & & \vdots \\[2mm] 0 & 0 & \cdots & \dfrac{1}{y_{lk}} & \cdots & 0 \\[2mm] \vdots & \vdots & & \vdots & \ddots & \vdots \\[2mm] 0 & 0 & \cdots & \dfrac{-y_{(m+1)k}}{y_{lk}} & \cdots & 1 \end{bmatrix} \qquad (4\text{-}53)$$

The update of $\widehat{B}$ inferred by this equation may be implemented on an element by element basis as

$$\widehat{b}\,'_{ij} = \widehat{b}_{ij} - \frac{y_{ik}}{y_{lk}}\,\widehat{b}_{lj} \quad \text{for } i \neq l \quad i = 1 \text{ to } m+1 \qquad (4\text{-}54)$$
$$j = 1 \text{ to } m+1$$

and

$$\hat{b}_{ij}' = \frac{\hat{b}_{ij}}{y_{lk}} \quad \text{for } i = l \quad j = 1 \text{ to } m+1$$

<div align="right">(4-55)</div>

Thus by updating the inverse of the augmented basis directly the computation of the (m+1) dimensional inverse $\hat{B}^{-1}$ and a full set of combination coefficients has been avoided.

4.4 Implementation of the Revised Simplex Jet Select Algorithm [2,16]

The jet select algorithm employed as part of the cooperative autopilot developed in this thesis is a nine dimensional implementation of the Revised Simplex method described in the last section. The principle input to the algorithm is the nine dimensional rate change request (ΔW_c) generated by the steering algorithms. The jet select software assigns appropriate firing times to the reaction control jets on a pair of spacecraft in order to implement the requested impulse.

The example under study in this thesis is a system of two space shuttles. Each shuttle has a complement of 44 stationary reaction control thrusters; 38 primaries (870 lbf) and six verniers (24 lbf). Each jet is described by its body fixed position vector, body fixed thrust direction vector, an availability flag, and a scalar cost coefficient. Table 4.1 gives the location and thrust direction of each jet in the shuttle body frame. The primary thrusters on each shuttle are grouped into 14 clusters of two to four jets, (see figure 4.3). The jets within each cluster have similar locations, similar thrust directions, and consequently, deliver similar torques and forces. Though the six vernier jets are physically located adjacent to the primary jet clusters, the magnitude of a vernier activity vector is significantly smaller than those of the neighboring primaries. For the purpose of jet selection each available vernier jet is considered to be a separate single jet cluster and is included in the formulation of the constraint coefficient matrix A.

Due to the similarity of the activity vectors of the primary reaction control jets in each cluster, a single primary jet is designated as the cluster representative and (at least initially) is the only jet included in the constraint coefficient matrix. This approach provides substantial computation benefits and does not significantly affect the maneuverability of the shuttle during normal operations.

Table 4.1
Shuttle Reaction Control Jet Data.

JET NUMBER	DESIG- NATION	CLUSTER NUMBER	LOCATION (FT)			THRUST DIRECTION*			THRUST MAGNITUDE (LBF)*
PRIMARY JETS									
1	F1F	1	99.440	-1.221	0.567	-0.990	0.030	0.135	867.922
2	F3F	1	99.440	0.000	0.463	-0.990	0.000	0.136	868.018
3	F2F	1	99.440	1.221	0.567	-0.990	-0.030	0.135	867.922
4	F1L	2	94.777	-5.792	2.189	-0.030	0.999	0.021	874.185
5	F3L	2	94.607	-5.971	3.396	-0.024	1.000	0.001	870.553
6	F1U	3	95.756	-1.199	-1.122	-0.037	0.013	0.999	875.074
7	F3U	3	95.757	0.000	-1.211	-0.036	0.000	0.999	874.082
8	F2U	3	95.756	1.199	-1.122	-0.037	-0.013	0.999	875.074
9	F1D	4	97.180	-5.118	3.560	-0.032	0.694	-0.720	888.646
10	F3D	4	95.963	-5.519	3.463	-0.028	0.692	-0.722	885.847
11	F2R	5	94.777	5.792	2.189	-0.030	-0.999	0.021	874.185
12	F4R	5	94.607	5.971	3.396	-0.024	-1.000	0.001	870.553
13	F2D	6	97.180	5.118	3.560	-0.032	-0.694	-0.720	888.646
14	F4D	6	95.963	5.519	3.463	-0.028	-0.692	-0.722	885.847
15	L1A	7	-4.607	-10.333	-6.088	0.985	0.000	0.174	870.021
16	L3A	7	-4.607	-11.417	-6.088	0.985	0.000	0.174	870.021
17	L4L	8	-1.333	-12.469	-4.917	0.004	1.000	0.006	868.819
18	L2L	8	-2.417	-12.469	-4.917	0.004	1.000	0.006	868.819
19	L3L	8	-3.500	-12.469	-4.917	0.004	1.000	0.006	868.819
20	L1L	8	-4.583	-12.469	-4.917	0.004	1.000	0.006	868.819
21	L4U	9	-1.333	-11.000	-6.708	0.000	0.087	0.996	875.531
22	L2U	9	-2.417	-11.000	-6.708	0.000	0.087	0.996	875.531
23	L1U	9	-3.500	-11.000	-6.708	0.000	0.087	0.996	875.531
24	L4D	10	-1.333	-9.329	-3.117	0.305	0.461	-0.834	691.018
25	L2D	10	-2.417	-9.250	-3.333	0.305	0.461	-0.834	691.018
26	L3D	10	-3.500	-9.172	-3.550	0.305	0.461	-0.834	691.018
27	R1A	11	-4.607	10.333	-6.088	0.985	0.000	0.174	870.021
28	R3A	11	-4.607	11.417	-6.088	0.985	0.000	0.174	870.021
29	R4R	12	-1.333	12.469	-4.917	0.004	-1.000	0.006	868.819
30	R2R	12	-2.417	12.469	-4.917	0.004	-1.000	0.006	868.819
31	R3R	12	-3.500	12.469	-4.917	0.004	-1.000	0.006	868.819
32	R1R	12	-4.583	12.469	-4.917	0.004	-1.000	0.006	868.819
33	R4U	13	-1.333	11.000	-6.708	0.000	-0.087	0.996	875.531
34	R2U	13	-2.417	11.000	-6.708	0.000	-0.087	0.996	875.531
35	R1U	13	-3.500	11.000	-6.708	0.000	-0.087	0.996	875.531
36	R4D	14	-1.333	9.329	-3.117	0.305	-0.461	-0.834	691.018
37	R2D	14	-2.417	9.250	-3.333	0.305	-0.461	-0.834	691.018
38	R3D	14	-3.500	9.172	-3.550	0.305	-0.461	-0.834	691.018
VERNIER JETS									
39	F5L	4	97.971	-4.975	4.157	-0.033	0.694	-0.719	24.463
40	F5R	6	97.971	4.975	4.157	-0.033	-0.694	-0.719	24.463
41	L5L	8	-5.417	-12.469	-4.917	0.000	1.000	-0.025	24.007
42	L5D	10	-5.417	-9.833	-4.620	0.000	0.000	-1.000	13.200
43	R5R	12	-5.417	12.469	-4.917	0.000	-1.000	-0.025	24.007
44	R5D	14	-5.417	9.833	-4.620	0.000	0.000	-1.000	13.200

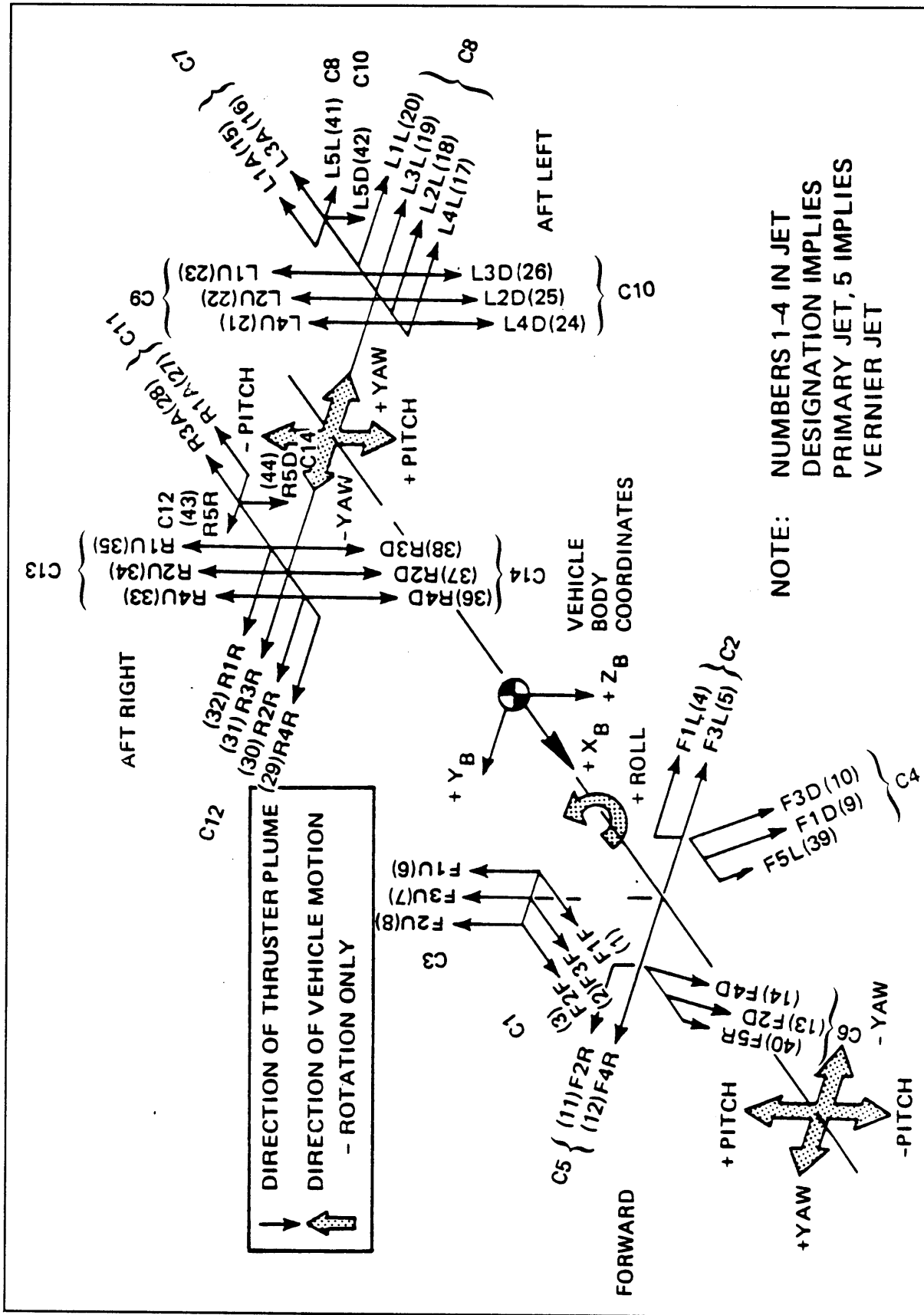* Includes effects of jet plume impingement

Figure 4.3
Reaction Control Jet locations and thrust directions

Each reaction control thruster also has an associated availability flag and cost coefficient. The availability flag indicates whether or not a jet may be included in the jet selection solution. A jet may be designated as unavailable by the crew, a failure detection module, or a heuristic supervisor module (e.g. a plume avoidance algorithm). If a cluster representative is unavailable the jet select module attempts to replace it with another member of the cluster. If all members of a cluster are unavailable, the linear programing problem is formulated without a representative from the cluster and the dimension of the constraint coefficient matrix (A) is decreased by one. This flexibility is one of the major benefits of formulating the jet selection task as a linear programming problem.

The optimum solution of the linear programming formulation of the jet selection problem is selected from among the set of feasible solutions based on the value of the linear objective function

$$F(t) = C^T t \qquad (4\text{-}56)$$

The cost coefficients (c_j) associated with each jet are a quantitative representation of an operational preference to be applied during the jet selection process. A preference among the available jets may be motivated by several different objectives. The principle objective in this development is fuel conservation, thus all primary jets are costed equally and more heavily than the verniers, ($c_{primary} = 1.0$, $c_{vernier} = 0.0287$). Alternative realtime algorithms for the cost coefficients may be motivated by a need to perform fuel management either between the two spacecraft or among the propellent tanks on a single vehicle. Cost functions could also be developed to heavily penalize the use of jets which which may 'plume' a neighboring spacecraft. This approach to plume avoidance leaves the jet in the range of possible simplex solutions, so that it may be selected during an emergency maneuver. Designating a jet as unavailable removes it from the solution space and thus may adversely affect the controllability of the vehicle(s).

The simplex approach to linear programming systematically progresses from one basic feasible solution to a 'better' basic feasible solution until the optimal solution is achieved. The feasibility of the final optimal solution is therefore dependent on the feasibility of the initial solution. Though in some linear programming applications an initial basic solution is easily discerned , the complexity of jet selection problem makes this impractical. The initial basis must satisfy the constraint equation

$$B t = \Delta W_c, \qquad (4\text{-}57)$$

55

span nine dimensional space (it must be invertible), and it must provide a feasible solution t via

$$t = B^{-1} \Delta W_c \qquad (4\text{-}58)$$

Even if a basis could be easily derived form the combination coefficient matrix, performing the inversion of **B** required to seed the revised simplex method is also computationally burdensome.

To circumvent these difficulties, nine additional variables are introduced with a basis of corresponding "artificial activity vectors" B_0. If the artificial vectors are defined as

$$B_{0_j} = I_j \, \text{SIGN}\left(\Delta W_{c_j}\right) \qquad (4\text{-}59)$$

where I_j is the jth column of a 9x9 identity matrix then

$$B_o^{-1} = B_o \qquad (4\text{-}60)$$

and

$$\tilde{t}_j = \text{ABS}\left(\Delta W_{c_j}\right) \qquad (4\text{-}61)$$

Since the artificial vectors are mutually orthogonal, the inverse in equation 4-60 is guaranteed to exist. Equation 4-59 confirms that the initial solution satisfies the non-negativity constraints. Thus the addition of a set of slack variables avoids both a difficult search for an initial basis and the computational burden of inverting the basis to seed the revised simplex algorithm.

The artificial activity vectors are not however, representative of real reaction control jets and thus cannot appear in a real optimal solution. To ensure that these columns of **B** are rotated out of the basis during the simplex operations, the cost coefficient corresponding to each artificial activity vector is set to a maximum positive value. Simplex must iterate at least nine times to eliminate all the artificial vectors from the basis. Once removed from the basis the artificial vectors are discarded and are never used as potential incoming vectors.

Once the initial basis solution is set up, the jet select algorithm proceeds to solve the linear programming problem using the revised simplex method. Several pragmatic

implementation issues may have a significant impact on the performance of the jet select algorithm.

The activity vectors are calculated under the assumption that neither vehicle experiences a significant translation or rotation during the jet firing. During large ΔW maneuvers, some jets are assigned fairly long firing times as part of the optimal solution. If the vehicle has a significant angular velocity during the firing, the net translational impulse provided by a jet will not be aligned with the expected impulse vector. Several solutions have been proposed to alleviate this problem.

The revised simplex algorithm implementation by Persson and Cooke[16] compares the longest firing command in the optimal solution to a predetermined threshold. If the firing time exceeds the threshold, it is set equal to the threshold value and all the other jet firing times are scaled to preserve the direction of the impulse delivered.

$$\tilde{t}_j' = \frac{\tilde{t}_j}{\tilde{t}_{max}} t_{threshold}$$

(4-62)

Since the magnitude of the impulse delivered by this method will be less than the magnitude of the original impulse request, the state of the vehicles at the end of the burn is measured, a new ΔW_c calculated, and the jet selection algorithm immediately run to complete the maneuver. In this manner an extremely long burn may be accurately implemented in a piecewise optimal sense.

A revised simplex algorithm modified to incorporate an upper bound on the each solution variable $\tilde{t}_j$ has been implemented for control moment gyros by Paradiso[3]. In this algorithm the value of the $\tilde{t}_j$ is compared to a threshold after each simplex iteration. If $\tilde{t}_j$ exceeds this upper bound the corresponding actuator is considered saturated and it is removed from the basis and saved as a special adjunct command. The impulse provided by this saturated actuator is used to adjust the impulse request passed to the remaining true basis solution set. As the algorithm progresses toward the final basic solution it may be no longer be optimal for $\tilde{t}_j$ to remain at the maximum value. To allow this saturated actuator to become 'unsaturated' during the course of simplex convergence the sign of the corresponding activity vector is switched and re-admitted into the set of potential incoming activity vectors. If this *anti-vector* is selected then the firing time of the saturated jet is decreased and it is re-admitted into the basic solution in its positive sense.

The most striking feature of this approach is that **more than 9** jets could be fired simultaneously as part of a single solution. This enhancement of the linear programming approach to jet selection is promising and should be investigated further as a method of incorporating the secondary jets in each cluster.

In any iterative algorithm there exists a potential for build up of round off errors. The effect of the round off errors induced during the direct update of the B^{-1} matrix may be checked by calculating the impulse delivered by the current solution against the impulse request. The firing time solution vector is given by

$$\tilde{t} = B^{-1} \Delta W_c \qquad (4\text{-}63)$$

where B^{-1} is calculated during the most recent simplex iteration. Since the activity vectors corresponding to these firing times are columns of the known matrix A (equation 4-22) the actual basis B_a may be easily constructed and the actual impulse calculated as

$$B_a \tilde{t} = \Delta W_a \qquad (4\text{-}64)$$

The error in the velocity change due to the inaccuracy of B^{-1} is simply the difference between the actual and commanded velocity impulse.

$$\Delta W_{err} = \Delta W_a - \Delta W_c \qquad (4\text{-}65)$$

If the magnitude of this error vector exceeds 1% of the magnitude of ΔW_c, the actual basis B_a is inverted and substituted for the current value of B^{-1}. The round off errors do not grow rapidly and thus the basis is not re-inverted very often.

CHAPTER 5

TWO VEHICLE TRAJECTORY SOLVER

5.0 Introduction

The cooperative trajectory solver generates a model trajectory consisting of a list of the jets to be fired, the corresponding burn times, and the state variable time histories which carry the two vehicle system from the initial state to a commanded final state. A solution to single spacecraft combined rotational and translational maneuvers has been presented using an open-loop "feed-forward" trajectory solver as part of a "feed-forward / feedback" closed-loop control architecture[9]. This section develops a similar open-loop trajectory solver for two vehicle cooperative maneuvers.

The two shuttle vehicles under consideration in this thesis are characteristic of a larger class of spacecraft which employ reaction control jets to perform rotational and translational maneuvers. Each shuttle reaction control jet applies a force along at least two of the vehicle body axes and (consequently) a torque about all three body axes. Current spacecraft control system designs tend to approach attitude and translation control as two separate, decoupled control problems. In addition, attitude and translation control is often performed by a set of uncoupled single axis controllers. Since the vehicle dynamics are coupled through the reaction control jets, attempts to control one set of the control variables with an uncoupled controller will often introduce large disturbances in other control variables. Compensating for these control induced disturbances consumes additional fuel and may cause the number of jet firings to drastically increase.

It has been demonstrated that optimal, three degree of freedom rotational maneuvers of a single linearized spacecraft model employ a jet activity profile which contains an acceleration phase, coast phase, and a deceleration phase[1], (see figure 5.1). The "staircase" clustering of the acceleration and deceleration jet firings at t_0 and t_f increases the average vehicle rate during the firings and thus decreases the overall maneuver time. During the intermediate coast period the external torque on the vehicle is assumed to be zero and the spacecraft angular velocity remains constant. This jet firing profile is the basis for the nine degree of freedom feed-forward trajectory solver developed here.
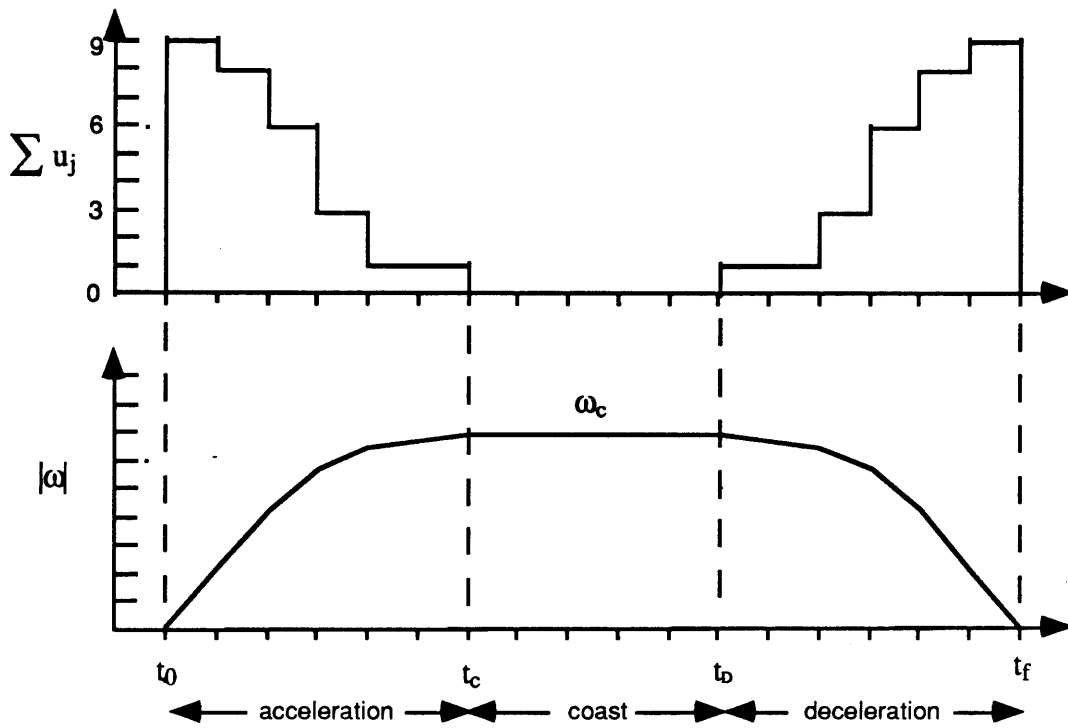
Figure 5.1
The Two Burn Jet Firing Profile.

5.1 Final State Equations

The two vehicle coordinated trajectory solver plans combined master vehicle rotations, slave/master relative rotations, and slave/master relative translations using the available reaction control jets on both vehicles. The rate of change of the velocity of each of the control variables induced by the jth reaction control jet is described by a nine dimensional activity vector A_j. As defined in chapter 4,

$$A_j = \begin{bmatrix} \alpha_a \\ \alpha_R \\ a_R \end{bmatrix}_j \tag{5-1}$$

where α_a is the angular acceleration of the master vehicle expressed in the master body frame, α_R is the rate of change of the relative angular velocity expressed in the master vehicle frame, and a_R is the rate of change of the relative linear velocity expressed in the LVLH frame.

60

The linearized equations governing the absolute attitude of the master vehicle and the relative attitude of the slave vehicle with respect to the master vehicle were derived in chapter 2 under the assumption that each vehicle is experiencing a small angular rate. Since the sub-vectors of the general activity vector (α_a, α_R) represent the angular accelerations induced by the jth jet, these equations may be written

$$\dot{\omega}_a = \sum_{j=1}^{N_1+N_2} \alpha_{a_j} u_j \tag{5-2}$$

$$\dot{\omega}_R = \sum_{j=1}^{N_1+N_2} \alpha_{R_j} u_j \tag{5-3}$$

Here $\mathbf{u}$ is the N_1+N_2 element control vector defined as

$$u_j = \begin{cases} 1 & \text{when the } j^{th} \text{ jet is firing} \\ 0 & \text{otherwise} \end{cases} \tag{5-4}$$

Integrating equation 5-2 from t_0 to t_f while following the jet firing profile in figure 5.1 yields:

$$\omega_a(t_c) = \sum_{j=1}^{N_1+N_2} \alpha_{a_j} t_j + \omega_a(t_0) \tag{5-5}$$

$$\omega_a(t_f) = \sum_{j=1}^{N_1+N_2} \alpha'_{a_j} t'_j + \omega_a(t_c) \tag{5-6}$$

$$\theta_a(t_f) = \sum_{j=1}^{N_1+N_2} \alpha_{a_j} \left(t_f t_j - \tfrac{1}{2} t_j^2 \right) + \sum_{j=1}^{N_1+N_2} \tfrac{1}{2} \alpha'_{a_j} \left(t'_j \right)^2 + \omega_a(t_0) t_f + \theta_a(t_0) \tag{5-7}$$

Similarly, integrating equation 5-3 for the attitude of the slave vehicle with respect to the master vehicle yields

$$\omega_R(t_c) = \sum_{j=1}^{N_1+N_2} \alpha_{R_j} t_j + \omega_R(t_0) \tag{5-8}$$

$$\omega_R(t_f) = \sum_{j=1}^{N_1+N_2} \alpha'_{R_j} t'_j + \omega_R(t_c) \tag{5-9}$$

$$\theta_R(t_f) = \sum_{j=1}^{N_1+N_2} \alpha_{R_j}\left(t_f t_j - \tfrac{1}{2}t_j^2\right) + \sum_{j=1}^{N_1+N_2} \tfrac{1}{2}\alpha'_{R_j}\left(t_j\right)^2 + \omega_R(t_0)\, t_f + \theta_R(t_0) \qquad (5\text{-}10)$$

In equations 5-5 thru 5-7 and 5-8 thru 5-10 the α'_{a_j}, α'_{R_j}, and t_j are the angular accelerations and firing times corresponding to the jth jet during the deceleration burn. As was shown in chapter 4, the activity vectors corresponding to the jets on the slave spacecraft are a function of the relative attitude of the two spacecraft. The set of activity vectors employed during the second burn must therefore be recomputed at the beginning of the deceleration burn. Since each burn is assumed to be impulsive, the relative attitude of the two spacecraft at the initiation of the second burn is considered to be equal to the commanded relative attitude for the purpose of activity vector calculation.

In chapter 3 the translational motion of a single spacecraft in a local vertical - local horizontal (LVLH) reference frame was shown to be governed by the Clohessy - Wiltshire equations. The complete solution of the C.W. equations for a period of constant external force was shown to be

$$\mathbf{x}(t) = \begin{bmatrix} \mathbf{r}(t) \\ \mathbf{v}(t) \end{bmatrix} = \Phi(t)\,\mathbf{x}(t_0) + \Gamma(t)\sum_{j=1}^{N} a_j u_j \qquad (5\text{-}11)$$

where $\Phi(t)$ is the state transition matrix,

$$\Phi(t) = \begin{bmatrix}
1 & 0 & 6\eta_0 t - 6S & \dfrac{4}{\eta_0}S - 3t & 0 & \dfrac{2}{\eta_0}(1-C) \\[2mm]
0 & C & 0 & 0 & \dfrac{1}{\eta_0}S & 0 \\[2mm]
0 & 0 & 4 - 3C & -\dfrac{2}{\eta_0}(1-C) & 0 & \dfrac{1}{\eta_0}S \\[2mm]
0 & 0 & 6\eta_0(1-C) & 4C - 3 & 0 & 2S \\[2mm]
0 & -\eta_0 S & 0 & 0 & C & 0 \\[2mm]
0 & 0 & 3\eta_0 S & -2S & 0 & C
\end{bmatrix} \qquad (5\text{-}12)$$

$\Gamma(t)$ is the control weighting matrix,

$$\Gamma(t) = \begin{bmatrix} \dfrac{4}{\eta_o^2}(1-C) - 3t^2 & 0 & \dfrac{2}{\eta_o}\left(t - \dfrac{S}{\eta_o}\right) \\[3mm] 0 & \dfrac{1}{\eta_o^2}(1-C) & 0 \\[3mm] \dfrac{-2}{\eta_o}\left(t - \dfrac{S}{\eta_o}\right) & 0 & \dfrac{1}{\eta_o^2}(1-C) \\[3mm] \dfrac{4}{\eta_o}S - 3t & 0 & \dfrac{2}{\eta_o}(1-C) \\[3mm] 0 & \dfrac{1}{\eta_o}S & 0 \\[3mm] \dfrac{-2}{\eta_o}(1-C) & 0 & \dfrac{1}{\eta_o}S \end{bmatrix} \qquad (5\text{-}13)$$

a_j is the translation acceleration sub-vector of the jth activity vector, and u is the control vector defined in equation 5-4. For simplicity, 'C' and 'S' have been substituted for 'cos $\eta_o t$' and 'sin $\eta_o t$' in the above expressions. Often the state transition matrix is written in terms of its 3x3 sub-matrices as

$$\Phi(t) = \begin{bmatrix} \Phi_{rr}(t) & \Phi_{rv}(t) \\ \Phi_{vr}(t) & \Phi_{vv}(t) \end{bmatrix} \qquad (5\text{-}14)$$

Since the relative motion of the master and slave spacecraft is defined by

$$x_R(t) = x_2(t) - x_1(t) \qquad (5\text{-}15)$$

the equation governing the relative motion of the two spacecraft during any period of constant thrust is

$$x_R(t) = \begin{bmatrix} r_R(t) \\ v_R(t) \end{bmatrix} = \Phi(t)\, x_R(t_0) + \Gamma(t) \sum_{j=1}^{N_1+N_2} a_{R_j} u_j \qquad (5\text{-}16)$$

This equation may be applied to each period of constant thrust along the accelerate, coast, decelerate jet firing profile of figure 5.1 to determine the final relative position states of the two spacecraft. The constant thrust periods during the acceleration and deceleration phases are very short compared to the period of the reference orbit. (A circular Low Earth Orbit has a period of approximately 90 min. and a mean motion $\eta_o = 0.00116$ rad/sec; a typical period of constant thrust during the jet firing phases is < 5 sec.). Since t is small during the acceleration and deceleration phases, $\eta_o t$ is a small angle and truncated series approximations for SIN and COS may be used without introducing significant errors. Neglecting terms of the order of η_o^2 and higher yields:

$$\Phi(t) = \begin{bmatrix} 1 & 0 & 0 & t & 0 & 0 \\ 0 & 1 & 0 & 0 & t & 0 \\ 0 & 0 & 1 & 0 & 0 & t \\ 0 & 0 & 0 & 1 & 0 & 2\eta_o t \\ 0 & 0 & 0 & 0 & 1 & 0 \\ 0 & 0 & 0 & -2\eta_o t & 0 & 1 \end{bmatrix} \qquad \Gamma(t) = \begin{bmatrix} 0 & 0 & 0 \\ 0 & 0 & 0 \\ 0 & 0 & 0 \\ t & 0 & 0 \\ 0 & t & 0 \\ 0 & 0 & t \end{bmatrix} \qquad (5\text{-}17)$$

The velocity coupling terms $2\eta_o t \ll 1$, and thus the velocity update performed by equation 5-16 is dominated by the effect of the thrusters during the acceleration and deceleration phases of the jet firing profile. If the change in velocity due to these coupling terms is neglected during short reaction control jet firings equation 5-16 becomes

$$\begin{bmatrix} r_R(t) \\ v_R(t) \end{bmatrix} = \begin{bmatrix} I & It \\ 0 & I \end{bmatrix} \begin{bmatrix} r_R(t_0) \\ v_R(t_0) \end{bmatrix} + \begin{bmatrix} 0 \\ It \end{bmatrix} \sum_{j=1}^{N_1+N_2} a_{R_j} u_j \qquad (5\text{-}18)$$

Here I is the 3x3 identity matrix. It should be noted that equation 5-18 represents simple rectangular integration of the initial velocities and constant forces to attain the new position and linear velocity. Using equation 5-18 to propagate the relative position state across each period of constant thrust during the acceleration burn, the relative position state at the end of the acceleration burn is calculated as

$$r_R(t_c) = r_R(t_0) + v_R(t_0) t_c + \sum_{j=1}^{N_1+N_2} a_{R_j}\left(t_c t_j - \tfrac{1}{2}t_j^2\right) \qquad (5\text{-}19)$$

$$v_R(t_c) = v_R(t_0) + \sum_{j=1}^{N_1+N_2} a_{R_j} t_j \qquad (5\text{-}20)$$

There are no feed-forward jet firings during the coast period. The state transition matrix is used to propagate the relative position state from the end of the acceleration burn to the beginning of the deceleration burn.

$$\begin{bmatrix} r_R(t_D) \\ v_R(t_D) \end{bmatrix} = \begin{bmatrix} \Phi_{rr}(t_D\text{-}t_c) & \Phi_{rv}(t_D\text{-}t_c) \\ \Phi_{vr}(t_D\text{-}t_c) & \Phi_{vv}(t_D\text{-}t_c) \end{bmatrix} \begin{bmatrix} r_R(t_c) \\ v_R(t_c) \end{bmatrix} \qquad (5\text{-}21)$$

The final relative position state is determined by propagating $x_R(t_D)$ and $v_R(t_D)$ thru the deceleration burn using equation 5-18 across each period of constant force.

$$r_R(t_f) = r_R(t_D) + v_R(t_D)(t_f\text{-}t_D) + \sum_{j=1}^{N_1+N_2} \tfrac{1}{2}a_{R_j} t_j^2 \qquad (5\text{-}22)$$

64

$$v_R(t_f) = v_R(t_0) + \sum_{j=1}^{N_1+N_2} a'_{R_j} t'_j \qquad (5\text{-}23)$$

In the above equations the contribution from each available reaction control jet has been included in the summations over 1 to N_1+N_2. If the jth jet is not firing during a portion of a maneuver then $t_j = 0$ during the corresponding integration step.

5.2 Trajectory Solution Algorithm [9]

The trajectory solver must solve the algebraic equations 5-7, 5-10, and 5-22 for the first and second burn firing times (t_j and t'_j) in terms of the boundary conditions and the activity vectors A_j, A'_j for j=1 to N_1+N_2. Since no manageable closed form solution is possible, the problem is parameterized in terms of the velocities at the beginning of the coast period, ($\omega_a(t_c)$, $\omega_R(t_c)$, $v_R(t_c)$) and solved iteratively using Newton's Iterative Method (Newton-Raphson Method). Each iteration consists of two computational phases:

- Solve the rate equations for the t_j and t'_j based on the current values of the coast velocity parameters and the initial and final velocity boundary conditions.

- Update the coast velocity parameters based on the final state error calculated using the jet firing times derived from the rate equations.

Since the rate equations for each burn are linear algebraic functions of the corresponding set of firing times, the first stage of the iteration process may be formulated as two separate problems; one for each burn. The acceleration burn rate equations 5-5, 5-8, and 5-20 may be written together in matrix form as

$$\begin{bmatrix} \omega_a(t_c) - \omega_a(t_0) \\ \omega_R(t_c) - \omega_R(t_0) \\ v_R(t_c) - v_R(t_0) \end{bmatrix} = \begin{bmatrix} \vdots & \vdots & & \vdots \\ A_1 & A_2 & \cdots & A_{(N_1+N_2)} \\ \vdots & \vdots & & \vdots \end{bmatrix} \begin{bmatrix} t_1 \\ t_2 \\ \vdots \\ t_{(N_1+N_2)} \end{bmatrix} \qquad (5\text{-}24)$$

The relative translational velocity at the end of the acceleration period may be propagated to the end of the coast period once the acceleration burn firing times are known

$$v_R(t_D) = \begin{bmatrix} \Phi_{vr}(t_D\text{-}t_c) & \Phi_{vv}(t_D\text{-}t_c) \end{bmatrix} \begin{bmatrix} r_R(t_c) \\ v_R(t_c) \end{bmatrix} \qquad (5\text{-}25)$$

and the deceleration rate equations may be written as

$$
\begin{bmatrix} \omega_a(t_f) - \omega_a(t_c) \\ \omega_R(t_f) - \omega_R(t_c) \\ v_R(t_f) - v_R(t_b) \end{bmatrix} = \begin{bmatrix} \vdots & \vdots & & \vdots \\ A_1' & A_2' & \cdots & A_{(N_1+N_2)}' \\ \vdots & \vdots & & \vdots \end{bmatrix} \begin{bmatrix} t_1' \\ t_2' \\ \vdots \\ t_{(N_1+N_2)}' \end{bmatrix} \tag{5-26}
$$

These equations for acceleration and deceleration (5-24, 5-26) may be considered as the structural constraint equation of a linear programming problem of the form

$$Minimize \quad F(t) = C^T t$$

$$subject\ to \quad \Delta W = A\,t \tag{5-27}$$

$$and \quad t_j \geq 0 \quad for\ j = 1,2,...,N_1+N_2$$

The **Revised Simplex** method of solving this nine dimensional linear programming problem is developed in detail in Chapter 4 of this thesis. The revised simplex algorithm selects a set of at most nine reaction control jets and computes the corresponding firing times t_j such that the structural and non-negativity constraints are satisfied and the objective function $F(t)$ is minimized. In this application $F(t)$ is a fuel usage function. The nine activity vectors A_j corresponding to the nine reaction control jets selected by the revised simplex algorithm for each burn may be collected into a *basis* matrix B. The corresponding nine firing times t_j are collected into the 9-vector $\tilde{t}$.

The second stage of the trajectory solver is the update of the values of the optimization parameter vectors $\omega_a(t_c)$, $\omega_R(t_c)$, $v_R(t_c)$) in order to decrease the final state errors.

The final values of the control variables $\theta_a(t_f)$, $\theta_R(t_f)$, $r_R(t_f)$, are a function of the values of the corresponding coast velocity parameter vectors. Define the error functions $g_1(\omega_a(t_c))$, $g_2(\omega_R(t_c))$, $g_3(v_R(t_c))$ as

$$g_1(\omega_a(t_c)) = \theta_a(t_f) - \theta_{a_{cmd}} \tag{5-28}$$

$$g_2(\omega_R(t_c)) = \theta_R(t_f) - \theta_{R_{cmd}} \tag{5-29}$$

$$g_3(v_R(t_c)) = r_R(t_f) - r_{R_{cmd}} \tag{5-30}$$

The optimal choice of the coast velocity parameters will result in g_1, g_2, $g_3 = 0$. If these error functions are not zero then the coast parameters must be altered. The required values

of the coast velocity vectors may be written as the current value plus the required adjustment

$$\omega_{a_{opt}} = \omega_a(t_c) + \Delta\omega_a \tag{5-31}$$

$$\omega_{R_{opt}} = \omega_R(t_c) + \Delta\omega_R \tag{5-32}$$

$$v_{R_{opt}} = v_R(t_c) + \Delta v_R \tag{5-33}$$

If the current value of the coast parameters are close to the optimal values, the adjustment vectors are small and each of the g_1, g_2, g_3 may be expanded in a Taylor series. Keeping only up to the first derivative terms

$$g_1\left(\omega_{a_{opt}}\right) = g_1\left(\omega_a(t_c)+\Delta\omega_a\right) \approx g_1\left(\omega_a(t_c)\right) + \frac{\partial g_1}{\partial \omega_a}\Delta\omega_a \tag{5-34}$$

$$g_2\left(\omega_{R_{opt}}\right) = g_2\left(\omega_R(t_c)+\Delta\omega_R\right) \approx g_2\left(\omega_R(t_c)\right) + \frac{\partial g_2}{\partial \omega_R}\Delta\omega_R \tag{5-35}$$

$$g_3\left(v_{R_{opt}}\right) = g_3\left(v_R(t_c)+\Delta v_R\right) \approx g_3\left(v_R(t_c)\right) + \frac{\partial g_3}{\partial v_R}\Delta v_R \tag{5-36}$$

Since the left side of the each approximation will be zero for the optimum parameter value, the approximate change required in each coast velocity vector is given by

$$\Delta\omega_a = -\left[\frac{\partial g_1}{\partial \omega_a}\right]^{-1} g_1\left(\omega_a(t_c)\right) \tag{5-37}$$

$$\Delta\omega_R = -\left[\frac{\partial g_2}{\partial \omega_R}\right]^{-1} g_2\left(\omega_R(t_c)\right) \tag{5-38}$$

$$\Delta v_R = -\left[\frac{\partial g_3}{\partial v_R}\right]^{-1} g_3\left(v_R(t_c)\right) \tag{5-39}$$

Since the command values of the control variables are constant, the partial derivatives of the error functions may be evaluated using equations 5-28 thru 5-30

$$\frac{\partial g_1}{\partial \omega_a} = \frac{\partial \theta_a(t_f)}{\partial \omega_a} \tag{5-40}$$

$$\frac{\partial g_2}{\partial \omega_R} = \frac{\partial \theta_R(t_f)}{\partial \omega_R} \tag{5-41}$$

$$\frac{\partial g_3}{\partial v_R} = \frac{\partial r_R(t_f)}{\partial v_R} \qquad (5\text{-}42)$$

Substituting these expressions into equation 5-37 thru 5-38 and combining the results with equations 5-31 thru 5-33 yields the three parameter update equations

$$\omega_a(t_c)^+ = \omega_a(t_c) - \left[\frac{\partial \theta_a(t_f)}{\partial \omega_a(t_c)}\right]^{-1} \left(\theta_a(t_f) - \theta_{a_{cmd}}\right) \qquad (5\text{-}43)$$

$$\omega_R(t_c)^+ = \omega_R(t_c) - \left[\frac{\partial \theta_R(t_f)}{\partial \omega_R(t_c)}\right]^{-1} \left(\theta_R(t_f) - \theta_{R_{cmd}}\right) \qquad (5\text{-}44)$$

$$v_R(t_c)^+ = v_R(t_c) - \left[\frac{\partial r_R(t_f)}{\partial v_R(t_c)}\right]^{-1} \left(r_R(t_f) - r_{R_{cmd}}\right) \qquad (5\text{-}45)$$

The partial derivatives in these equations are 3x3 Jacobian matrices. Since expressions for the final control variable values in terms of the coast velocity parameters is not available, a chain rule expansion is used in place of each Jacobian.

$$\frac{\partial \theta_a(t_f)}{\partial \omega_a(t_c)} = \frac{\partial \theta_a(t_f)}{\partial \tilde{t}} \frac{\partial \tilde{t}}{\partial \omega_a(t_c)} + \frac{\partial \theta_a(t_f)}{\partial \tilde{t}'} \frac{\partial \tilde{t}'}{\partial \theta_a(t_c)} \qquad (5\text{-}46)$$

$$\frac{\partial \theta_R(t_f)}{\partial \omega_R(t_c)} = \frac{\partial \theta_R(t_f)}{\partial \tilde{t}} \frac{\partial \tilde{t}}{\partial \omega_R(t_c)} + \frac{\partial \theta_R(t_f)}{\partial \tilde{t}'} \frac{\partial \tilde{t}'}{\partial \theta_R(t_c)} \qquad (5\text{-}47)$$

$$\frac{\partial r_R(t_f)}{\partial v_R(t_c)} = \frac{\partial r_R(t_f)}{\partial \tilde{t}} \frac{\partial \tilde{t}}{\partial v_R(t_c)} + \frac{\partial r_R(t_f)}{\partial \tilde{t}'} \frac{\partial \tilde{t}'}{\partial v_R(t_c)} \qquad (5\text{-}48)$$

The 9x9 matrix **B** has been defined as the collection of basis activity vectors for the first burn. Since each activity vector consists of three sub-vectors, the basis matrix may be partitioned into three 3x9 sub-matrices

$$\mathbf{B} = \begin{bmatrix} \mathbf{B}_{\alpha_a} \\ --- \\ \mathbf{B}_{\alpha_R} \\ --- \\ \mathbf{B}_{a_R} \end{bmatrix} \qquad (5\text{-}49)$$

The partial derivatives of the final values of the control variables with respect to the first set of firing times $\tilde{t}$ are then determined from equations 5-7, 5-10, and 5-22.

68

$$\frac{\partial \theta_a(t_f)}{\partial \tilde{t}} = \mathbf{B}_{\alpha_a} \ \mathrm{diag}\left[(t_f - \tilde{t}_j)\right] \tag{5-50}$$

$$\frac{\partial \theta_R(t_f)}{\partial \tilde{t}} = \mathbf{B}_{\alpha_R} \ \mathrm{diag}\left[(t_f - \tilde{t}_j)\right] \tag{5-51}$$

$$\frac{\partial r_R(t_f)}{\partial \tilde{t}} = \left\{\Phi_{rr} + (t_f - t_0)\Phi_{vr}\right\} \mathbf{B}_{a_R} \ \mathrm{diag}\left[(t_f - \tilde{t}_j)\right] + \left\{\Phi_{rv} + (t_f - t_0)\Phi_{vv}\right\} \mathbf{B}_{a_R} \tag{5-52}$$

If $\mathbf{B}'$ is the basis matrix corresponding to the second burn, the partial derivatives of the final values of the control variables with respect to the second set of firing times $\tilde{t}'$ are then determined from equations 5-7, 5-10, and 5-22 and written as

$$\frac{\partial \theta_a(t_f)}{\partial \tilde{t}'} = \mathbf{B}'_{\alpha_a} \ \mathrm{diag}\left[\tilde{t}_j'\right] \tag{5-53}$$

$$\frac{\partial \theta_R(t_f)}{\partial \tilde{t}'} = \mathbf{B}'_{\alpha_R} \ \mathrm{diag}\left[\tilde{t}_j'\right] \tag{5-54}$$

$$\frac{\partial r_R(t_f)}{\partial \tilde{t}'} = \mathbf{B}'_{a_R} \ \mathrm{diag}\left[\tilde{t}_j'\right] \tag{5-55}$$

The structural constraint equation for each burn may be re-written in terms of the basic solution provided by the revised simplex algorithm. Since the collections of activity vectors in the bases $\mathbf{B}$ and $\mathbf{B}'$ are by definition an linearly independent sets, they may be inverted.

$$\mathbf{B}^{-1} \begin{bmatrix} \omega_a(t_c) - \omega_a(t_0) \\ \omega_R(t_c) - \omega_R(t_0) \\ v_R(t_c) - v_R(t_0) \end{bmatrix} = \tilde{t} \qquad \mathbf{B}'^{-1} \begin{bmatrix} \omega_a(t_f) - \omega_a(t_c) \\ \omega_R(t_f) - \omega_R(t_c) \\ v_R(t_f) - v_R(t_c) \end{bmatrix} = \tilde{t}' \tag{5-56}$$

The partial derivatives of the firing times with respect to the coast parameters are

$$\frac{\partial \tilde{t}}{\partial \omega_a(t_c)} = \mathbf{B}_{\alpha_a}^{-1} \qquad \frac{\partial \tilde{t}}{\partial \omega_R(t_c)} = \mathbf{B}_{\alpha_R}^{-1} \qquad \frac{\partial \tilde{t}}{\partial v_R(t_c)} = \mathbf{B}_{a_R}^{-1} \tag{5-57}$$

and

$$\frac{\partial \tilde{t}'}{\partial \omega_a(t_c)} = \mathbf{B}'^{-1}_{a_R} \qquad \frac{\partial \tilde{t}'}{\partial \omega_R(t_c)} = \mathbf{B}'^{-1}_{\alpha_R} \qquad \frac{\partial \tilde{t}'}{\partial v_R(t_c)} = \mathbf{B}'^{-1}_{a_R} \tag{5-58}$$

For convenience the inverse basis matrices **B** and **B'** have been partitioned into 9x3 submatrices

$$B^{-1} = \left[\begin{array}{c|c|c} B^{-1}_{\alpha_a} & B^{-1}_{\alpha_R} & B^{-1}_{a_R} \end{array} \right]$$

(5-59)

$$B'^{-1} = \left[\begin{array}{c|c|c} B'^{-1}_{\alpha_a} & B'^{-1}_{\alpha_R} & B'^{-1}_{a_R} \end{array} \right]$$

(5-60)

Newton's method requires an initial approximation for the coast velocity parameters in order to begin the iteration process. The initial estimate of the rotation rate parameters for the absolute and relative attitude maneuvers is computed by approximating the entire maneuver as a constant rate *eigenaxis* rotation. The eigenaxis is defined as the unit vector perpendicular to the initial and final attitude quaternions. If $\tilde{q}_o$ represents the initial attitude and $\tilde{q}_f$ is the final attitude, then the maneuver quaternion $\tilde{q}_m$ satisfies

$$\tilde{q}_f = \tilde{q}_o \, \tilde{q}_m$$

(5-61)

and thus may be calculated as

$$\tilde{q}_m = \begin{bmatrix} \delta \\ \alpha \\ \beta \\ \gamma \end{bmatrix} = \tilde{q}_o^{-1} \, \tilde{q}_f$$

(5-62)

δ, α, β, γ are the Euler Parameters of the rotation. The quaternion $\tilde{q}_m$ represents a rotation by an angle

$$\varphi = 2 \, \mathrm{Cos}^{-1} \delta$$

(5-63)

about a unit vector

$$\hat{i}_\varphi = \left(\frac{1}{\sin \frac{1}{2}\varphi} \right) \left[\alpha \quad \beta \quad \gamma \right]$$

(5-64)

A constant rate rotational maneuver can then be described by the angular velocity vector

$$\omega_{coast} = |\omega| \, \hat{i}_\varphi$$

(5-65)

where

$$|\omega| = \frac{d\varphi}{dt} = \frac{\varphi}{\Delta t}$$

(5-66)

70

The initial approximations for the coast angular velocities for the absolute and relative rotational maneuvers are computed using equations 5-61 thru 5-66.

The initial relative translational velocity approximation is derived from the Clohessy-Wiltshire formulation for the relative motion of the two spacecraft (equation 5-11). Since the initial velocity estimate should be chosen to provide a final relative position near the commanded position, the estimate is computed from the first three of the six C-W equations. If the initial and final burns are truly impulsive, then the displacements of the vehicles will only take place during the coast portion of the maneuver and the position equations are written as

$$r_R(t_f) = \Phi_{rr}\, r_R(t_o) + \Phi_{rv}\, v_R(t_c) \tag{5-67}$$

This expression is solved for the desired coast velocity by multiplying thru by Φ_{rv}^{-1} and rearranging terms:

$$v_R(t_c) = \Phi_{rv}^{-1}\left[r_R(t_f) - \Phi_{rr}\, r_R(t_o)\right] \tag{5-68}$$

The state transition matrix sub-matrices in these expressions are computed for the fixed length of the maneuver. Equation 5-68 provides a reasonable estimate of the translation coast velocity parameter as long as the inverse Φ_{rv}^{-1} exists. From equation 5-12

$$\Phi_{rv}(t) = \frac{1}{\eta_o}\begin{bmatrix} 4\,S - 3\eta_o t & 0 & 2(1 - C) \\ 0 & S & 0 \\ -2(1 - C) & 0 & S \end{bmatrix} \tag{5-69}$$

and the inverse is

$$\Phi_{rv}^{-1}(t) = \frac{\eta_o}{S\big(S(4S - 3\eta_o t) + 4(1 - C)^2\big)}\begin{bmatrix} S^2 & 0 & -2S(1 - C) \\ 0 & S(4S - 3\eta_o t) + 4(1 - C)^2 & 0 \\ 2S(1 - C) & 0 & S(4S - 3\eta_o t) \end{bmatrix} \tag{5-70}$$

This inverse will exist everywhere except where the denominator of the coefficient term is zero. The factors in the denominator may be expanded and like terms collected yielding

$$S\big(S(4S - 3\eta_o t) + 4(1 - C)^2\big) \;\Rightarrow\; S(8 - 8C - 3\eta_o t S) \tag{5-71}$$

By inspection this last expression is zero whenever $\sin \eta_0 t$ is zero. The factor in parenthesis is also zero when $\sin \eta_0 t = 0$ and $\cos \eta_0 t = 1$. Figure 5.2 shows a plot of this function for the range $0 \le \eta_0 t \le 4\pi$.
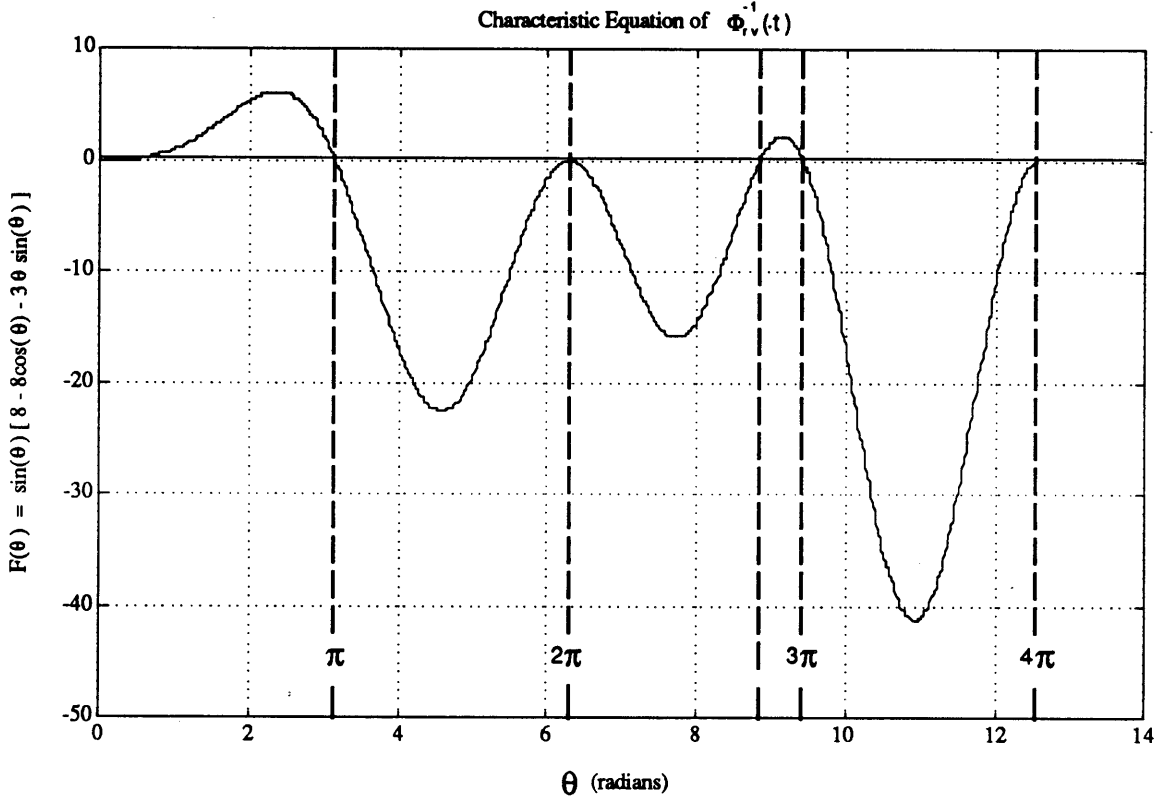

Figure 5.2

Determinant of Φ_{rv} vs $\theta = \eta_0 t$ Φ_{rv}^{-1} does not exist at the zero crossing angles.

In addition to the zeroes at multiples of π, ($\eta_0 t = 0$, π, 2π, $3\pi \cdots$), a zero occurs at approximately 2.81346π. At the zeroes the state transition sub-matrix Φ_{rv} becomes

$$\Phi_{rv}(t) = \frac{1}{\eta_o} \begin{bmatrix} -3\eta_o t & 0 & 0 \\ 0 & 0 & 0 \\ 0 & 0 & 0 \end{bmatrix} \text{ for } \eta_0 t = 0, 2\pi, \ldots$$

(5-72)

$$\Phi_{rv}(t) = \frac{1}{\eta_o} \begin{bmatrix} -3\eta_o t & 0 & -4 \\ 0 & 0 & 0 \\ 4 & 0 & 0 \end{bmatrix} \text{ for } \eta_0 t = \pi, 3\pi, \ldots$$

(5-73)

72

$$\Phi_{rv}(t) = \frac{1}{\eta_o} \begin{bmatrix} -24.30400 & 0 & 3.66628 \\ 0 & 0.55306 & 0 \\ -3.66628 & 0 & 0.55306 \end{bmatrix} \text{ for } \eta_o t \approx 2.83416\pi \tag{5-74}$$

Equation 5-72 shows that the out-of-plane and radial components of the final position are not effected by the coast velocity during maneuvers lasting one reference orbit period. Equation 5-73 demonstrates that the out-of-plane final position is also not effected by the coast velocity for maneuvers lasting half a reference orbit period. The first and third columns of the matrix in equation 5-74 are parallel vectors and therefore the change in the x and z components of the final position cannot be independently varied by adjusting the coast velocity when the maneuver is scheduled for approximately 1.4 nominal orbits. When the inverse Φ_{rv}^{-1} does not exist the system is not completely controllable using a single two burn maneuver. To reach the final state a sequence of maneuvers must be performed. The planning and optimization of these multi-maneuver sequences is beyond the scope of this thesis.

5.3 Nominal Trajectory Generator

The trajectory solution algorithm described in the last section determines a set of feed forward jet firing commands for both the acceleration and deceleration burns of the two burn maneuver based on a linearized model of the two vehicle system. During the coast portion of the maneuver a feedback controller is employed to compensate for non-linearities in the actual vehicle dynamics and unmodelled environmental disturbances. The primary inputs to the feedback controller are the current values of the desired attitude of the master vehicle with respect to an external reference frame, the desired attitude of the slave vehicle with respect to the master, and the desired position of the slave vehicle with respect to the master. The nominal trajectory generator computes the desired states at each point in the coast phase of the maneuver using the linearized models employed by the trajectory solution algorithm.

The linearized equations governing the absolute attitude of the master vehicle and the relative attitude of the slave vehicle with respect to the master vehicle have been derived under the assumption that each vehicle is experiencing a small angular rate. In section 5.1 it was shown that the angular velocities at the end of the acceleration burn are

$$\omega_a(t_c) = \sum_{j=1}^{N_1+N_2} \alpha_{a_j} t_j + \omega_a(t_0) \tag{5-75}$$

$$\omega_R(t_c) = \sum_{j=1}^{N_1+N_2} \alpha_{R_j} t_j + \omega_R(t_0) \tag{5-76}$$

Integrating these equations across the acceleration burn (t_0 to t_c) while following the jet firing profile in figure 5.1 yields the angular displacement vectors at the beginning of the coast phase.

$$\theta_a(t_c) = \sum_{j=1}^{N_1+N_2} \alpha_{a_j} \left(t_c t_j - \tfrac{1}{2} t_j^2 \right) + \omega_a(t_0) \left(t_c - t_0 \right) \tag{5-77}$$

$$\theta_R(t_c) = \sum_{j=1}^{N_1+N_2} \alpha_{R_j} \left(t_c t_j - \tfrac{1}{2} t_j^2 \right) + \omega_R(t_0) \left(t_c - t_0 \right) \tag{5-78}$$

During the coast phase of the maneuver the vehicles are assumed to be experiencing torque free motion. The equations of motion may be written

$$\dot{\omega}_a = 0 \quad \Rightarrow \quad \omega_a = constant \tag{5-80}$$

$$\dot{\omega}_R = 0 \quad \Rightarrow \quad \omega_R = constant \tag{5-81}$$

Integrating each of these equations from the end of the acceleration burn to the current time yields an attitude change vector which is used to update the quaternions representing the absolute attitude of the master vehicle and the attitude of the slave relative to the master.

$$\Delta\theta_a(t - t_c) = \omega_a(t - t_c) \qquad \text{for } t_c \le t \le t_D \tag{5-82}$$

$$\Delta\theta_R(t - t_c) = \omega_R(t - t_c) \qquad \text{for } t_c \le t \le t_D \tag{5-83}$$

The quaternions representing the rotations $\Delta\theta_a$ and $\Delta\theta_R$ are (see equation 2-50)

$$\tilde{q}_{\Delta a}(t-t_c) = \begin{bmatrix} \delta_a \\ q_a \end{bmatrix} \qquad\qquad \tilde{q}_{\Delta R}(t-t_c) = \begin{bmatrix} \delta_R \\ q_R \end{bmatrix} \tag{5-84}$$

where the 3-vectors q_a and q_R are defined in terms of the magnitudes of the rotations $\Delta\theta_a$ and $\Delta\theta_r$ and the corresponding rotation axes $\hat{i}_a$ and $\hat{i}_R$ as

74

$$q_a = \left(\sin\tfrac{1}{2}\Delta\theta_a\right)\hat{i}_a \tag{5-85}$$

$$q_R = \left(\sin\tfrac{1}{2}\Delta\theta_R\right)\hat{i}_R \tag{5-86}$$

.er parameters δ_a and δ_R are defined as

$$\delta_a = \cos\tfrac{1}{2}\Delta\theta_a \tag{5-87}$$

$$\delta_R = \cos\tfrac{1}{2}\Delta\theta_R \tag{5-88}$$

Similarly, the attitude quaternions at the end of the acceleration burn are calculated (t_c) and $\theta_a(t_c)$ as

$$\tilde{q}_a(t_c) = \begin{bmatrix} \delta_a(t_c) \\ q_a(t_c) \end{bmatrix} \qquad \tilde{q}_R(t_c) = \begin{bmatrix} \delta_R(t_c) \\ q_R(t_c) \end{bmatrix} \tag{5-89}$$

;ired absolute and relative attitude quaternions are then calculated during the coast rom the expected attitude at the end of the acceleration burn and the quaternions iting the change due to the constant coast rate.

$$\tilde{q}_a(t) = \tilde{q}_a(t_c)\,\tilde{q}_{\Delta a}(t\text{-}t_c) \tag{5-90}$$

$$\tilde{q}_R(t) = \tilde{q}_R(t_c)\,\tilde{q}_{\Delta R}(t\text{-}t_c) \tag{5-91}$$

The translational motion of the slave spacecraft relative to the master in a near orbit was shown to be governed by the Clohessy - Wiltshire equations in Chapter relative position and translational velocity of the two spacecraft at the end of the ition burn are given by

$$r_R(t_c) = r_R(t_0) + v_R(t_0)\,t_c + \sum_{j=1}^{N_1+N_2} a_{R_j}\!\left(t_c\,t_j - \tfrac{1}{2}t_j^2\right) \tag{5-92}$$

$$v_R(t_c) = v_R(t_0) + \sum_{j=1}^{N_1+N_2} a_{R_j}\,t_j \tag{5-93}$$

There are no feed-forward jet firings during the coast period. The homogeneous the C.W. equations is used to propagate the relative position state from the end of :leration burn to the current time.

$$\begin{bmatrix} \mathbf{r}_R(t) \\ \mathbf{v}_R(t) \end{bmatrix} = \begin{bmatrix} \Phi_{rr}(t\text{-}t_c) & \Phi_{rv}(t\text{-}t_c) \\ \Phi_{vr}(t\text{-}t_c) & \Phi_{vv}(t\text{-}t_c) \end{bmatrix} \begin{bmatrix} \mathbf{r}_R(t_c) \\ \mathbf{v}_R(t_c) \end{bmatrix} \qquad (5\text{-}94)$$

The quaternions $\tilde{q}_a(t)$, $\tilde{q}_R(t)$ and the vectors ω_a, ω_R, $\mathbf{r}_R$, $\mathbf{v}_R$ are computed on each autopilot pass during the coast phase of the two burn maneuver and passed to the feedback level of the cooperative autopilot.

76

CHAPTER 6

PHASE SPACE REGULATOR

6.0 Introduction

During the coast phase of the two burn maneuver the two spacecraft are perturbed from the nominal trajectory by environmental disturbances, the unmodelled non-linear dynamics and the granularity of the reaction control jet firings. A feedback control loop is used to generate jet firing commands in order to compensate for these effects and keep the spacecraft tracking the desired trajectory within a specified tolerance. In this thesis a *Phase Space Regulator* [2] is employed as the feedback controller.

The Phase Space control law was developed for the control of a single spacecraft performing six degree of freedom on-orbit maneuvers and was successfully flight tested as part of the shuttle OEX autopilot in 1985. The Phase Space control law combines the *velocity to be gained* principle with concept of a *phase sphere* in order to compute a velocity impulse request to drive the system to the commanded state. This section presents the Phase Space control law and develops the nine degree of freedom cooperative control phase space regulator.

6.1 Velocity to be Gained

Originally developed as a method of formulating guidance equations, the *velocity to be gained* algorithm computes the change in the velocity required for the system to follow a coasting trajectory from the current state to the specified target state. The state of a general n-degree of freedom system is described by the n-dimensional state vector x and the first derivative of the state $\dot{x}$. Given a target state x_d and a target velocity $\dot{x}_d$ the state error and velocity error are defined as

$$x_e = x - x_d \tag{6-1}$$

$$\dot{x}_e = \dot{x} - \dot{x}_d \tag{6-2}$$

The velocity to be gained vector v_g is defined as the difference between the velocity required to satisfy the *coast to target* constraints (v_r) and the current velocity of the system.

$$v_g = v_r - \dot{x} \qquad (6\text{-}3)$$

The determination of an appropriate expression for the required velocity v_r in terms of the current error state of the system is a central issue in most guidance problems. For the phase space controller the required velocity is expressed as the sum of a *convergent velocity* v_c and the desired velocity at the target state $\dot{x}_d$.

$$v_r = v_c + \dot{x}_d \qquad (6\text{-}4)$$

The velocity to be gained can be re-written in terms of the convergent velocity as

$$v_g = v_c + \dot{x}_d - \dot{x}$$

$$= v_c - \dot{x}_e \qquad (6\text{-}5)$$

This states that the velocity to be gained is simply the convergent velocity minus the current velocity error. The purpose of the convergent velocity is to drive the current vehicle state x toward the desired state x_d and thus the state error vector toward zero. An efficient method of driving a vector to zero is to align the time rate of change of the vector with the vector itself. Thus the convergent velocity vector is aligned with the current state error vector and may be written as

$$v_c = -c\,\hat{i}_e \qquad (6\text{-}6)$$

Here $\hat{i}_e$ is the unit vector in the direction of the state error and 'c' is the desired *convergence rate*. The velocity to be gained is thus written in terms of the direction of the state error and the velocity error as

$$v_g = -c\hat{i}_e + \dot{x}_d - \dot{x}$$

$$= -c\hat{i}_e - \dot{x}_e \qquad (6\text{-}7)$$

Ideally this velocity to be gained control law precisely controls the state and the velocity of the system at the desired state. In practice however, several difficulties arise. In systems employing on/off (bang-bang) actuators, precise control of the system velocity is especially difficult. Each actuator provides a finite acceleration and thus truly impulsive rate changes are not possible. As a result the implementation of the velocity requests lags

78

the velocity to be gained computation. Additional rate errors are introduced during the implementation of the velocity request due to the minimum impulse and discrete on/off switch time constraints on the actuators. These small rate errors cause the system to overshoot or drift away from the target state. Consequently attempts to control the system state to an exact target point will result in excessive actuator activity. In the next section the *phase sphere* concept is introduced as a method of accommodating these rate errors while controlling the system state to a desired accuracy.

6.2 Phase Sphere

A standard method of circumventing the difficulty of imprecise rate control inherent in the use of on/off actuators is the introduction of a small target region representing the acceptable levels of error in each state variable in place of the single target state. The target region is defined as an n-dimensional *deadband* in which actuator activity is inhibited and in which the system is allowed to coast freely. This approach increases fuel economy and decreases the number of actuator on/off cycles at the cost of a small amount of accuracy.

The control objective of the deadband control approach is to maintain each element of the state vector x_i within a specified 'deadband' of the corresponding target state element x_{d_i}. The target region is described by the n deadband constraints

$$-db_i < x_{e_i} < +db_i \tag{6-8}$$

The full set of these n double sided constraints on the n state variables defines a $2n$ sided rectangular parallelepiped centered on the origin in the n-dimensional error space. The length of a side of this rectangular parallelepiped is twice the value of the corresponding deadband db_i. Figure 6.1 shows a deadband volume defined in 3-space.

Since the numerical values of the individual db_i may be very different, the error vector x_e indicates the direction of the largest errors rather than the direction in which the state variables are furthermost from the established target volume. In practice the numerically largest element of the error vector could be within its deadband while the numerically smallest element could be outside its deadband. In order to apply control in a direction which will cause the state to most rapidly converge on the deadband volume a new *normalized* error vector is calculated by normalizing each component of the error
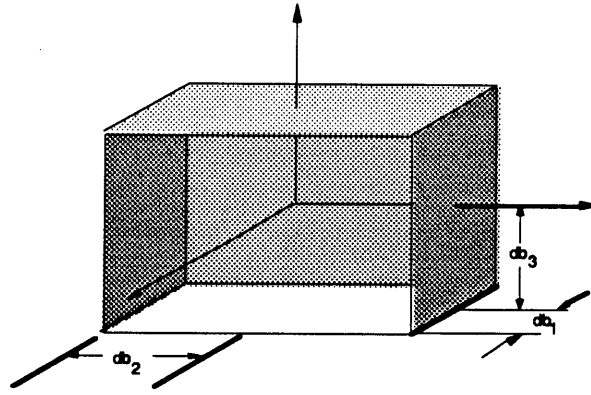
Figure 6.1
A deadband volume in the 3-dimensional
state error space.

vector x_{e_i} by the corresponding deadband value db_i. The elements of the normalized error vector are

$$\tilde{x}_{e_i} = \frac{x_{d_i} - x_i}{db_i}$$

$$= \tilde{x}_{d_i} - \tilde{x}_i \qquad (6\text{-}9)$$

Where $\tilde{x}_{d_i}$ and $\tilde{x}_i$ are the ith elements of the normalized desired state and current state vectors. Note that though $\tilde{x}_e$, $\tilde{x}_d$, and $\tilde{x}$ are referred to as *normalized* vectors, in general, they are not unit vectors and their direction is not the same as the original x, x_d, x_e. vectors. In addition note that each element of these *normalized* vectors is a dimensionless quantity.

The deadband constraints of equation 6-8 are expressed in the n-dimensional *normalized* error space as

$$-1 < \tilde{x}_{e_i} < +1 \qquad (6\text{-}10)$$

In this form the constraints define a hypercube centered at the origin of the n-dimensional *normalized* state error space. The length of each side of the hypercube is 2.

A simpler, though slightly more restrictive deadband volume is described by the n-dimensional unit hypersphere inscribed in the hypercube, (figure 6.2). Using this simpler deadband volume the n control objective constraints (equation 6-10) may be replaced by a single scalar constraint in terms of the *normalized* state error vector $\tilde{x}_e$

$$\left[\tilde{x}_e^T \tilde{x}_e \right]^{\frac{1}{2}} < 1 \qquad (6\text{-}11)$$

80

The inscribed hypersphere is referred to as a *phase sphere*. The unit radius phase sphere represents the state target region in the normalized error space.
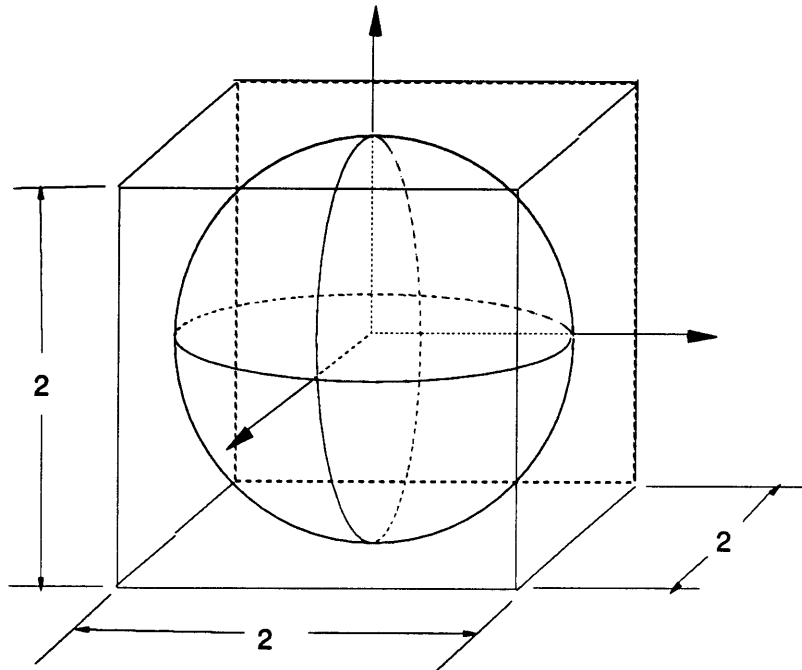

Figure 6.2
The unit phase sphere in the 3-dimensional
normalized state error space.

6.3 Phase Space Control Law

The Phase Space Control Law utilizes the phase sphere concept as the primary method for scheduling the values of the convergence rate parameter (c) in the velocity to be gained calculation (equation 6-7). When the normalized error state lies within the unit radius phase sphere the state control objective is satisfied and the convergence rate parameter is set to a small value. Conversely, outside the phase sphere the state error has exceeded the acceptable threshold and the value of the convergence rate parameter is increased in order to supplement the velocity error correction with a velocity component along the current error vector and drive the state back toward the deadband region.

As discussed the in the previous section, the convergent velocity component of the velocity to be gained vector should be aligned in the direction of the largest state excursion relative to the defined deadband region rather than in the direction of the numerically largest

81

error. The velocity to be gained calculation is thus modified to incorporate the *normalized* state error unit vector in the convergent velocity calculation.

$$V_g = -c\hat{i}_\epsilon + \dot{x}_d - \dot{x} \tag{6-12}$$

Due to the inability to precisely control the system velocity in the presence of environmental disturbances, actuator restrictions and/or state measurement errors, the phase space controller is unable to maintain the system state at the commanded value with zero velocity error. Consequently the state of the system tends to drift away from the target state and toward the perimeter of the deadband region. Ideally, when the state error encounters the edge of the phase sphere, control is applied and the component of the drift velocity in the direction of the normalized error is reversed. The system then coasts back through the deadband volume with the new convergent velocity until it again reaches the perimeter of the deadband volume and an additional velocity correction is made. As this process continues the system tends to oscillate within the deadband region. This oscillation about the target state is the well known *limit cycling* phenomena.

It is impractical to attempt to reverse the velocity at the precise moment when the state error reaches the edge of the phase sphere. During the finite amount of time required to implement the velocity change request the system state will travel beyond the phase sphere boundary. The amount and direction the system will overshoot the specified control tolerance is determined by the effectiveness of the actuators and the velocity of the system at the time it encounters the phase sphere perimeter.

To prevent any control variable from exceeding its maximum allowable value the velocity correction must be initiated before the normalized state error intercepts the perimeter of the unit radius phase sphere. As a divergent drift rate in the ith control direction ($\dot{x}_i$) is driven to zero by a constant actuator acceleration component in the ith direction (a_i) the system will travel a distance

$$\Delta x_i = \frac{\dot{x}_i^2}{2a_i} \tag{6-13}$$

Expressed as a fraction of the specified maximum allowable error in the ith control variable direction (db_i) this becomes

$$b_i = \frac{\Delta x_i}{db_i} = \frac{\dot{x}_i^2}{2a_i db_i} \tag{6-14}$$

82

Thus in order to prevent undesirable excursions of the system state away from the target state a new set of error thresholds described by

$$-(1 - b_i) < \tilde{x}_{e_i} < +(1 + b_i) \qquad (6\text{-}15)$$

must be employed to determine the appropriate points at which a corrective maneuver should be initiated. These n double sided constraints describe a parallelepiped in the n-dimensional normalized error space. Since the values used for $\dot{x}_i$ and a_i are not precisely known and may vary with disturbance levels and the state of the system, a second n-dimensional hypersphere is defined as a practical approximation of this complex surface. The radius of this second phase sphere is calculated as

$$r_{P2} = 1 - b \qquad (6\text{-}16)$$

where

$$b = \frac{\dot{x}_{i_{max}}^2}{2a_{i_{min}}db_i} \qquad (6\text{-}17)$$

The values used for $\dot{x}_{i_{max}}$ and $a_{i_{min}}$ are *anticipated* maximum and minimum values and should be determined empirically for the specific system under consideration. The inner sphere convergence rate parameter 'c' is a reasonable first approximation for $\dot{x}_{i_{max}}$.

This second phase sphere provides an error threshold at which control may be applied with a high confidence of reversing the divergent drift velocity before any error state exceeds its maximum allowable value. The second phase sphere is centered at the origin of the normalized error space, concentric with the original unit radius phase sphere. The two phase spheres partition the normalized error space into three distinct regions, (figure 6.3).

Region 1: The volume inside the inner phase sphere. When the normalized error vector lies within the inner sphere actuator activity is inhibited and the convergence rate parameter (c) is set to a small value.

Region 2: The buffer region between the two phase spheres. In this region the actuators may be employed to implement the calculated velocity change request (v_g). The convergence rate parameter (c) is set to a small value since the normalized error vector still lies within the unit phase sphere.

Region 3: The region outside the unit phase sphere. In this region the actuators may be employed to implement the calculated velocity change request (v_g). The convergence rate parameter (c) is set to a large value since the normalized error vector lies outside the unit phase sphere; indicating at least one of the control variables has travelled an unacceptable distance from the target state.
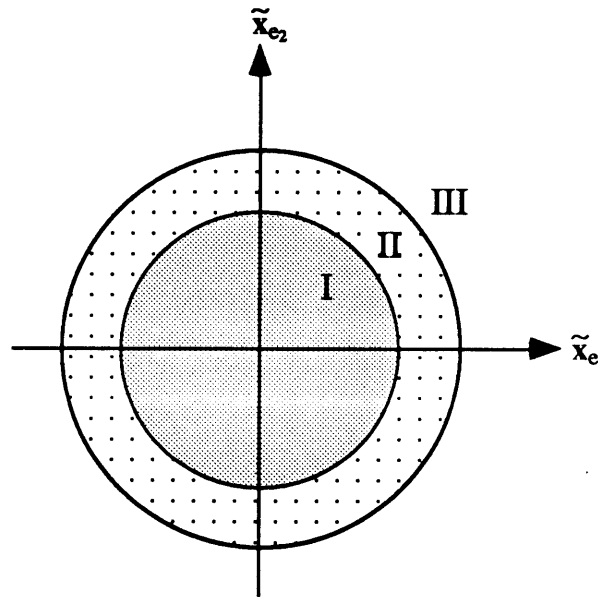

Figure 6.3
Two dimensional cross section of the
phase sphere geometry

The value of the convergence rate parameter takes on two distinct values. In regions 1 and 2 the convergence rate is selected to be large enough to generate at least the minimum impulse velocity request required to drive the system away from the phase sphere perimeter and small enough to provide a reasonable coast time between limit cycle velocity corrections. The value of the convergence rate in region 3 must be large enough to provide a timely convergence on the target region but must not exceed any system velocity constraints.

Figure 6.4 is a limit cycle error trajectory. At the point a the system is at the target state but has a small drift velocity. The normalized error grows as the system drifts away from the target state until it intersects the inner phase sphere (point b). A corrective velocity change is then implemented and the system re-enters the inner phase sphere at the point c. Actuator activity is then inhibited and the system coasts until it encounters the perimeter at point d and another corrective velocity change is implemented.
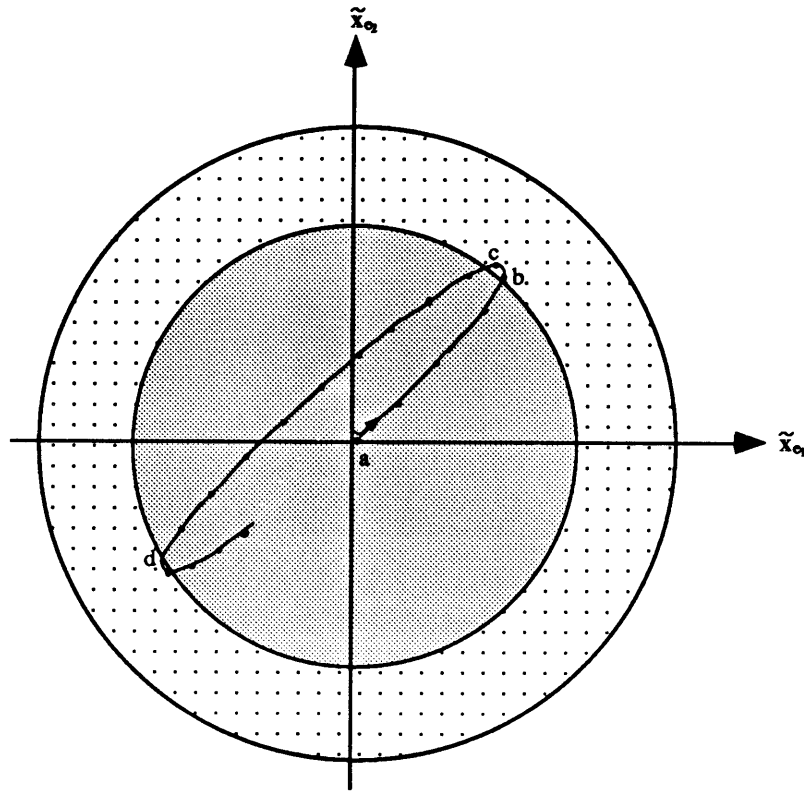
84

Figure 6.4
Two dimensional view of a limit cycle trajectory.

Each corrective velocity change adds the calculated velocity to be gained to the current system velocity.

$$\dot{x}^+ = \dot{x}^- + v_g^-$$

$$= \dot{x}^- + \left(-c\hat{i}_e^- + \dot{x}_d - \dot{x}^-\right) \tag{6-18}$$

$$= \dot{x}_d - c\hat{i}_e^-$$

The new velocity to be gained is then calculated as

$$v_g^+ = -c\hat{i}_e^+ + \dot{x}_d - \dot{x}^+$$

$$= -c\hat{i}_e^+ + \dot{x}_d - \left(\dot{x}_d - c\hat{i}_e^-\right) \tag{6-19}$$

$$= -c\left(\hat{i}_e^+ - \hat{i}_e^-\right)$$

Ideally the velocity imparted to the system is exactly the calculated v_g^- and the direction of the normalized error vector is not altered significantly during the burn. In that case the new

85

velocity to be gained is a very small vector. As the system coasts through the inner phase sphere the direction of the normalized error will change and the velocity of the system will be altered in response to system dynamics and external disturbances. The velocity to be gained gradually increases as the system travels away from the state corresponding to point *b*.

Figure 6.5 is a convergent normalized error trajectory. The system state is initially outside the acceptable state error range (point *a*). A velocity correction, or a series of velocity corrections, are implemented in order to provide and maintain the appropriate convergence velocity. The system state encounters the outer phase sphere at *b* and the convergence rate parameter is reduced to the limit cycle rate value. At the point *c* the velocity has been reduced to this smaller convergence rate and the limit cycle motion begins.
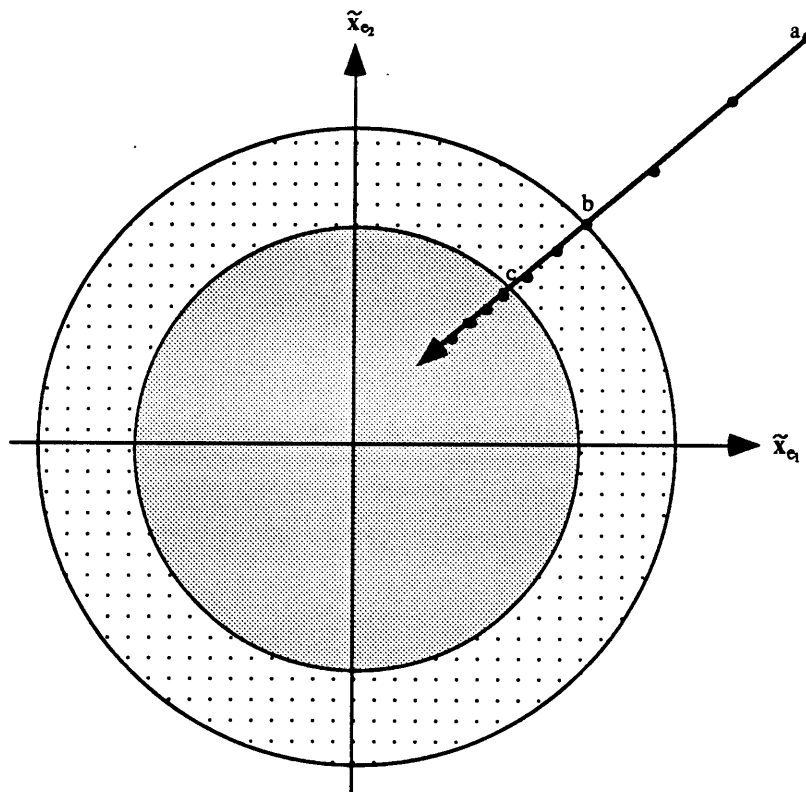

Figure 6.5
Two dimensional view of a convergent trajectory.

6.4 The Cooperative Control Phase Space Regulator

The application of interest in this thesis is the control of the motion of two space shuttles operating in close proximity. The linearized equations of motion of the vehicles are derived in chapters 2 and 3. The 9-dimensional state of the two vehicle system is specified by the current attitude of the master vehicle with respect to the M50 inertial coordinate frame (θ_A), the attitude of the slave vehicle with respect to the master vehicle (θ_R), and the position of the slave vehicle with respect to the master (r_R). The velocity of the system is the first derivative of the state, $(\omega_A, \omega_R, \dot{r}_R)$.

A cooperative maneuver is commanded by specifying a final command state, final command velocity, and a coast time of flight. The nominal trajectory generator provides a nominal trajectory consisting of an open loop set of jet of acceleration jet firings, nominal time histories of each state variable during the coast phase of the maneuver, and an open-loop set of deceleration jet firing commands. During the coast phase of this maneuver the system will be perturbed from this nominal trajectory as a result of the actual non-linear vehicle dynamics, environmental disturbances, and the granularity of the reaction control jets. The purpose of the cooperative control phase space regulator is to compensate for these effects and keep the two vehicle system tracking the nominal linear trajectory to within the specified tolerance by commanding corrective jet firings.

The phase space regulator for this 9-dimensional system is formulated as three separate 3-dimensional phase space algorithms; one for the absolute attitude channel, one for the relative attitude channel, and one for the relative position channel. Each 3-dimensional phase space is described by a set of three deadband values (db_i), a low and high convergence rate parameter (c_{12}, c_3), and an inner sphere radius (r_{P2}). The three phase space algorithms are operated in parallel, each generating a three dimensional velocity to be gained vector.

The velocity to be gained vector for each control channel is computed as described in the last section. The normalized error vector is calculated and its magnitude compared to the radii of the phase spheres in order to determine the value of the convergence rate. The convergent velocity is calculated as the product of this convergence rate and the negative of the normalized error unit vector. The velocity to be gained is the difference between the convergent velocity and the velocity error.

A corrective jet firing is executed whenever any of the three normalized error vectors

(1) traverses its inner phase sphere boundary from region I to region II of the normalized error space,

(2) traverses its outer phase sphere boundary from region II to region II of the normalized error space,

(3) lies in region II of its normalized error space and is increasing,

(4) lies in region III of its normalized error space and the corresponding 3-dimensional velocity error exceeds a specified threshold.

The third condition for initiating a feedback jet firing causes the state to converge more rapidly to the desired target rather than remain near the outer sphere boundary. This has the effect of lowering the value of the average error during a maneuver. The fourth condition for initiating a feedback jet firing is included to ensure a sufficiently rapid convergence of large state errors while keeping the number of jet firings reasonably small.

When at least one of the above conditions is met the three 3-dimensional velocity to be gained vectors are assembled as a single 9 dimensional velocity request and passed to the jet selection algorithm (Chapter 4). The jet selection algorithm determines the appropriate jets and corresponding firing times to impart the nine dimensional velocity change. Thus though the velocity requests are computed on a channel by channel basis all channels are compensated when one channel satisfies one of the three conditions above.

CHAPTER 7

PERFORMANCE VERIFICATION TESTS

The development and verification testing of the cooperative controller included both module level and system level testing. This section describes the test environment and presents a discussion of the system performance. Three test scenarios demonstrating the features, operation, and performance of the cooperative controller are examined in detail:

(1)   A long duration maneuver consisting of a commanded change in the attitude of the master vehicle with respect to the M50 frame, the attitude of the slave with respect to the master, and the position of the slave with respect to the master.

(2)   A short duration translation maneuver performed both with and without reaction control jet failures.

(3)   A V-bar docking approach using different jet cost coefficient values in the jet selection cost algorithm.

In each case the ability of the system to design a satisfactory maneuver, execute this planned trajectory within specified accuracy limits, and to hold the specified final state after the maneuver is complete is evaluated.

7.1 The Test Environment

The system level tests of the cooperative controller are conducted using the C.S. Draper Laboratory two vehicle simulator. This simulator is a derivative of the Draper Space Station simulator and has been adapted to run on an IBM PS2 Model 50 desk top computer. The simulator is coded in FORTRAN and is currently running under IBM DOS 3.3.

The simulator models the independent rigid body motion of two active spacecraft. Each spacecraft is modelled using an input deck containing the vehicle mass properties (I, r_{cm}, m) and the locations and thrust directions of the reaction control jets. Due to the relatively short duration of the maneuvers of interest in this thesis, the mass property values are modelled as constants. The rotational motion of each spacecraft is modelled using the non-linear Euler's Moment Equations. The translational motion of each spacecraft is

89

modelled using Kepler 's equation for the motion of two bodies using a spherical gravity field. The equations of motion are integrated using a Fourth Order Runge-Kutta method.

The simulator provides a sequencer to supervise the execution of the environment and flight control software. Data links from the flight control modules to the sensor and actuator modules are provided. In this thesis, no attempt to model sensor dynamics or other sensor noise sources has been made. All controller inputs are thus the *truth* values computed by the environment software.

Data recording is performed at approximately 1.04 hz. (every 0.96 seconds).

7.2 Long Maneuver Test

The cooperative controller employs the "two burn" trajectory solver (chapter 5) to generate a linearized trajectory which carries the two spacecraft from the initial state to the commanded final state. During long maneuvers small rate errors generate attitude and position errors large enough to require the cooperative controller to command midcourse correction maneuvers. A failure to perform appropriate midcourse corrections will allow the system state to diverge from the planned trajectory and will result in large final state errors. The accuracy of the implementation of the midcourse corrections is limited due to reaction control jet minimum impulse constraints and the granularity of the on/off switch times. As a result new small rate errors are introduced as the system compensates for current state errors. The cooperative control system should drive the two shuttle system to the commanded state using a reasonably small number of corrective jet firings. The purpose of the long duration maneuver test is to demonstrate the ability of the cooperative controller to plan and track a somewhat complex relative motion trajectory and then formationkeep at the final commanded state. For comparison purposes the maneuver is also implemented using two separate single vehicle maneuvers. The fuel efficiency of this cooperative maneuver is then compared to a similar maneuver implemented using two separate single vehicle maneuvers.

7.2.1 Cooperative Control During a Long Maneuver

In this test, the two space shuttles are travelling in a circular low earth orbit with zero relative translational and relative rotational velocity (figure 7.1). Both vehicles are initially aligned with their respective LVLH coordinate frames. The slave vehicle is positioned forward of the master vehicle. Neither spacecraft is rotating with respect to its LVLH coordinate frame: i.e. the inertial angular velocity vector of each vehicle is equal to

90

the angular velocity vector of the circular orbit. The quaternions describing the initial attitude of the master vehicle with respect to the M50 coordinate frame and the initial attitude of the slave vehicle with respect to the master vehicle are respectively

$$Q\_B\_M50 = [\ .452676 \quad .845757 \quad .280830 \quad -.030224 \ ]$$
$$Q\_V2\_B = [\ .9999998 \quad 0.0 \quad .00001157 \quad 0.0 \ ] \qquad (7\text{-}1)$$

The initial relative position of the two shuttles is

$$REL\_POS = [\ 507.6 \quad 0.0 \quad 0.0 \ ] \ \text{(ft)} \qquad (7\text{-}2)$$

The initial angular velocity of the master vehicle with respect to the M50 frame and the initial angular velocity of the slave with respect to the master are respectively

$$\omega\_V1 = [\quad 0.0 \quad -.001161 \quad 0.0 \ ] \ \text{(rad/sec)}$$

$$\omega\_V2\_V1 = [\ 0.0 \quad 0.0 \quad 0.0 \ ] \ \text{(rad/sec)} \qquad (7\text{-}3)$$

The initial relative translational velocity is

$$REL\_VEL = [\ 0.0 \quad 0.0 \quad 0.0 \ ] \ \text{(ft/sec)} \qquad (7\text{-}4)$$

The two vehicle system is commanded to a new state described by :

$$Q\_B\_M50 = [\ .0320071 \quad -.3752774 \quad -.5317485 \quad .7585419 \ ]$$

$$Q\_V2\_B = [\quad 0.0 \quad 0.0 \quad -1.00000 \quad 0.0 \ ]$$

$$REL\_POS = [\ 100.0 \quad 0.0 \quad 60.0 \ ] \ \text{(ft)}$$

$$\omega\_V1 = [\ 0.0 \quad 0.0 \quad 0.0 \ ] \ \text{(rad/sec)} \qquad (7\text{-}5)$$

$$\omega\_V2\_V1 = [\ 0.0 \quad 0.0 \quad 0.0 \ ] \ \text{(rad/sec)}$$

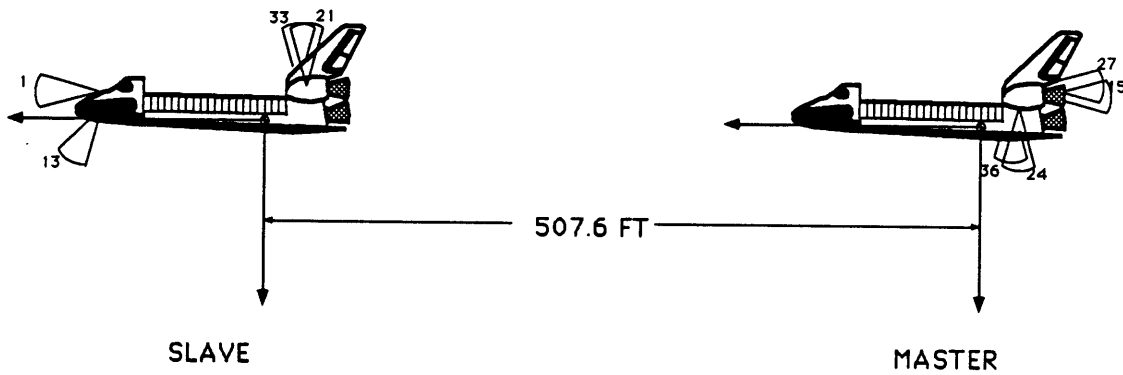$$REL\_VEL = [\ 0.0 \quad 0.0 \quad 0.0 \ ] \ \text{(ft/sec)}$$

Figure 7.1
The initial state of the two vehicle system
and the acceleration phase jet firings.

The commanded final attitude of the master vehicle has been specified such that at the end of the maneuver the vehicle will be in a $90°$ pitch down orientation with respect to the final LVLH coordinate frame. The slave vehicle is commanded to a final orientation pitched $180°$ with respect to the master vehicle. The relative position command places the center of mass of the slave shuttle 100 ft below and 60 ft ahead of the center of mass of the master shuttle, (figure 7.2). The commanded coast time for the maneuver is 500 seconds.
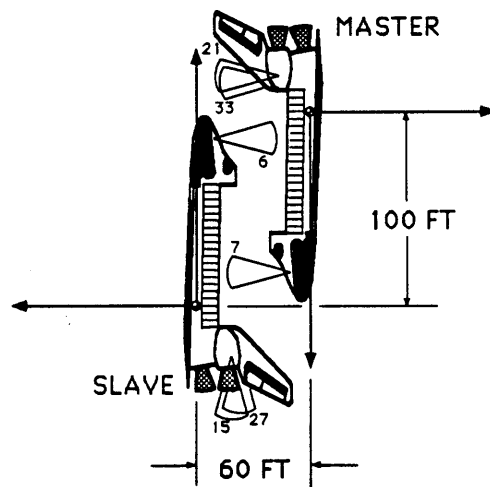

Figure 7.2
The final state for the two vehicle system
and the deceleration phase jet firings.

The commanded final translational velocity, angular velocity of the master with respect to the M50 inertial coordinate frame, and the angular velocity of the slave with respect to the master are all zero. Note that since the vehicles are originally aligned with the LVLH frames and thus rotating with respect to M50, the controller must perform the maneuver and dissipate the initial angular velocity of the two spacecraft.

In addition to initial state and commanded state values, the cooperative controller requires an array of nine deadband values (one per control variable), a value for the radius of the inner phase sphere and convergent rate for each of the three control channels, as well as cost coefficient values for the primary and vernier reaction control jets on each spacecraft. Table 7.1 and table 7.2 give the values of these parameters used in this test. These values have been selected as a nominal set and are not intended to represent an extreme controller configuration.

Table 7.1
Phase Space Regulator Parameters

Parameter	Master Attitude Phase Space	Rel Attitude Phase Space	Rel Position Phase Space
Inner PhaseSphere Radius	.85	.85	.85
Convergence rate (Reg 1&2)	.0005 (rad/sec)	.0005 (rad/sec)	0.05 (ft/sec)
Convergence rate (Reg 3)	.00284 (rad/sec)	.00284 (rad/sec)	0.10 (ft/sec)
deadband (x,y,z)	.05, .05, .05(rad)	.05, .05, .05(rad)	5.0, 5.0, 5.0(ft)

Table 7.2
Reaction Control Jet Cost Coefficients.

	RCS Cost Coefficient	
	Veh #1	Veh #2
Primary Jets	1.0	1.0
Vernier Jets	0.0287	0.0287

The cooperative controller computes and then implements a maneuver profile consisting of an acceleration phase, a coast phase, a deceleration phase, and a formationkeeping phase. Figure 7.1 shows the original configuration of the two shuttle system and indicates the jets fired during the acceleration phase. The jet numbers and

corresponding firing times for the acceleration burn are shown in table 7.3. Since the flight control software module is executed at 12.5 hz. the on/off status of a jet may only be changed every 0.08 seconds. The times given in table 7.3 are the actual implementation times; the commanded firing time rounded to the nearest 0.08 seconds. Note that jet number 29 on the slave vehicle was not actually fired since the commanded firing time was less than 0.04 seconds.

Table 7.3
Acceleration phase jet firings.

Master		Slave	
Jet #	Time	Jet #	Time
27	1.52	1	2.96
15	1.42	33	0.72
24	0.40	21	0.64
36	0.40	13	0.08
		29	0.00

Figure 7.2 shows the configuration of the two shuttles at the end of the maneuver and the jets fired to eliminate the residual coast velocities and bring the system to rest at the desired state. The corresponding jet numbers and firing times are in table 7.4. Note that three of the jets selected by simplex for this deceleration firing were assigned firing times less than 0.04 seconds and thus were not fired by the jet sequencer.

Table 7.4
Deceleration jet firings.

Master		Slave	
Jet #	Time	Jet #	Time
33	1.60	15	2.72
21	1.52	27	2.64
7	1.12	6	0.08
27	0.0	33	0.00
		11	0.00

The relative position trajectory in the x-z plane of the reference LVLH coordinate system centered on the master vehicle is shown in figure 7.3. The pitch profiles of the master vehicle with respect to the reference LVLH frame and the slave vehicle with respect to the master are shown in figures 7.4 and 7.5.
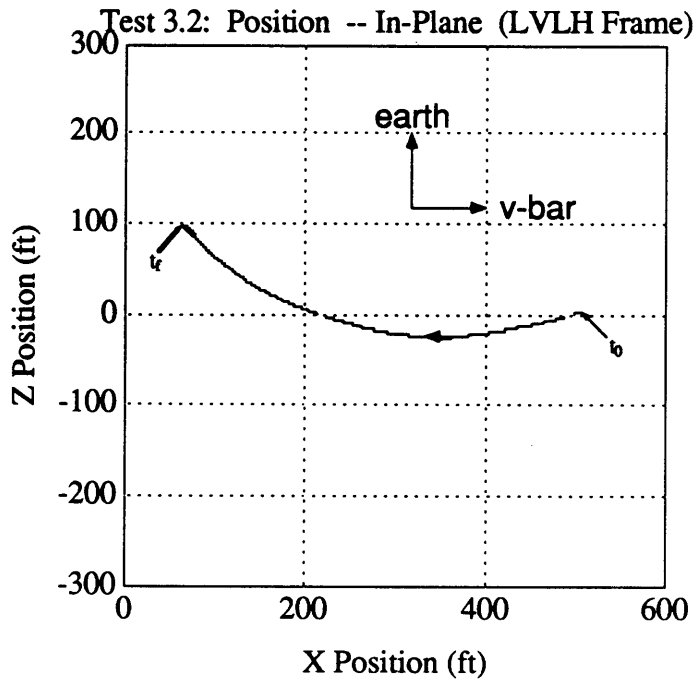
94

Test 3.2: Position -- In-Plane (LVLH Frame)

Figure 7.3
Relative Position Trajectory (LVLH)

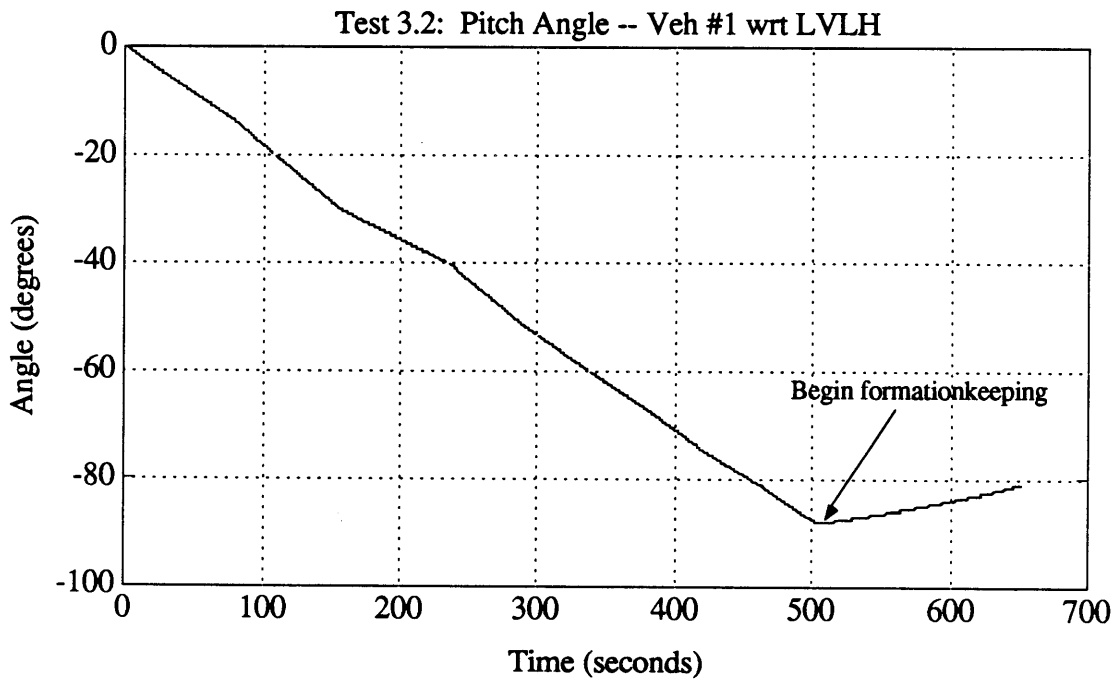Test 3.2: Pitch Angle -- Veh #1 wrt LVLH

Begin formationkeeping

Figure 7.4
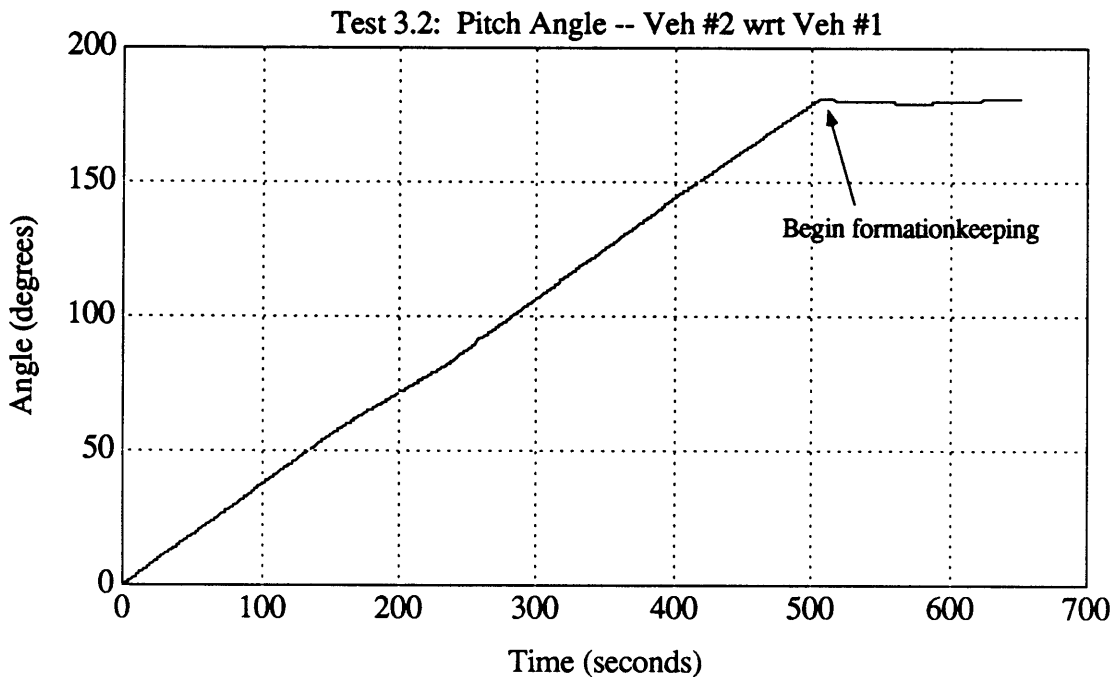Pitch Profile of Master Vehicle with respect to LVLH.

Figure 7.5
Pitch Profile of Slave Vehicle with respect to Master

During the 500 sec. coast phase of the maneuver the Phase Space Regulator (chapter 6) monitors the state and velocity errors, formulates a velocity to be gained request, and determines when corrective jet firings should be implemented. Eleven corrective actions were implemented during the coast phase of this maneuver. The average time between corrective actions was 45 sec.; the longest time between corrective actions was over 100 sec. Table 7.5 summarizes the jet firing activity during the coast phase of this test.

Table 7.5
Coast Phase Reaction Control Jet Activity.

	Master	Slave	Total
Primary	20 / 3.12	14 / 2.32	34 / 5.44
Vernier	5 / 1.76	0 / 0.00	5 / 1.76
Total	25 / 4.88	14 / 2.32	39 / 7.20

values are {# of firings } / { aggregate firing time}

The velocity to be gained request to be implemented during a corrective set of jet firings is often small, thus the simplex jet selection algorithm frequently assigns firing times which are below the minimum jet on time. As a result most of the corrective maneuvers are performed with fewer than nine reaction control jets and do not deliver the

96

precise velocity requested by the phase space controller. Small rate errors are responsible for the cycling of the state variable errors visible in figures 7.6 thru 7.8.
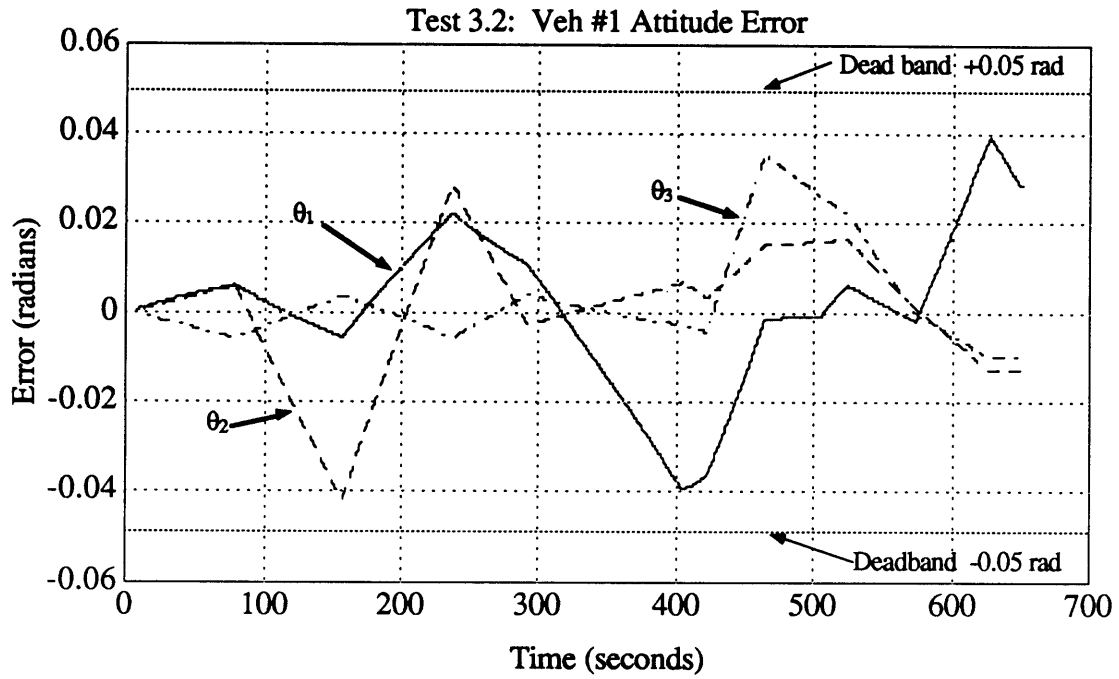
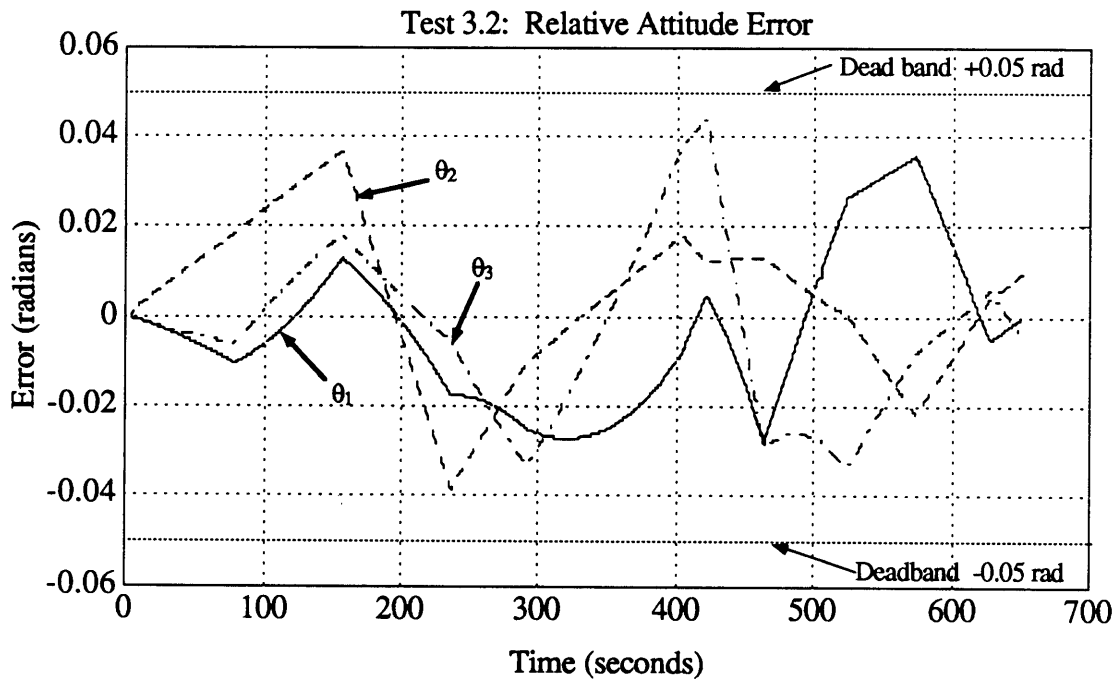

Figure 7.6
Attitude Error: Master Vehicle wrt M50

Figure 7.7
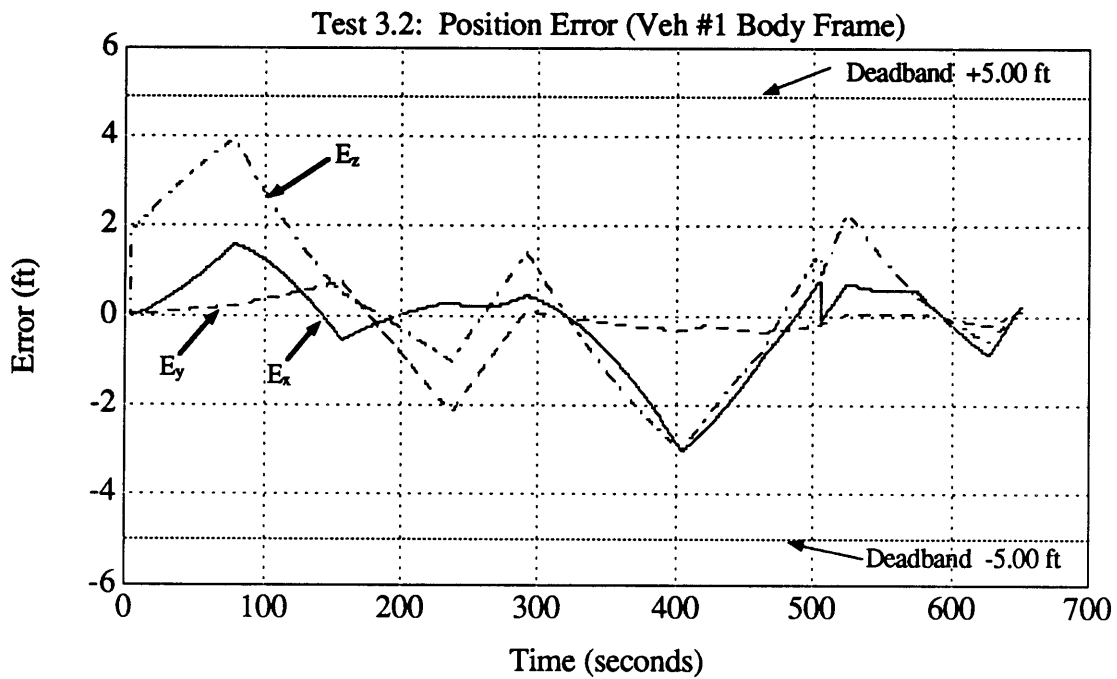Attitude Error: Slave Vehicle wrt Master

Figure 7.8
Relative Position Error.

During the formationkeeping phase of the maneuver (505.76 - 650.88 sec.) the phase space regulator is used to maintain the current state at the commanded state value. In this 145 sec. period the cooperative controller implements three corrective maneuvers. Table 7.6 summarizes this jet activity.

Table 7.6
Formationkeeping Reaction Control Jet Activity.

	Master	Slave	Total
Primary	11 / 1.44	7 / 0.66	18 / 2.10
Vernier	3 / 3.92	0 / 0.00	3 / 3.92
Total	14 / 5.36	7 / 0.66	21 / 6.02

values are {# of firings } / { aggregate firing time}

98

The cooperative controller maintained each of the control variable errors within its specified deadband throughout the 650 sec. test, (figure 7.6 - 7.8). As described in chapter 6, the phase space regulator initiates a corrective action whenever the normalized error state crosses the inner phase sphere. Figure 7.9 shows the magnitude of each of the normalized error vectors and indicates the cross over points corresponding to the initiation of corrective jet firings.
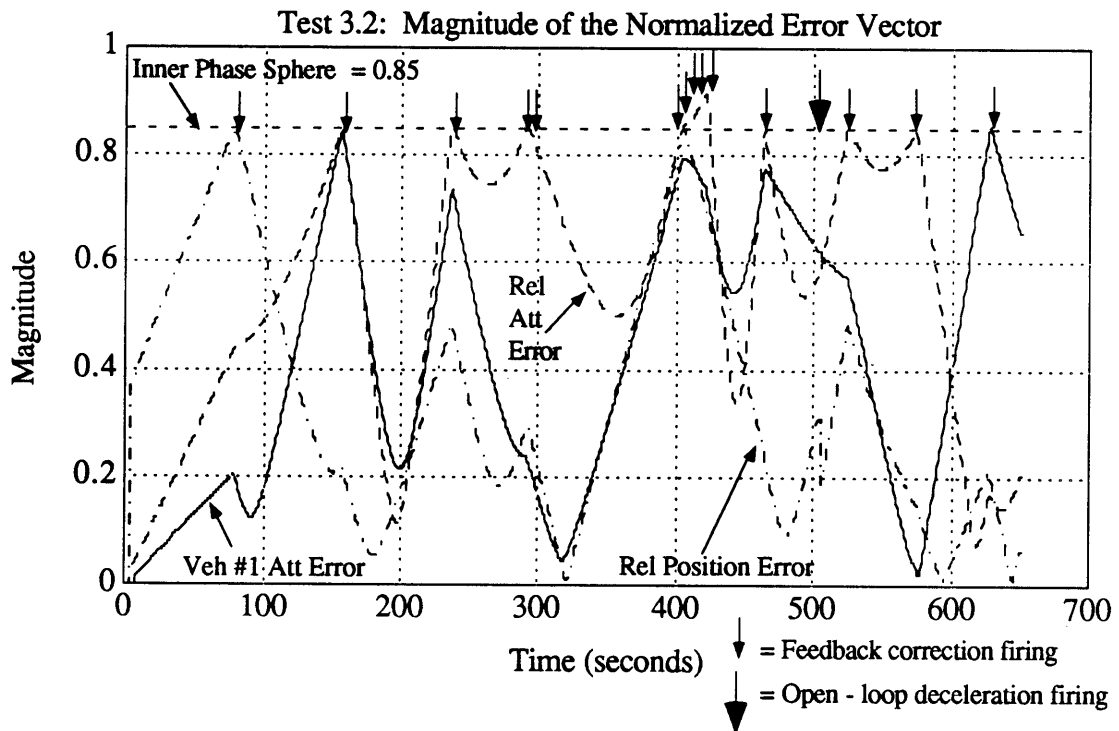

Figure 7.9
Magnitude of the Normalized Error Vector.

The state variable errors at the end of the coast phase, at the end of the deceleration maneuver, and at the end of the test are given in table 7.7. All compare favorably with the specified deadbands.

Table 7.7
State Variable Errors.

	@ end of coast phase	@ end of deceleration	@ end of test
V1_Att_Err (rad)	-.00072 .01589 .0264407	.0006689 .0160397 .0266003	.0282891 -.0127713 -.0099812
Rel_Att_Err (rad)	.0088385 .0040098 -.0272224	.0114901 .0033326 -.0277083	-.000264 .0094189 -.003866
Rel_Pos_Err (ft)	.7540 -.1973 1.3516	.0108 -.1362 1.0914	.2240 .1010 .2285

7.2.2 Non - Cooperative Maneuver

In this test the cooperative maneuver described in the last section is divided into two single vehicle maneuvers. The slave vehicle performs a +90 degree pitch maneuver and translates 407.6 ft. aft and 60 ft. down relative to an LVLH reference coordinate system centered on the location of the master vehicle. The master vehicle holds its position relative to the LVLH frame and performs a -90 degree pitch maneuver. Each vehicle plans its own trajectory and performs its maneuver without knowledge of the motion of the other vehicle. This test emulates a scenario where two separate autopilots agree to perform a pre-planned coordinated operation.

This test involved two computer runs: one for the slave vehicle motion and one for the master vehicle motion. The motion of each vehicle is controlled using the cooperative controller designed in this thesis with the jets on the other vehicle flagged as unavailable. The command input for the "ghost" vehicle state is set at its initial state so that its error state could not cause feedback initiated corrective maneuvers.

The final state command for each vehicle is selected so that the final state of the two vehicle system is identical to the final state command used in the cooperative control case. Table 7.8 shows the jet firings used by the two vehicles during the acceleration burns.

100

Table 7.8
Acceleration phase jet firings.

Master		Slave	
Jet #	Time	Jet #	Time
6	.24	1	6.0
24	.16	33	.72
1	.08	21	.56
36	.08	13	.32
		9	.24
		29	.08

Table 7.9 gives the deceleration burn activity for each vehicle.

Table 7.9
Deceleration jet firings.

Master		Slave	
Jet #	Time	Jet #	Time
9	.24	27	2.48
13	.24	15	2.40
21	.16	6	1.36
33	.16	33	1.28
1	.16	21	1.04

A comparison of these tables to the corresponding acceleration and deceleration tables in the last section show that the jets selected in each case are very similar. Table 7.10 summarizes the jet firing activity for both the cooperative control and the non-cooperative open-loop maneuvers. The cooperative and non-cooperative open-loop trajectories use the same amount of total fuel (18 sec) even though the fuel usage is different on each vehicle. In the non-cooperative case the slave spacecraft performs the entire translation whereas in the cooperative case each vehicle performed a portion of the translation. The rotational maneuver performed by each vehicle is the same in both the cooperative and non-cooperative tests.

Since the two spacecraft are identical and are aligned during the acceleration and deceleration burns, the amount of fuel consumed performing the translation maneuver is expected to be insensitive to to variations in the percentage of the translation performed by each vehicle. If the two spacecraft are not aligned during the acceleration and deceleration burns, have different mass properties, different actuator characteristics, or are otherwise

not equally efficient in translation then the fuel usage in the cooperative and non-cooperative case would not be equal.

Table 7.10
Feed-Forward Jet Firing Activity Comparison.

		Master	Slave	Total
Cooperative Control	Accel	3.74	4.40	8.14
	Decel	4.42	5.44	9.86
	total	8.16	9.84	18.00
Non-Cooperative Control	Accel	0.56	7.92	8.48
	Decel	0.96	8.56	9.52
	total	1.52	16.48	18.00

(values are seconds of jet activity)

Table 7.11 compares the corrective jet firing activity for the two tests. In the non-cooperative case each vehicle attempts to independently compensate for the small rate errors which cause its state error to exceed the phase sphere threshold. In the cooperative control architecture each corrective maneuver is computed to compensate for error components in all 3 control channels. For example, using cooperative control the relative position error rate will be reversed when a corrective firing is initiated due to errors on either the absolute attitude or the relative attitude channels. In the non-cooperative control case jet firings on one vehicle do not effect the errors on the other vehicle. The cooperative control approach eliminates the duplication of effort inherent in the non-cooperative corrective jet firings. As a result the cooperative controller performed coast phase regulation of the state of the two vehicle system using 68 % less fuel and implementing 51% fewer jet firings than the non-cooperative approach.

Table 7.11
Corrective Jet firings.

	Master	Slave	Total
Cooperative Control	25 firings 4.88 sec	14 firings 2.32 sec	39 firings 7.20 sec
Non-Cooperative Control	31 firings 15.62 sec	49 firings 6.96 sec	80 firings 22.58 sec

7.3 Jet Failure Test

The purpose of the short maneuver test is to investigate the effects of jet failures on the performance of the cooperative controller during a simple translational maneuver. The test is executed under four different conditions:

(1)   All reaction control jets available on both the master and slave vehicle.

(2)   Forward jets on the slave vehicle unavailable. This situation could arise if there was a major failure in the forward RCS system or if firings of the forward jets were inhibited by the crew in order to prevent jet plume impingement on the master vehicle during a *nose first* close inspection or docking approach maneuver.

(3)   Forward jets on the slave vehicle *and* all the down (+Z in body frame) firing jets on the master vehicle are unavailable. In this scenario neither the master or slave vehicle is completely controllable in six degrees of freedom. This test investigates the ability of the cooperative controller to exploit the available control assets on both vehicles in order to control the state of the system.

(4)   Forward jets on the slave vehicle and all the primary jets of the master vehicle unavailable. The remaining jets on the master vehicle provide low authority attitude control only; they do not provide translational control. This scenario is designed to demonstrate the effect of unavailable jets on the performance of a single maneuvering vehicle during an approach to a vehicle which is only capable of performing attitude corrections.

Identical initial state and final commanded state values are used in the four test cases. In each test case the two space shuttles are initially travelling in low earth orbit as shown in figure 7.10(a). The master vehicle is in a circular orbit and is aligned with the LVLH coordinate frame. The slave vehicle is orbiting above the master and is pitched -90° with respect to the master vehicle. Neither vehicle is rotating with respect to the LVLH frame.
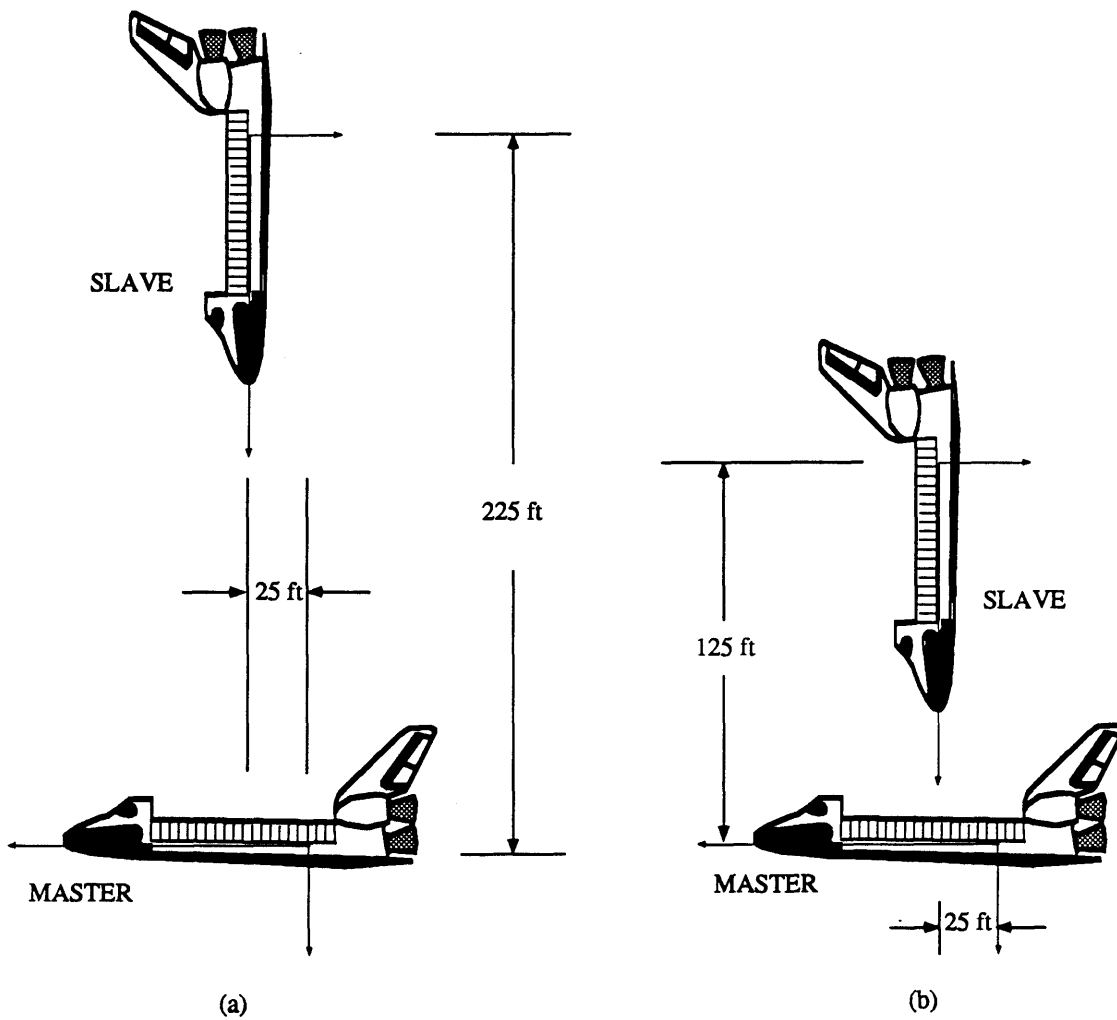
103

Figure 7.10
Initial state (a) and final state (b) of the two vehicle system.

The attitude quaternions, position vector, angular and linear velocity vectors describing the initial state of the system are given as:

$$Q\_B\_M50 = [\ .452676 \quad .845757 \quad .280830 \quad -.030224\ ]$$

$$Q\_V2\_B = [\ .7071068 \quad 0.0 \quad .7071068 \quad 0.0\ ]$$

$$REL\_POS = [\ 25.0 \quad 0.0 \quad -225.0\ ]\ (ft)$$

$$\omega\_V1 = [\ 0.0 \quad -.001161 \quad 0.0\ ]\ (rad/sec) \qquad (7\text{-}6)$$

$$\omega\_V2\_V1 = [\ 0.0 \quad 0.0 \quad 0.0\ ]\ (rad/sec)$$

$$REL\_VEL = [\ 0.0 \quad 0.0 \quad 0.0\ ]\ (ft/sec)$$

The desired maneuver for this test is a relative translation of -100 ft. in the direction of the master vehicle Z body axis. The coast time for the maneuver is set at 90 sec. The relative position in the x and y directions as well as the relative attitude are commanded to remain constant. The attitude of the master vehicle is command to be aligned with the reference LVLH frame at the end of the coast period. The slave vehicle therefore remains in a -90 pitch attitude with respect to the master vehicle and the LVLH frame. The values describing the commanded final state for this test are

$$Q\_B\_M50 = [\quad .4365087 \quad\quad .8428057 \quad\quad .3053541 \quad\quad -.07679619 \ ]$$

$$Q\_V2\_B = [\ .7071068 \quad\quad 0.0 \quad\quad .7071068 \quad\quad 0.0 \quad]$$

$$REL\_POS = [\quad 25.0 \quad\quad 0.0 \quad\quad -125.0 \ ] \ (ft)$$

$$\omega\_V1 \quad = [\ 0.0 \quad 0.0 \quad 0.0 \ ] \ (rad/sec) \qquad\qquad (7\text{-}7)$$

$$\omega\_V2\_V1 = [\ 0.0 \quad 0.0 \quad 0.0 \ ] \ (rad/sec)$$

$$REL\_VEL = [\ 0.0 \quad 0.0 \quad 0.0 \ ] \ (ft/sec)$$

The phase space parameters used in this test are the same as those used in the long duration maneuver described in the last section. The values of the inner phase sphere radii, the convergence rates, and the deadband values are given in table 7.1 and 7.2. The following sections present the results from each test cases.

7.3.1 All Jets Available

The "all jets available" test case provides a performance benchmark against which the cases using a partially depleted set of reaction control jets may be compared. In this run the full set of 38 primary jets and 6 vernier jets are "available" on each vehicle for a total of 88 jets. As outlined in chapter 4, the jets on each vehicle are considered as clusters of similar jets for the purpose of jet selection. A representative jet from each of the 20 clusters on each vehicle (40 jets total) is used as an input to the simplex jet selection algorithm.

In this test the cooperative controller computes and then implements a maneuver trajectory which satisfied the initial and final states specified above. Figure 7.11 shows the original configuration of the two spacecraft and indicates the jets fired during the acceleration phase of the "all jets available" maneuver. The corresponding firing times are given in table 7.12.
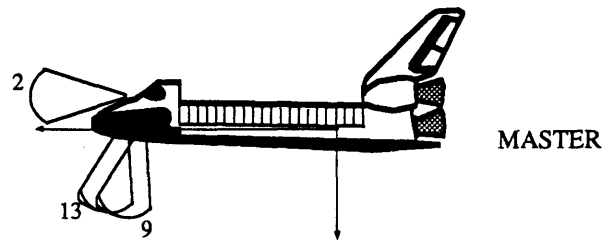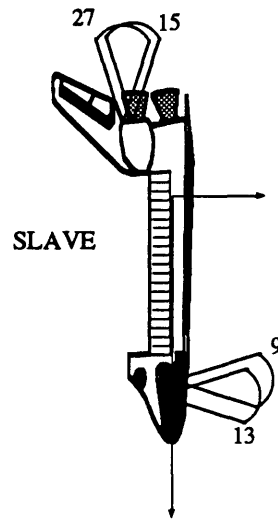
Figure 7.11
Acceleration jet firings. (All jets available)

Table 7.12
Acceleration jet firings   (All jets available)

Master		Slave	
Jet #	Time	Jet #	Time
2	2.00	27	3.92
9	0.16	15	3.84
13	0.16	9	0.16
29	0.0	13	0.16
43	0.0		

Figure 7.12 shows the vehicles at the command state and indicates the jets fired during the deceleration phase of the maneuver. The corresponding firing times are provided in table 7.13
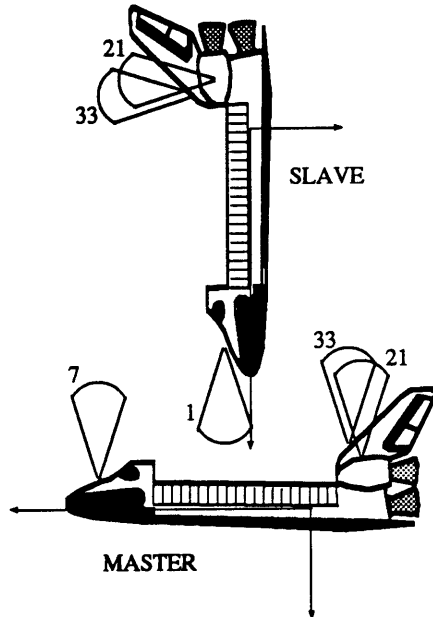

Figure 7.12
Deceleration jet firings. (All jets available)

Table 7.13
Deceleration jet firings (All jets available)

Master		Slave	
Jet #	Time	Jet #	Time
21	1.12	1	3.84
33	1.12	33	0.64
7	1.04	21	0.56
17	0.0	11	0.08
		29	0.0

Note the extensive use of jet #1 on the slave shuttle during the deceleration firings. Though at the time of the deceleration firings the mass centers of the vehicles are separated by 125 ft in the master vehicle z-body axis direction, this jet is located approximately 67 ft

forward of the center of mass of the slave vehicle. The hot gas plume from this jet is impinging upon all equipment in the open payload bay of the master vehicle. From an operational standpoint this is undesirable and should be avoided.

The simple relative position trajectory of the spacecraft is shown in figure 7.13 in the x-z plane of the reference LVLH coordinate frame centered on the master vehicle. Since the commanded final attitude of the master vehicle is specified with respect to M50 and the relative position of the slave vehicle is specified in the master vehicle coordinate system, the relative position vector appears to rotate in the LVLH frame during the formationkeeping phase of the test.
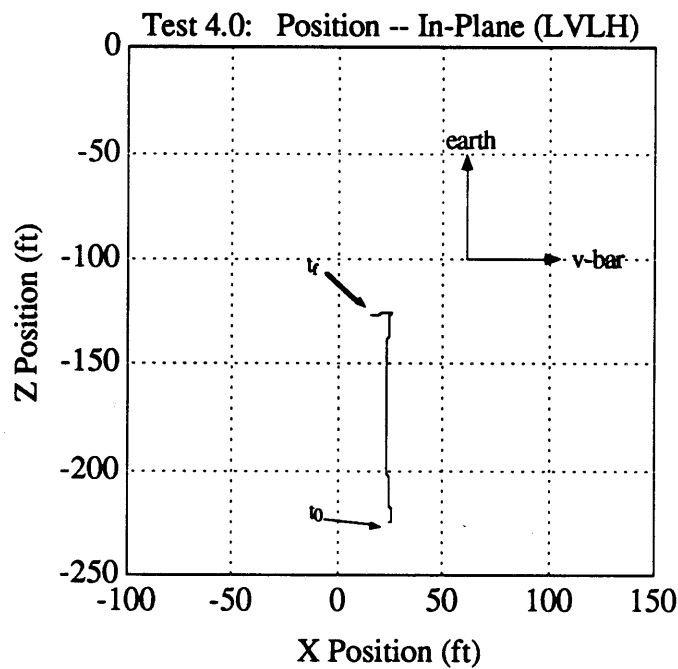

Figure 7.13
Relative Position Trajectory (LVLH)

During the 90 second coast phase and the 83 second formationkeeping phase of the maneuver the phase space regulator monitors the state and velocity errors, computes the velocity to be gained request, and initiates corrective jet firings when these errors approach the specified thresholds. Figure 7.14 shows the magnitude of the normalized error vectors for this test case. The errors remained small during the coast phase of the maneuver and no corrective burns were required. However, as a consequence of the granularity of the individual reaction control jet firing times during the implementation of the deceleration

108

burn, slightly larger relative angular velocity errors are induced and the relative attitude error eventually exceeds the inner phase sphere threshold at 125.44 seconds. Table 7.14 shows the actual firing times for this corrective maneuver.
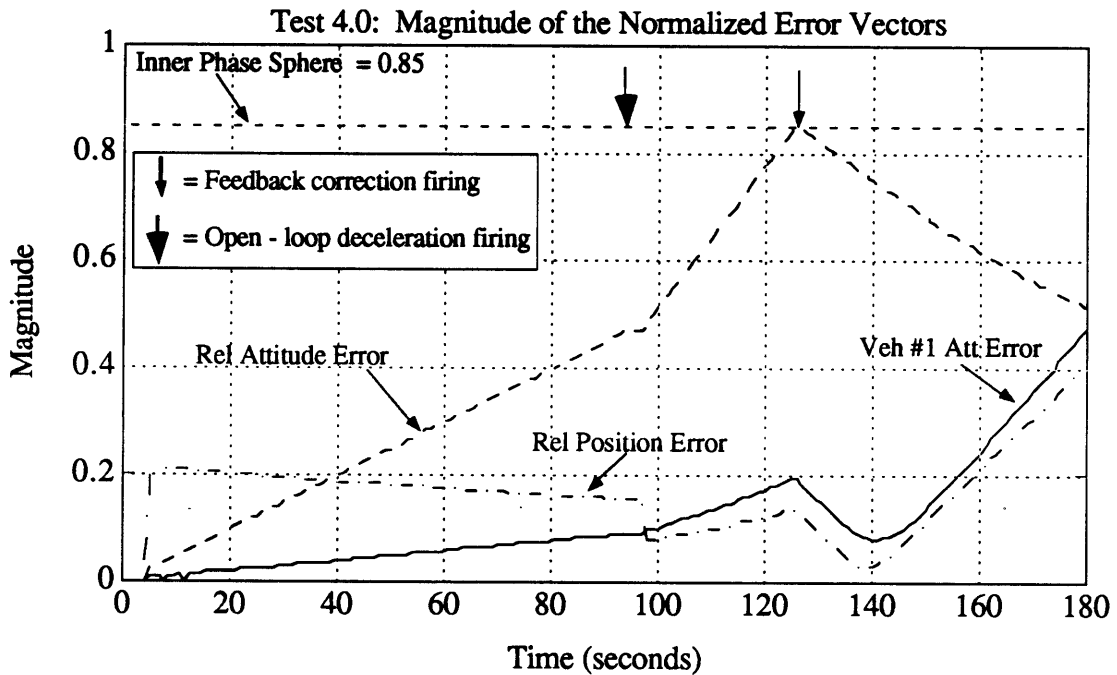

Figure 7.14
Magnitude of the Normalized Error vectors.

Table 7.14
Corrective Jet Firings, initiated @ 125.44 sec.

Master		Slave	
Jet #	Time	Jet #	Time
2	0.24	15	0.08
9	0.08	24	0.08
17	0.08	36	0.08

The final state errors at the end of the coast phase, the end of the deceleration burn, and the end of the test are in table 7.15. Figures 7.15 - 7.17 are respectively the time

histories of the master vehicle attitude error, the relative attitude error, and the relative position error. In all cases the errors are within the specified deadband tolerances.

Table 7.15
State Variable Errors.

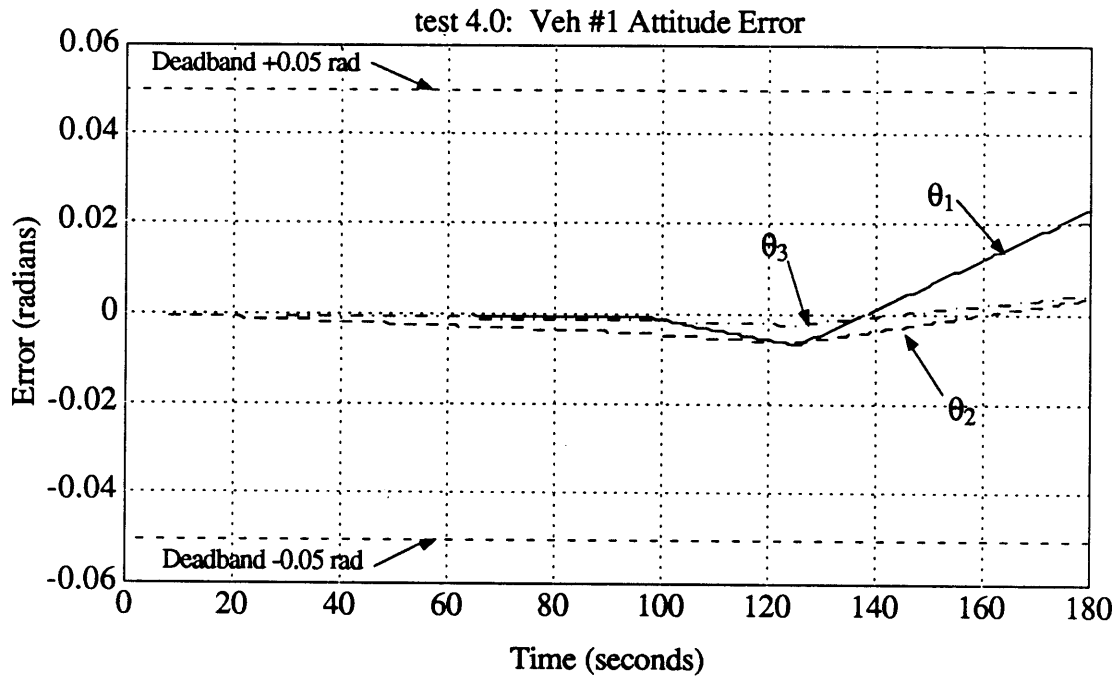|	@ end of coast phase	@ end of deceleration	@ end of test
V1_Att_Err (rad)	-.000737 -.004279 -.001572	-.001014 -.004587 -.001657	.023130 .003542 .004288
Rel_Att_Err (rad)	.003114 .022364 .006493	.0037338 .0231894 .006673	-.003068 .024800 .005888
Rel_Pos_Err (ft)	.7447 .0353 -.1943	-.3771 .0396 -.0740	1.9310 -.6427 -.1709

Figure 7.15
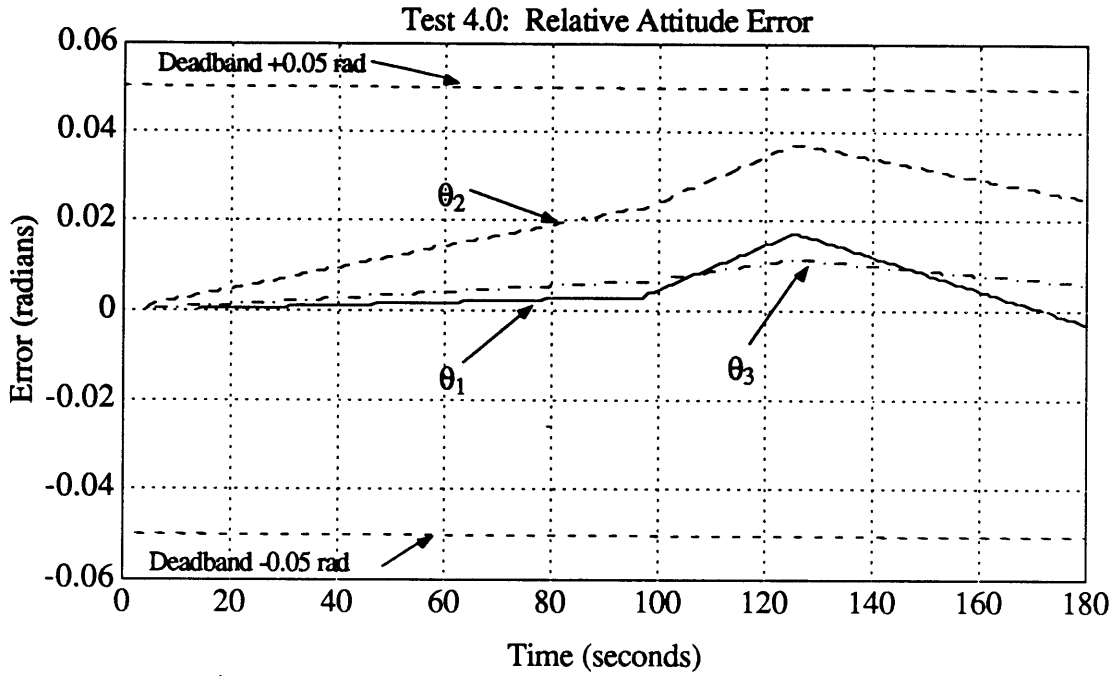Attitude Error: Master Vehicle wrt M50. (All jets available)

110

Test 4.0: Relative Attitude Error

Figure 7.16
Attitude Error: Slave Vehicle wrt Master (All jets available)

test 4.0: Relative Position Error (Veh #1 Body Frame)
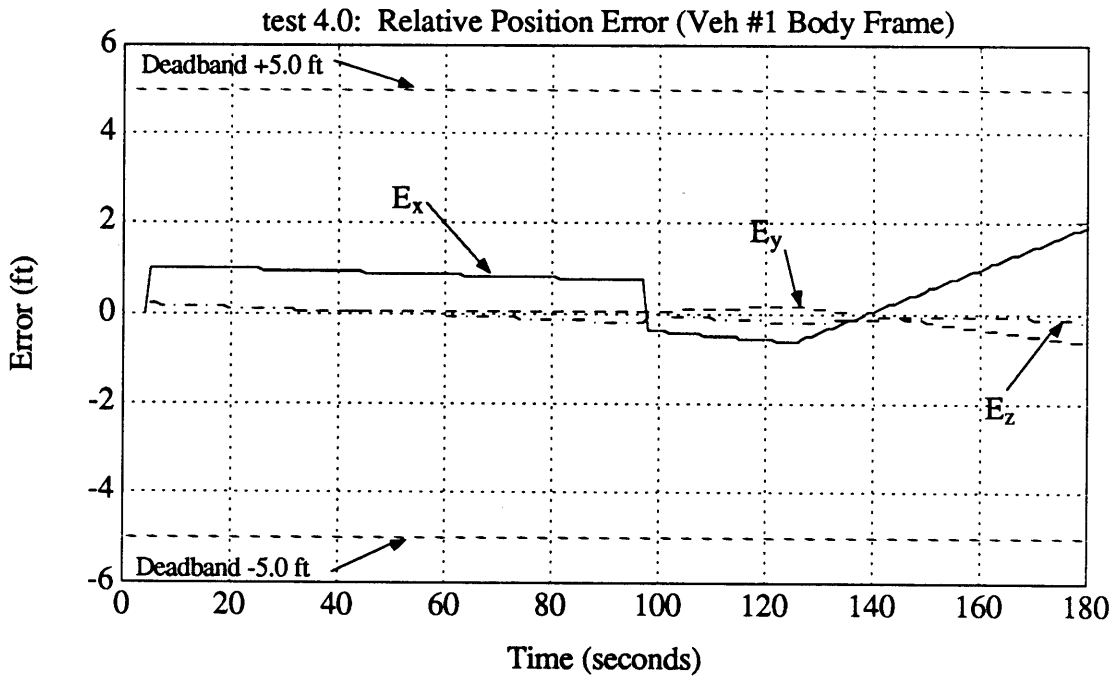

Figure 7.17
Relative Position Error. (All jets available)

7.3.2 Slave Shuttle's Forward Jets Unavailable

The system is commanded to perform the z axis transition described by the initial and final states given in equations 7-6 and 7-7 above. In this case however, primary jets #1 thru #14 and vernier jets #39 and #40 on the slave shuttle are flagged as unavailable. This set comprises the entire suite of reaction control jets forward of the center of mass of the slave shuttle and effectively removes 8 of the 40 cluster representatives nominally available to the two spacecraft simplex jet selection algorithm. Since these jets are unavailable, the simplex jet selection algorithm cannot employ them as part of acceleration, deceleration or any of the feedback initiated corrective jet firings.

The cooperative controller computes an open-loop trajectory consisting of an acceleration phase, a coast phase, and a deceleration phase. Figure 7.18 shows the initial configuration of the two spacecraft and indicates the acceleration jets fired to begin the maneuver. Note that slave vehicle jets #9 and #13 (forward-down-left and forward-down-right) are not selected as in the "all jets available" case; slave aft jets #21 and #31 are fired instead. Table 7.16 gives the complete set of jet firings and the corresponding firing times for the acceleration phase of the maneuver.

Table 7.16
Acceleration jet firings.

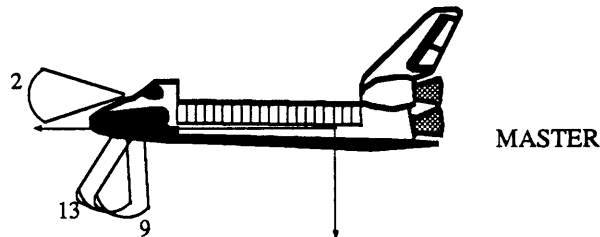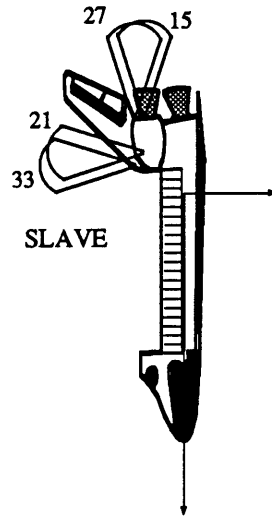| Master		Slave	
Jet #	Time	Jet #	Time
2	2.64	27	4.00
9	0.24	15	3.92
13	0.24	33	0.24
43	0.08	21	0.16
		17	0.0

112

Figure 7.18
Acceleration jet firings. (Slave forward jets unavailable)

The deceleration burn is executed as the vehicle reaches the commanded state. Figure 7.19 shows the jets fired and table 7.17 contains the corresponding jet firing times for the deceleration phase of the maneuver. Note the absence of slave vehicle jet #1 from the firing pattern and the significant increase in the firing times of the upwardly firing jets (#7,21, 33) on the master vehicle. The cooperative control trajectory planner has computed a new accelerate, coast, decelerate trajectory which can be flown using only the available reaction control jets. The resulting relative position trajectory of the two spacecraft in the x-z plane of the reference LVLH coordinate frame centered on the master vehicle is shown in figure 7.20.
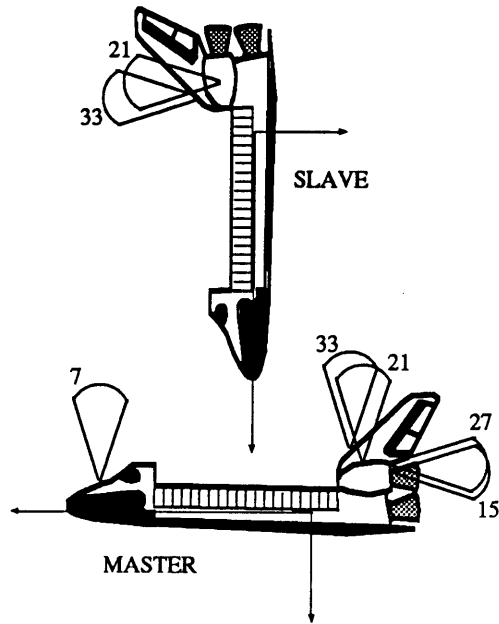
113

Figure 7.19
Deceleration jet firings. (Slave forward jets unavailable)

Table 7.17
Deceleration jet firings.

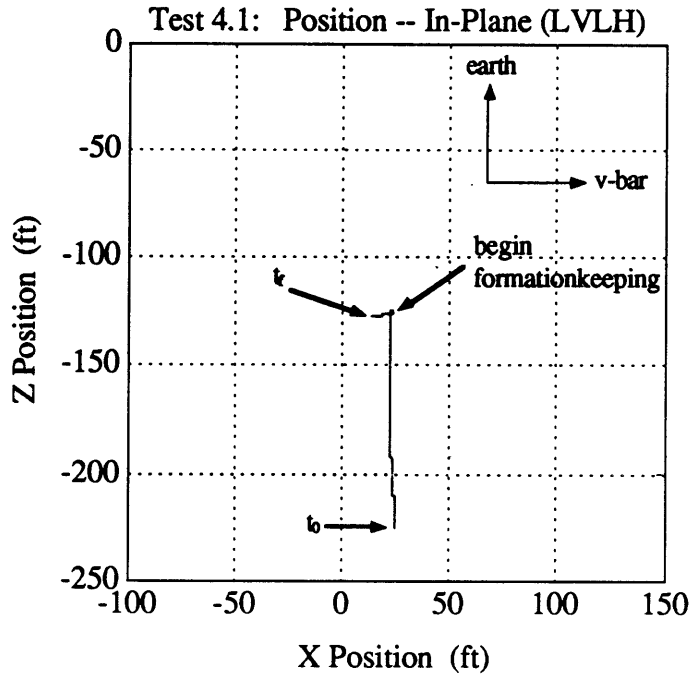| Master		Slave	
Jet #	Time	Jet #	Time
33	2.40	21	0.16
21	2.32	33	0.16
7	2.24	29	0.0
15	0.80		
27	0.80		
4	0.0		

Test 4.1: Position -- In-Plane (LVLH)

Figure 7.20
Relative Position Trajectory (Slave forward jets unavailable, LVLH frame).

The performance of the system during the coast maneuver is only slightly degraded by the unavailability of the slave shuttle's forward RCS jets. Figures 7.21 - 7.23 show the errors in the master vehicle attitude with respect to M50, the relative attitude errors, and the relative position errors. In this test case slightly larger rate errors are induced by the granularity of the jet firings than in the "all jets available" case. Consequently the relative attitude error exceeds its inner phase sphere threshold at 52.56 seconds and the master vehicle attitude error exceeds its inner sphere threshold at 120.56 seconds.
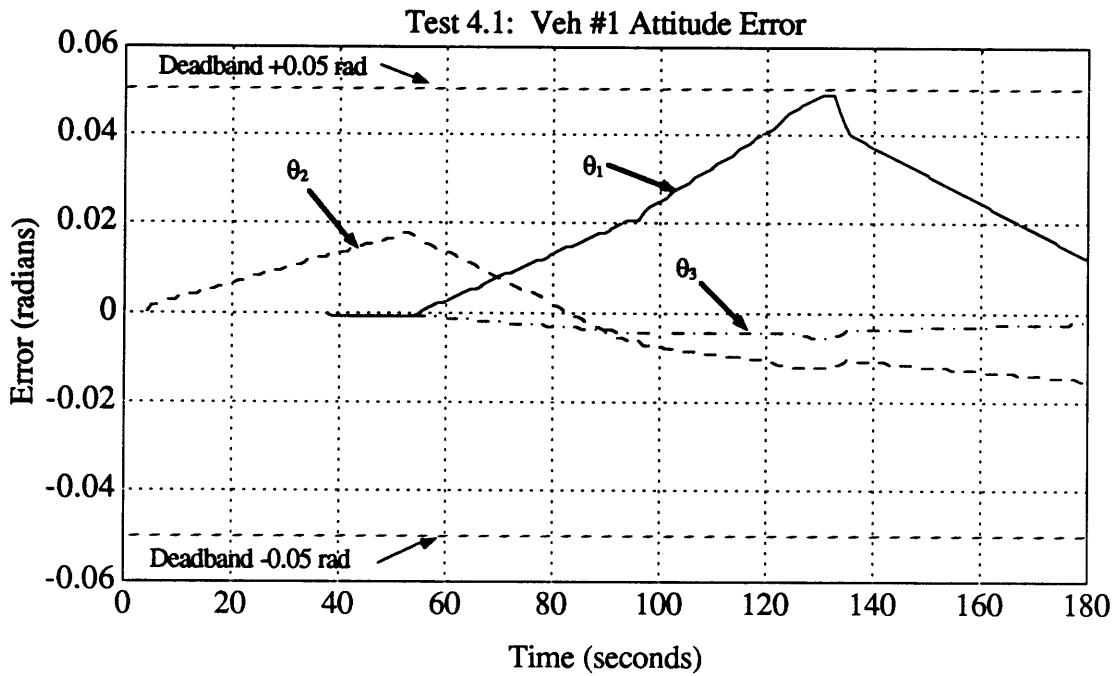
Figure 7.21
Attitude Error: Master Vehicle wrt M50. (Slave forward jets unavailable)
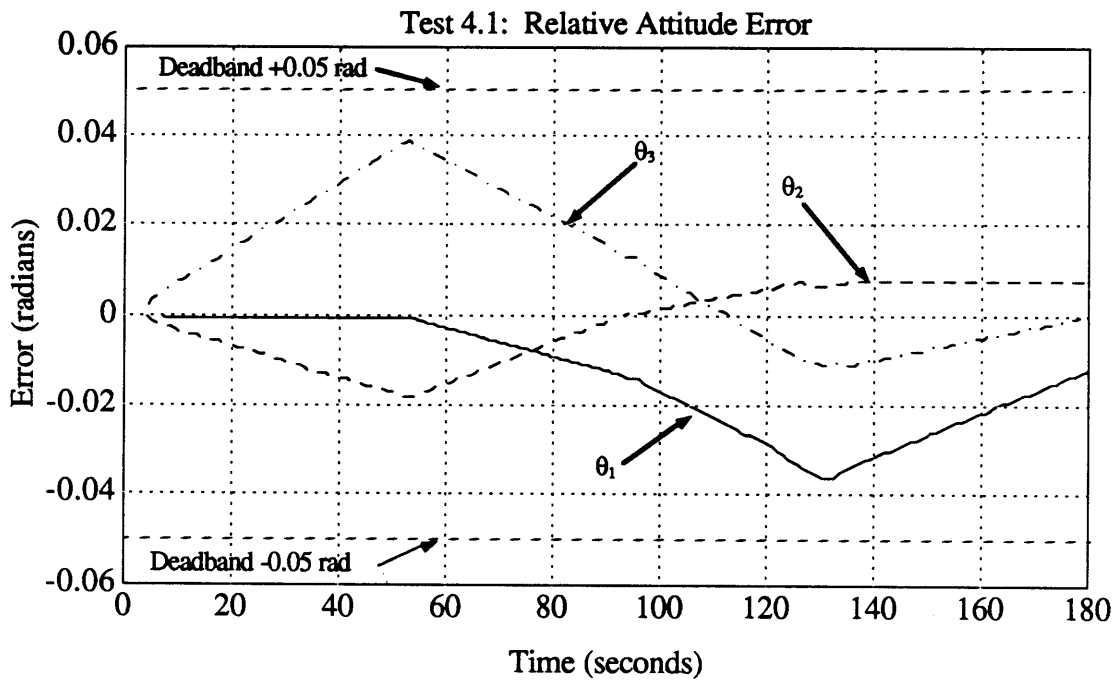

Figure 7.22
Attitude Error: Slave Vehicle wrt Master (Slave forward jets unavailable)
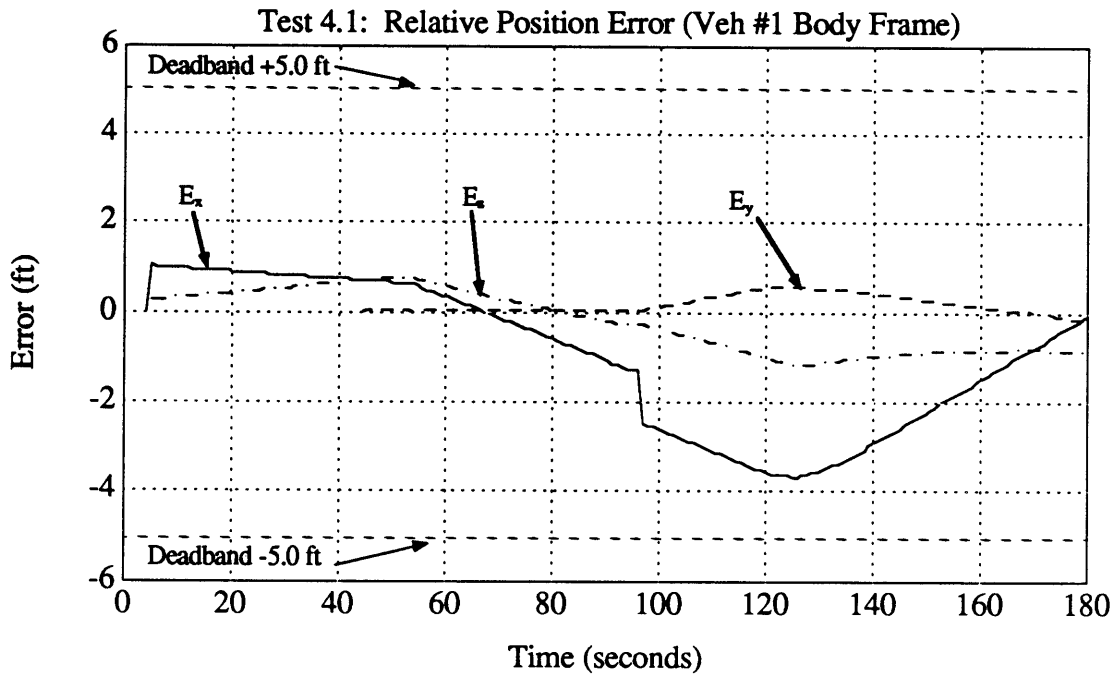
116

Test 4.1: Relative Position Error (Veh #1 Body Frame)

Figure 7.23
Relative Position Error. (Slave forward jets unavailable)

Note that the rate of change of the normalized magnitude of the master vehicle attitude error is not rapidly reversed as the normalized error exceeds the inner phase sphere at 120.56 sec (figure 7.24). During this corrective maneuver, simplex assigned long firing times to a pair of the low acceleration vernier jets instead of selecting the higher acceleration primaries and the correspondingly shorter firing times. The simplex cost of each jet firing is directly proportional to the firing time of the jet and includes no additional penalty for undesirably long firing times. Thus the optimal choice is dependent on the direction of the 9-dimensional velocity to be gained vector and the cost per second of each of the available jets. In this case the velocity to be gained vector is more closely aligned along the direction of the activity vectors of master vehicle verniers #39 and #44 than any primary jet.

To implement an excessively long set of jet firing commands, the cooperative controller scales each firing time such that the longest corresponds to a value of 4.96 seconds. In this manner the direction of the velocity change is preserved though its magnitude is diminished. At the end of the 4.96 sec firing a new velocity correction is computed and immediately implemented. Using this method a long corrective maneuver is implemented in a piecewise optimal sense.
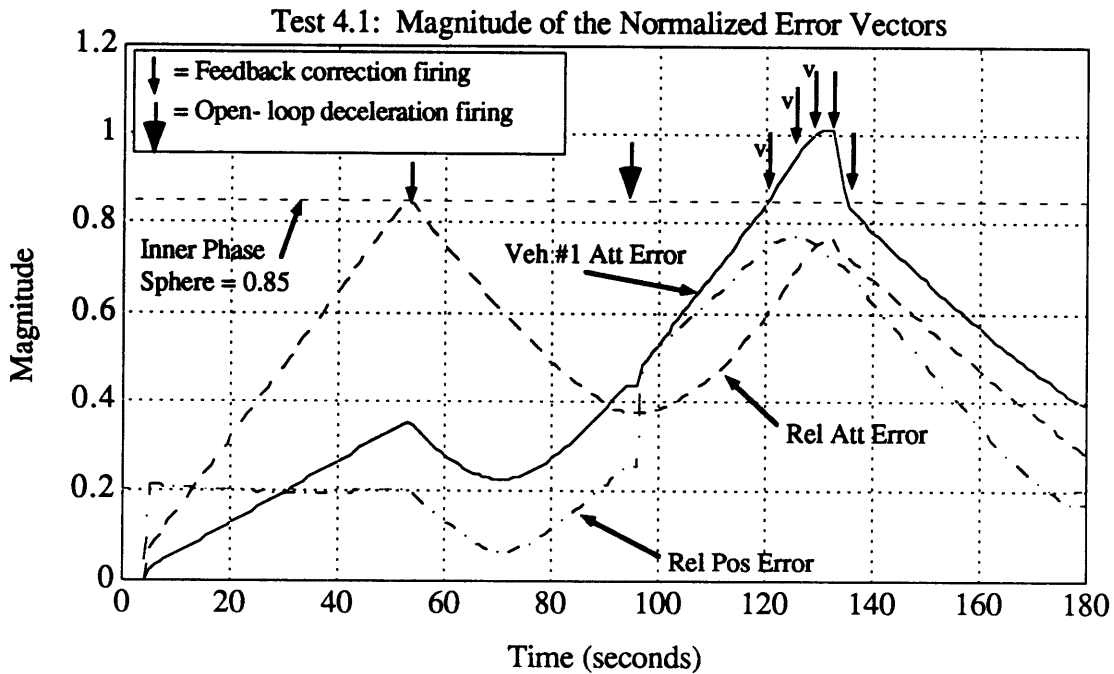
Figure 7.24
Magnitude of the Normalized Error Vector. (Slave forward jets unavailable)

Figure 7.24 shows that during the corrective maneuver (120.56 - 132.08 sec) the rate of change of the normalized master vehicle attitude error is decreased. However due to the duration of the maneuver the error has drifted beyond the unit phase sphere threshold. When the next segment of the corrective maneuver is computed at 132.24 sec the larger "region #3" value of the convergence rate (c) is used in the velocity to be gained calculation (equation 6-12). In order to deliver the new larger velocity change simplex selects a set of primary jets and the errors on all three phase space channels are rapidly decreased.

Since the slave shuttle reaction control jets have no effect on the absolute attitude of the master shuttle with respect to M50, the unavailability of the forward slave vehicle jets did not interfere with a rapid reversal of the master vehicle attitude rate error. This behavior was a consequence of the relative weight assigned to the primary and vernier jets in the simplex cost function. The determination of a method of blending vernier and primary jet commands while satisfying maximum firing time constraints is an area of possible future study.

118

Table 7.18 summarizes the feedback initiated jet activity during the coast and formationkeeping phases of this test.

Table 7.18
Feedback initiated jet firings. (Slave forward jets unavailable)

	Master	Slave	Total
Primary	22 / 3.12	12 / 2.56	34 / 5.68
Vernier	7 / 17.04	0 / 0.00	7 / 17.04
Total	29 / 20.16	12 / 2.56	41 / 22.72

values are {# of firings } / { aggregate firing time}

7.3.3 Slave's Forward Jets & Master's +Z Jets Unavailable

In this test the system is commanded to perform the z axis translation described by the initial and final states given in equations 7-6 and 7-7 above. In addition to the slave vehicle forward jets disallowed during the last test (#1 thru #14, #39, #40), all the down firing (+z) jets on the master shuttle are flagged unavailable (9,10,13,14,24,25,26, 36,37,38, and verniers 39,40,42,44). Specifically, jets used in the last test and their obvious replacements are now unavailable; this test stresses the ability of the system to accommodate jet failures. In this configuration neither of the individual shuttles is completely controllable in 6 degrees of freedom, and therefore neither is capable of performing a single pursuit vehicle approach to the other.

The cooperative controller computes an open-loop trajectory consisting of an acceleration phase, a coast phase, and a deceleration phase. Figure 7.25 shows initial configuration of the two spacecraft and indicates the acceleration jets fired to begin the maneuver. Note that since the +z jets on the master vehicle are unavailable, the cooperative controller uses jets #21 and #33 to provide the required + pitch impulse. Table 7.19 gives the complete set of jet firings and the corresponding firing times for the acceleration phase of the maneuver.
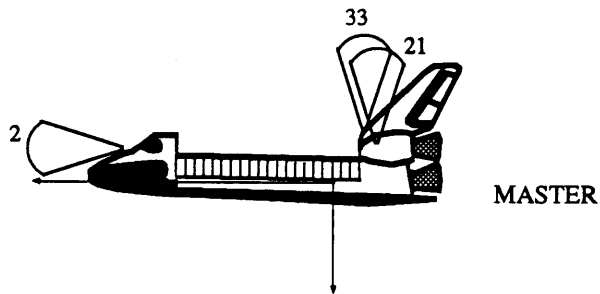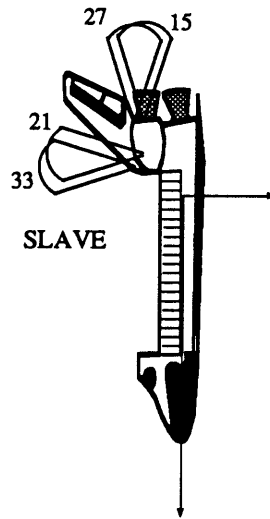
Figure 7.25
Acceleration jet firings. (Slave forward and master +Z jets unavailable)

Table 7.19
Acceleration jet firings.

Master		Slave	
Jet #	Time	Jet #	Time
2	2.88	27	4.48
33	0.32	15	4.40
21	0.32	21	.24
43	0.08	33	.24
4	0.0		

The deceleration burn is executed as the vehicle reaches the commanded state. Figure 7.26 shows the jets fired and table 7.20 contains the corresponding jet firing times for the deceleration phase of the maneuver. Similar to the last test, the impulse provided by the #1 jet on the slave vehicle in the "all jets available case" has been replaced by a significant increase in the firing times of the up firing jets (#7,21, 33) on the master vehicle. The resulting relative position trajectory of the two spacecraft in the x-z plane of the reference LVLH coordinate frame centered on the master vehicle is shown in figure 7.27.
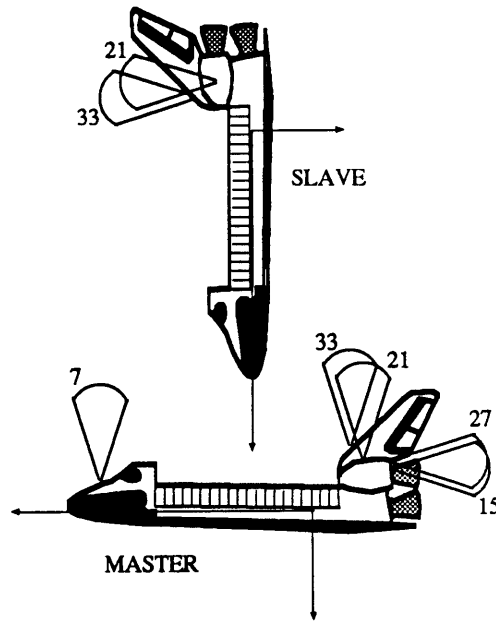

Figure 7.26
Deceleration jet firings. (Slave forward and master +Z jets unavailable)

Table 7.20
Deceleration jet firings.

Master		Slave	
Jet #	Time	Jet #	Time
33	2.40	21	0.16
7	2.32	33	0.16
21	2.32	29	0.00
27	0.80		
15	0.72		

Test 4.4: Position -- In-Plane (LVLH)

(plot)

earth

v-bar

begin
formationkeeping

t_f

t_0

Z Position (ft)
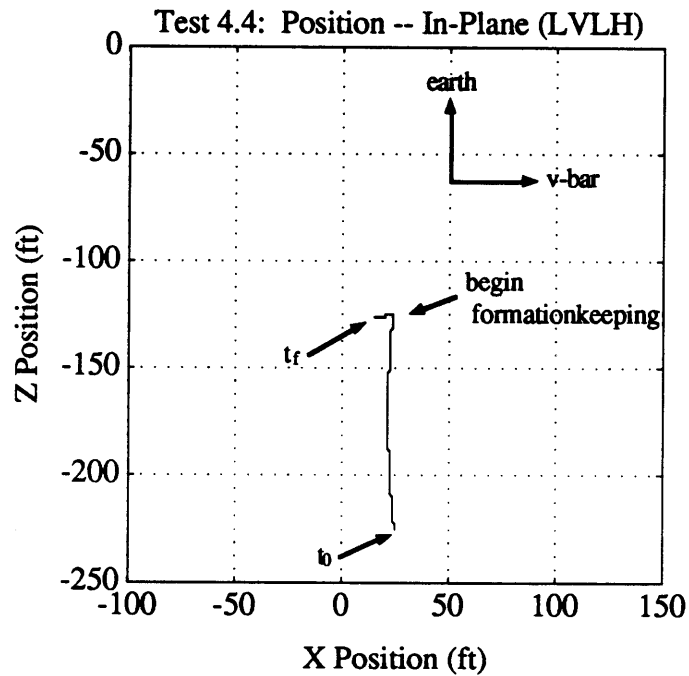
X Position (ft)

Figure 7.27
Relative Position Trajectory
(Slave forward and Master +Z jets unavailable, LVLH frame).

Though neither spacecraft is completely controllable in six degrees of freedom, their relative motion and the absolute attitude of the two vehicle system is controllable as a 9 degree of freedom system. The cooperative controller accurately controls the relative states of the two vehicles in a scenario where either vehicle acting as a single pursuit vehicle could not. Figure 7.28 - 7.30 show the errors in the master vehicle attitude with respect to M50, the relative attitude errors, and the relative position errors.

Figure 7.28
Attitude Error: Master Vehicle wrt M50.
(Slave forward and Master +Z jets unavailable)

Figure 7.29
Attitude Error: Slave Vehicle wrt Master
(Slave forward and Master +Z jets unavailable)
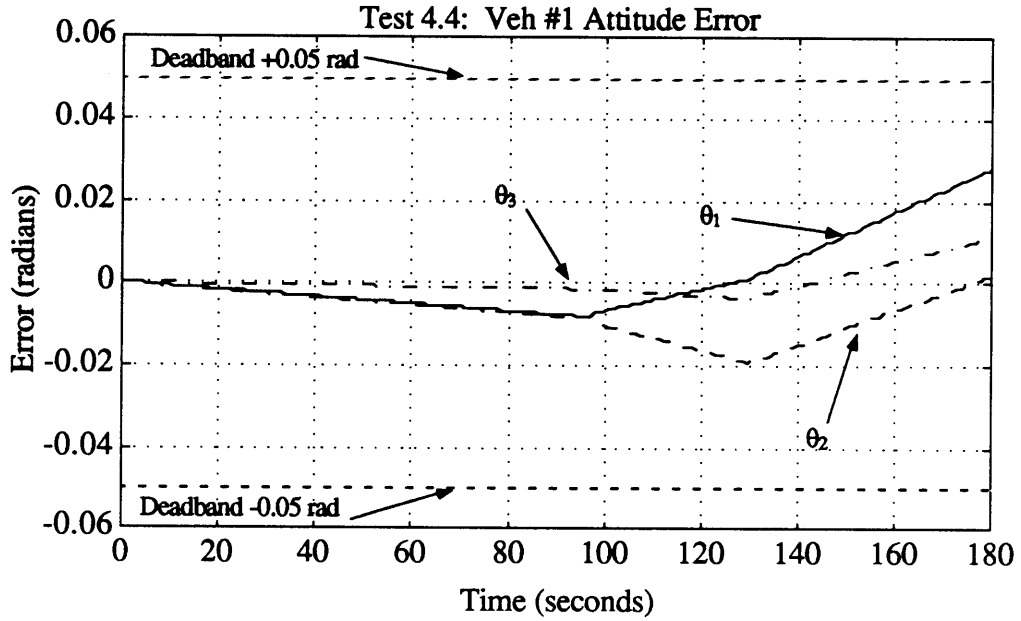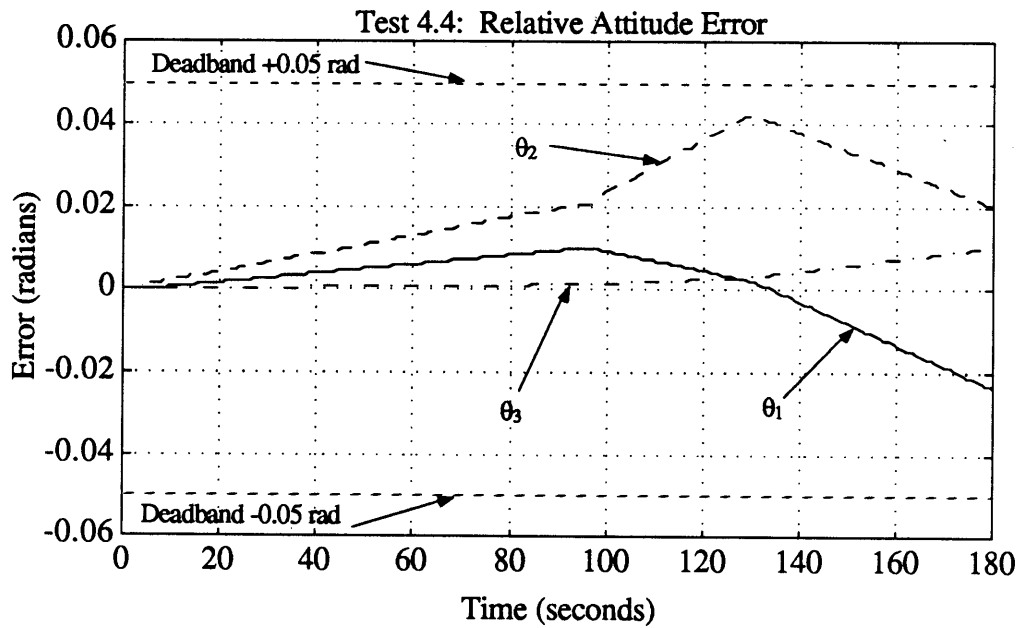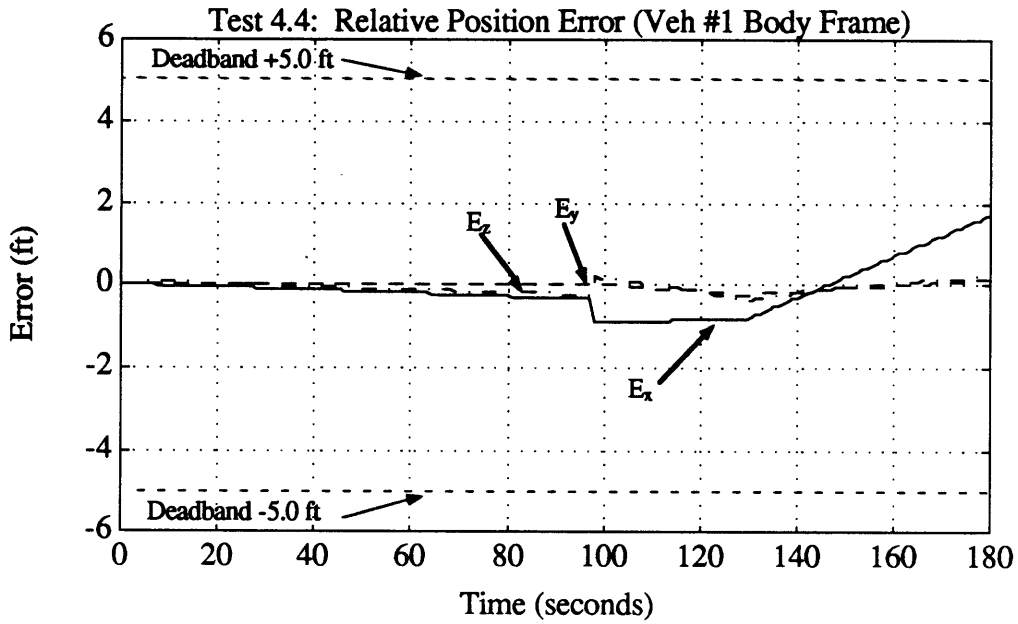
Figure 7.30
Relative Position Error.
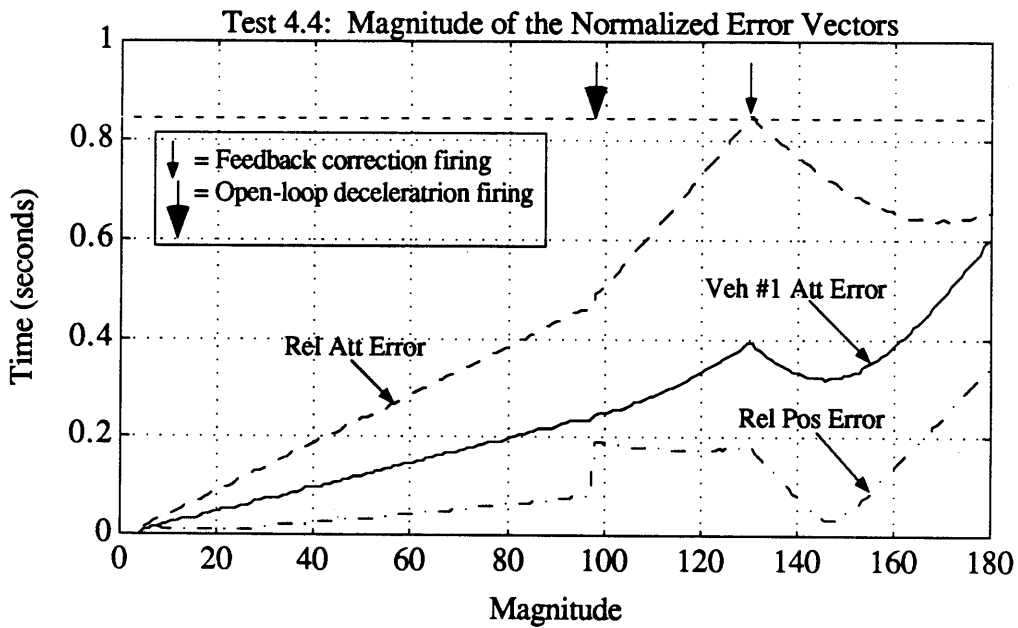(Slave forward and Master +Z jets unavailable)

Figure 7.31
Magnitude of the Normalized Error Vector.
(Slave forward and Master +Z jets unavailable)

124

The plot of the magnitude of the normalized error vectors in figure 7.31 shows that as in the other test cases the errors are well controlled and remain within the unit phase sphere. In this test a single corrective jet firing maneuver was required at t = 129.92 seconds during the formationkeeping phase of the test.

7.3.4 Slave's Forward Jets & Master's Primary Jets Unavailable

Traditional proximity operations are conducted using a single pursuit vehicle to approach or formationkeep with a passive target vehicle. The target vehicle may not actually be passive and may be capable of performing independent attitude control. This test case investigates the performance of this traditional approach during a period of degraded control authority of the pursuit vehicle.

Similar to the test case described in the last section, primary jets #1 thru #14 and vernier jets #39 and #40 on the slave shuttle are flagged as unavailable to simulate either a serious reaction control system failure or a desire to avoid forward jet plume impingement on the target (master) vehicle. In addition to these jets all the primary jets on the master vehicle (jets #1 thru #38) are also flagged as unavailable. The translational control authority provided to the master vehicle by the remaining low acceleration vernier jets is insignificant and the vehicle may be considered only capable of attitude control. Under these conditions the master vehicle provides an adequate approximation of a passive target vehicle.

The system is commanded to perform the z axis translation described by the initial state and commanded final state in equations 7-6 and 7-7 above. The cooperative controller parameters used in this test case are identical to those used in the previous two test cases and are given in table 7.1 and table 7.2.

The cooperative controller attempts to compute an open-loop trajectory consisting of an acceleration phase, a coast phase, and a deceleration phase which carries the system to the commanded final state. Due to the degraded control authority of the system, the simplex jet selection algorithm is unable to select a set of reaction control jets to satisfy the velocity change requirements. In both the "all jets available" and the "forward slave jets unavailable" test cases the acceleration maneuver utilized primary jet #2 on the master vehicle, (see tables 7.12 and 7.16). This jet provides an impulse in the -x direction without applying a torque to the slave spacecraft. In this test case all the primary jets on the master

vehicle are unavailable and no combination of the jets available on the slave spacecraft can provide an equivalent relative velocity impulse without also generating a significant relative rotational velocity impulse. In the terminology used in chapter 4, the set of jets available in this test fails to span the 9 dimensional velocity space and thus the system is not completely controllable.

7.3.5 Summary of Jet Failure Tests

In this section the robustness of the cooperative controller to reaction control jet unavailability was investigated. The four test cases conducted provided examples of varying degrees of degraded control authority of the two vehicle system.

In the first test case (all jets available) both the master and the slave vehicle are completely controllable. The cooperative controller performs the commanded maneuver using a total of 19.44 sec of jet on time; the smallest amount used in any of the four cases.

In the second case the slave vehicle is uncontrollable in 6 degrees of freedom. The cooperative controller is able to control the 9 dimensional state of the two vehicle system by exploiting the natural actuator redundancy provided by the reaction control jets available on the "healthy" master vehicle.

In the third test case neither the slave or the master spacecraft is completely controllable in six degrees of freedom. Even so, the cooperative controller is again able to coordinate reaction control jet firings on the two vehicles and control the system in the nine dimensional state space.

The fourth test case is the traditional pursuit vehicle control approach to proximity operations. Since the master vehicle is completely passive in translation, the controllability of the relative position of the two vehicles is entirely dependent on the controllability of the pursuit vehicle. Since the forward jets on the pursuit vehicle are unavailable, the pursuit vehicle is not completely controllable in translation and the maneuver cannot be accomplished.

The ability of the cooperative controller to maintain control of the system of two spacecraft when the single pursuit vehicle control system cannot control the relative states

126

of the vehicles is a principle benefit of the cooperative control approach to proximity operations.

7.4 V-Bar Approach Test

The purpose of this test is to demonstrate the ability of the cooperative controller to exploit the control assets available on both vehicles in order to perform fuel efficient maneuvers. The cooperative controller is exercised in several test cases using different jet costs and jet availability configurations. Performance comparisons are made based on the jets selected, the duration of the jet firings (fuel consumed) and the behavior of the two vehicles. A standard docking approach along the mean velocity vector of the target vehicle is commanded in each instance.

In the Clohessy - Wiltshire equations developed in chapter 3, (equation 3-43), when $z=0$, and $\dot{x}$, $\dot{z} = 0$ then $\ddot{x}$, $\ddot{z} = 0$. The x axis of the local LVLH coordinate system is a locus of equilibrium points which may be exploited during proximity operations. Since the direction of the x-axis corresponds to the direction of the orbital velocity vector of the reference circular orbit, this direction is referred to as V-BAR. Standard pursuit vehicle rendezvous operations often involve a v-bar approach.

In the v-bar approach test the master and the slave vehicle are travelling in the same circular orbit, (figure 7.32a). The slave vehicle is positioned 150 ft forward of the master vehicle. The master vehicle is pitched +90° with respect to its LVLH frame and the slave vehicle is aligned with the master. The complete description of the initial state of the two shuttle system is given by the absolute and relative attitude quaternions, the relative position vector (body frame), the absolute and relative angular velocity vectors, and the relative linear velocity vector.

$$Q\_B\_M50 = [\quad .518667 \quad .619413 \quad -.121514 \quad .576669 \quad]$$

$$Q\_V2\_B = [\quad 1.0 \quad 0.0 \quad 0.0 \quad 0.0 \quad]$$

$$REL\_POS = [\quad 0.0 \quad 0.0 \quad 150.0 \quad] \text{(ft)}$$

$$\omega\_V1 = [\quad 0.0 \quad 0.0 \quad 0.0 \quad] \text{(rad/sec)} \tag{7-8}$$

$$\omega\_V2\_V1 = [\quad 0.0 \quad 0.0 \quad 0.0 \quad] \text{(rad/sec)}$$

$$REL\_VEL = [\quad 0.0 \quad 0.0 \quad 0.0 \quad] \text{(ft/sec)}$$

(a)

(b)
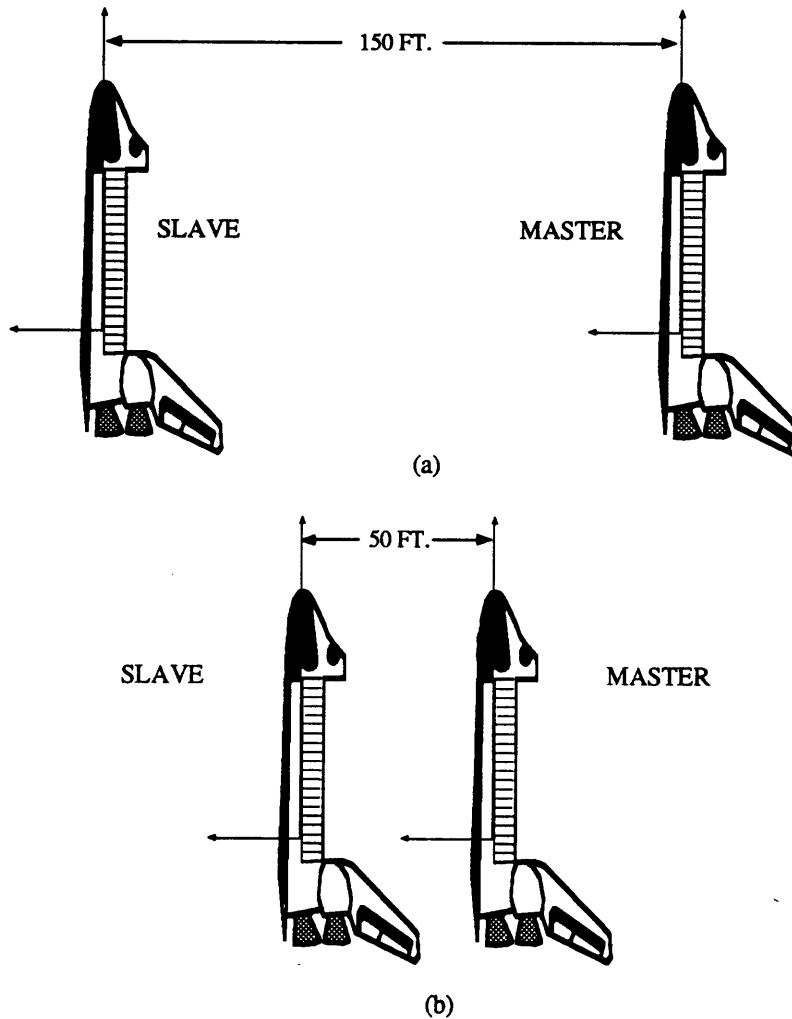
Figure 7.32
(a)The initial state of the two vehicle system
(b) The commanded final state of the two vehicle system.

The vehicles are commanded to decrease the distance between them to 50 ft while maintaining the attitude of the master vehicle with respect to the M50 frame and the attitude of the slave vehicle relative to the master vehicle constant, (figure 7.32b). The coast time for the maneuver is 100 seconds. The final state of the maneuver is given by

$$Q\_B\_M50 = [\ .518667 \quad .619413 \quad -.121514 \quad .576669\ ]$$

$$Q\_V2\_B = [\ 1.0 \quad 0.0 \quad 0.0 \quad 0.0\ ]$$

$$REL\_POS = [\ 0.0 \quad 0.0 \quad 50.0\ ] \text{(ft)}$$

$$\omega\_V1 = [\ 0.0 \quad 0.0 \quad 0.0\ ] \text{(rad/sec)} \tag{7-9}$$

$$\omega\_V2\_V1 = [\ 0.0 \quad 0.0 \quad 0.0\ ] \text{(rad/sec)}$$

$$REL\_VEL = [\ 0.0 \quad 0.0 \quad 0.0\ ] \text{(ft/sec)}$$

128

This test is executed four times using different actuator descriptions in order to demonstrate the ability of the cooperative controller to perform the maneuver using different subsets of the jets residing on the two vehicles. The differences in both fuel efficiency and the behavior of the system will be highlighted. The cases presented are:

(1) Master vehicle reaction control jets unavailable. All slave vehicle jets available.

(2) All reaction control jets available on the both vehicles.

(3) Master vehicle reaction control jets twice as fuel efficient as slave reaction control jets. All jets available.

(4) "Upward firing" (-z in body frame) reaction control jets on both the master and the slave vehicle are three time less fuel efficient than the other jets. All jets available.

These test cases are discussed individually in the following sections.

7.4.1 Master Vehicle Jets Unavailable

In this test case all of the reaction control jets on the master shuttle are flagged as unavailable and may not be fired by the cooperative controller. This test case reduces to the single vehicle pursuit solution to the proximity operations problem. The entire maneuver is performed by the slave vehicle. Figure 7.33 shows the initial state of the two shuttles and indicates the jets fired during the acceleration burn. Table 7.21 contains the actual firing times for each jet.

Figure 7.33
The initial state of the two vehicle system
Acceleration jet firings indicated.

Table 7.21
Acceleration phase jet firings.

Master		Slave	
Jet #	Time	Jet #	Time
-	0.0	24	3.44
		36	3.44
		13	1.76
		9	1.76
		1	1.52

The slave vehicle coasts toward the master at a velocity of approximately 1 ft/sec. After 100 sec the slave performs the deceleration set of jet firings in order to null the relative velocity and begin formationkeeping at the target 50 ft point. Figure 7.34 shows the jet firing pattern at the final state. Table 7.22 gives the actual firing times.
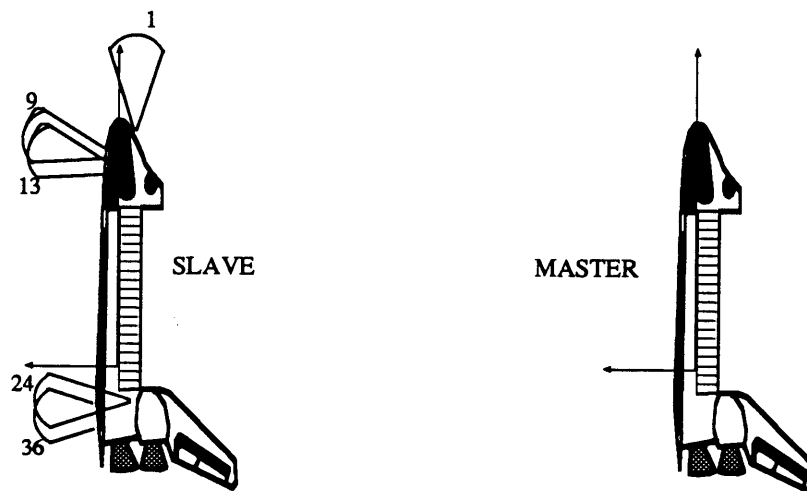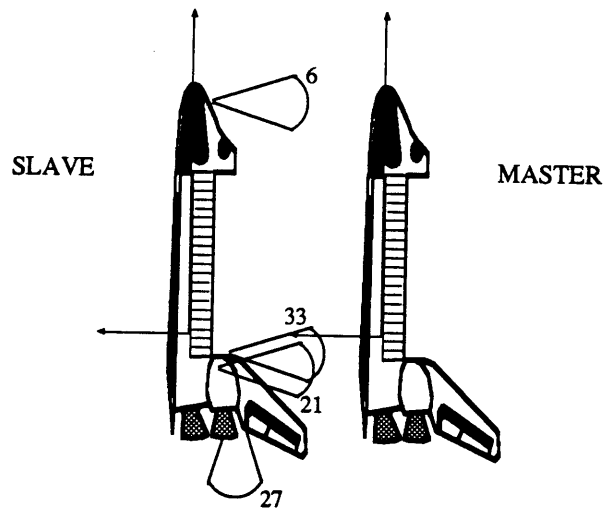

Figure 7.34
The final state of the two vehicle system
Deceleration jet firings indicated.

Table 7.22
Deceleration phase jet firings.

Master		Slave	
Jet #	Time	Jet #	Time
-	0.0	33	2.48
		6	2.40
		21	2.08
		27	0.08

Firing the up (-z) jets on the slave shuttle nulls its velocity in the LVLH frame and concludes the two burn maneuver. The slave then begins to formationkeep at the commanded final state. The master shuttle has not been perturbed from reference circular orbit and thus the two vehicle system is not translating with respect to the reference LVLH frame.

During this maneuver the phase space regulator commanded two corrective sets of jet firings, one at 16.80 sec (during coast) and one at 124.88 sec. (during formationkeeping). These two corrective maneuvers account for 12 jet firings and for a total of 3.84 seconds of firing time.

7.4.2 All Jets Available

In this test case all reaction control jets on both the master and the slave vehicles are available to the cooperative controller. The cooperative controller selects the most efficient combinations of jets based on the geometry of the activity vectors and the thrust level of each jet. In the jet select cost function the cost coefficient value used for all the primary jets is $c=1.0$, for all the vernier jets $c=0.0287$. Figure 7.35 show the acceleration jets fired in this test case. Table 7.23 shows the actual firing times used for each jet.

Table 7.23
Acceleration phase jet firings.

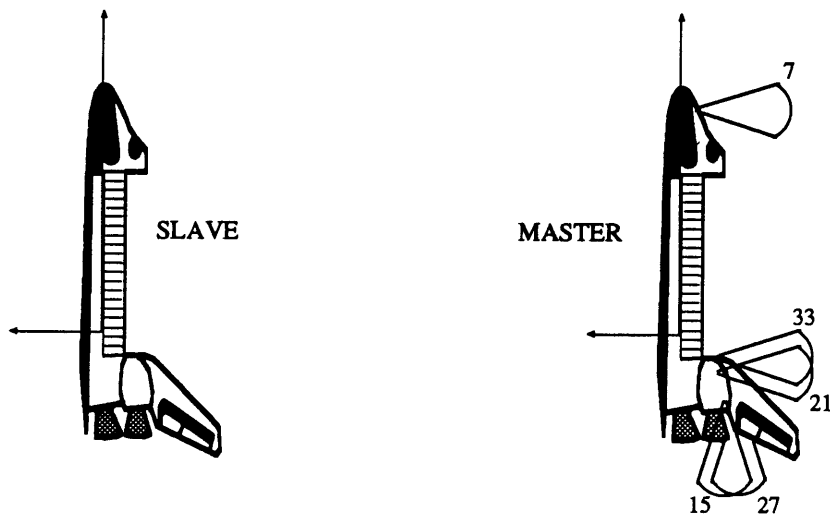| Master		Slave	
Jet #	Time	Jet #	Time
7	2.40	-	0.0
33	2.40		
21	2.24		
15	0.08		
27	0.08		

Figure 7.35
The initial state of the two vehicle system
Acceleration jet firings indicated.

From the firing pattern in figure 7.35 it is clear that the cooperative controller is performing a single vehicle approach by the master vehicle. This solution is primarily a result of an asymmetry in the reaction control jets on a shuttle spacecraft. Though each primary reaction control jet used on the shuttle is identical to all the other primaries, the effectiveness of each jet is altered by its placement on the vehicle. Specifically, on the space shuttle the aft downward firing (+z) jets impinge upon the shuttle itself. This impingement has the effect of decreasing the net thrust attained by firing the jet.

The cost coefficients for the aft +z jets are traditionally set to the same value as the other primary jets (see section 7.2.4 below) because they consume fuel at the same rate. Since the two vehicles in this test have been commanded to perform an approach maneuver, the cooperative controller must select the acceleration jets to be fired from either the set of down firing jets on the slave vehicle or the up (-z) firing jets on the master. Since the up jets do not impinge on the vehicle, and cost the same as the down jets, they are more efficient and are selected.

It must be emphasized that the shuttle reaction control jet model accounts for the forces and torques on a shuttle due to impingement *from its own jets*. It does not account for impingement effects due to jets from a neighboring vehicle.

132

The vehicles coast for 100 sec and then perform the open-loop deceleration firings. Figure 7.36 shows the firing pattern and table 7.24 contains the actual firing times.

Figure 7.36
The final state of the two vehicle system
Deceleration jet firings indicated.

Table 7.24
Deceleration phase jet firings.

Master		Slave	
Jet #	Time	Jet #	Time
-	0.0	33	2.48
		6	2.40
		21	2.08
		27	0.08

In the deceleration maneuver the relative efficiency of upward firing (-z) jets is again the dominant consideration in optimizing the fuel consumption of the two burn approach. In order to null the relative approach velocity the cooperative controller must select the deceleration jets from either the master vehicle -z jets or the slave vehicle +z jets.

Firing the less efficient master vehicle +z jets will cause the velocity of the master vehicle in the LVLH frame to decrease and the two vehicle system to formationkeep about a fixed point in the LVLH frame. The cooperative controller selects the more efficient solution, and fires a set of -z jets on the slave vehicle. As a result the slave vehicle accelerates to match the LVLH velocity of the master vehicle. The two vehicles attain the commanded final state and formationkeep about a point moving slightly faster than the reference circular orbit.

During this maneuver the phase space controller did not initiate any corrective jet firings.

7.4.3 Master Vehicle More Efficient Than Slave Vehicle

In this test case the cost coefficient for the jets on the master vehicle are set to values equal to half the values used for the jets on the slave vehicle. The smaller cost coefficient indicates to the cooperative controller that the master vehicle jets use fuel at half the rate of the slave vehicle jets. In this test all reaction control jets on both the master and the slave vehicles are available to the cooperative controller. The cooperative controller selects the most efficient combinations of jets based on the geometry of the activity vectors, the thrust levels of each, and the cost per second of firing time. Figure 7.37 shows the acceleration jets fired in this test case. Table 7.25 shows the actual firing times used for each jet.
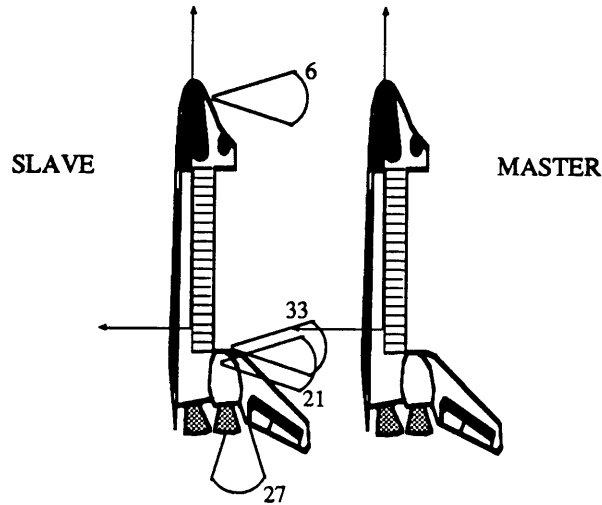

Figure 7.37
The initial state of the two vehicle system
Acceleration jet firings indicated.

Table 7.25
Acceleration phase jet firings.

Master		Slave	
Jet #	Time	Jet #	Time
7	2.32	-	0.0
21	2.24		
33	2.24		
27	0.08		

The firing pattern in figure 7.37 shows that in this case the most efficient solution to the two burn maneuver employs the master vehicle -z jets during the acceleration burn. As a result the master vehicle closes at approximately 1 ft/sec on the slave vehicle which remains in an unperturbed circular orbit.

The vehicles coast for 100 sec. and then the deceleration set of jet firings is implemented. Figure 7.38 shows the jet firing pattern and table 7.26 contains the corresponding jet firing times.

Figure 7.38
The final state of the two vehicle system
Deceleration jet firings indicated.

135

Table 7.26
Deceleration phase jet firings.

Master		Slave	
Jet #	Time	Jet #	Time
36	3.52	-	0.0
24	3.44		
9	1.76		
13	1.76		
2	1.44		

In this test the decrease in the cost of the master vehicle primary jets has offset the inefficiency of the +z primaries discussed in the last section. The +z jets on the master vehicle are fired, the closure velocity reduced, and the final command state reached. As in the test case presented in section 7.4.1 the system is not translating with respect to the LVLH frame at the end of the deceleration burn.

It should be noted that the cooperative controller did not "blend" jets from both vehicles during the maneuver due to constraints on the attitudes of the vehicles. Each jet provides a torque as well as a linear force. Thus to perform a pure translation the torques on each vehicle must sum to zero. It would be inefficient to fire "translation" jets on both vehicles and additional "torque nulling" jets as well.

7.4.4 Upward Firing Jets Less Efficient

In this test case the cost coefficient parameters for the upward firing (-z) jets on both vehicles are set to a value three times the standard value used for the other jets. This situation could actually arise if a spacecraft had two sets of very dissimilar actuators. In this test all reaction control jets on both the master and the slave vehicles are available to the cooperative controller. The cooperative controller selects the most efficient combinations of jets based on the geometry of the activity vectors, the thrust levels of each, and the cost per second of firing time. Figure 7.39 shows the acceleration jets fired in this test case. Table 7.27 shows the actual firing times used for each jet.
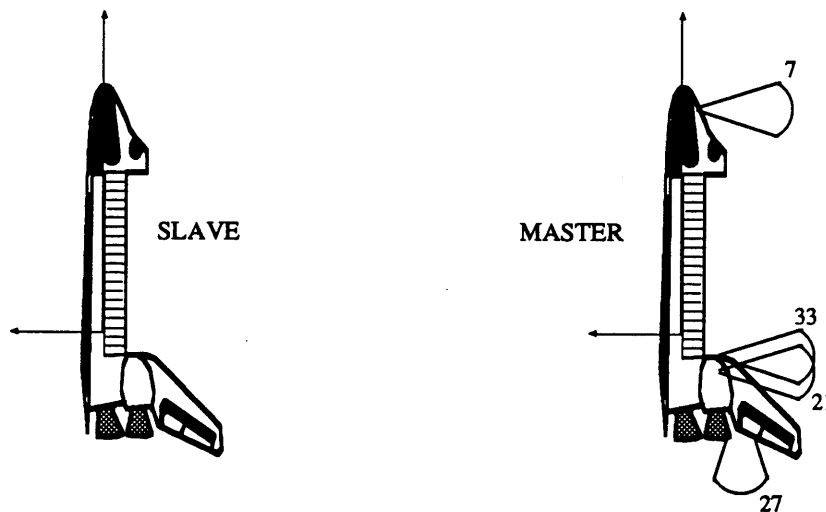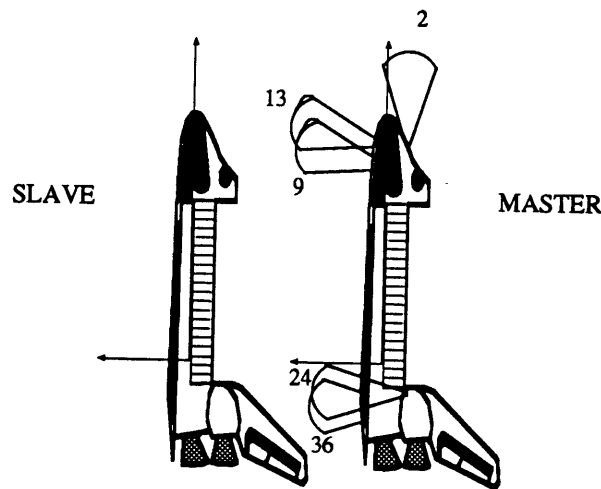
Figure 7.39
The initial state of the two vehicle system
Acceleration jet firings indicated.

Table 7.27
Acceleration phase jet firings.

Master		Slave	
Jet #	Time	Jet #	Time
15	0.80	36	3.28
27	0.64	24	3.20
33	0.08	9	1.52
		13	1.52

The jet firing pattern in figure 7.39 is different than the pattern observed in the three prior approach cases. Due to the high cost of the master vehicle up firing (-z) jets, the down firing (-z) jets on the slave vehicle are used to impart the required translation velocity to the system. This combination produces an additional velocity component in the +x body axis direction which caused jet #1 on the slave vehicle to be employed during the single vehicle case presented in section 7.4.1 (figure 7.33). In this test case the cooperative controller employs the +x jets on the master vehicle (these jets were unavailable during the single vehicle test). Jet #33 is used for only one control cycle to counter the small torque associated with the jet 15 & 27 combination.

The slave vehicle coasts toward the master for 100 sec and then the deceleration jets are fired. Figure 7.40 shows the firing pattern and table 7.28 contains the actual firing times.
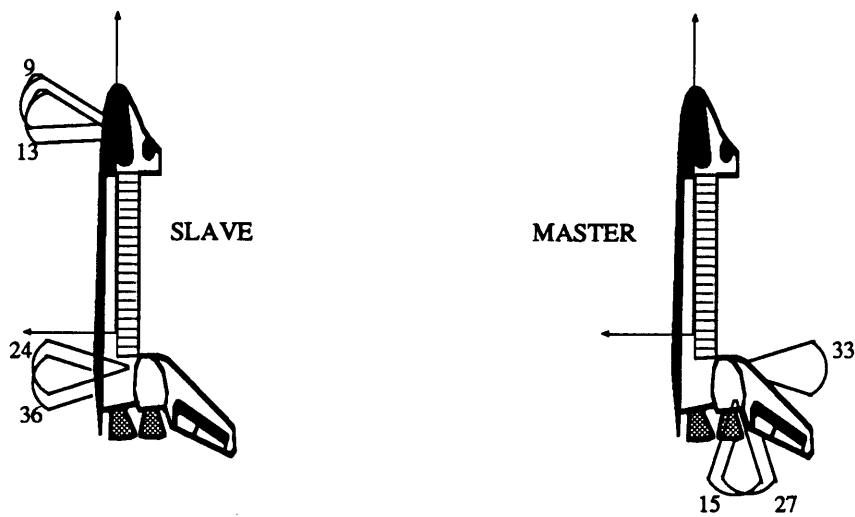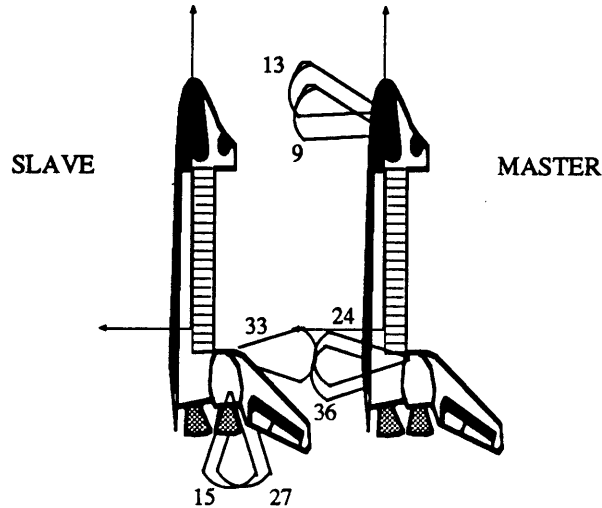

Figure 7.40
The final state of the two vehicle system
Deceleration jet firings indicated.

Table 7.28
Deceleration phase jet firings.

Master		Slave	
Jet #	Time	Jet #	Time
24	3.28	15	0.72
36	3.28	27	0.56
9	1.60	33	0.08
13	1.60		
44	0.32		

In this deceleration maneuver the cooperative controller selects the down (+z) master vehicle jet combination over the costlier up firing slave vehicle jets. The master vehicle is thus accelerated until its translational velocity matches the approach velocity of the slave vehicle. The cooperative controller compensates for the additional velocity in the +x body direction induced by the 9,13,24,36 jet combination by commanding short firings

138

of the +x jets on the slave vehicle. The two vehicles attain the commanded final state at the end of the deceleration burn and formationkeep about a point moving slightly slower than the reference circular orbit.

During this test the phase space controller initiated 3 corrective maneuvers consisting of 25 individual jet firings for a total of 8.72 seconds of firing time.

7.4.5 Summary of V-bar Tests

This series of four tests demonstrated the fuel efficiency and the versatility of the cooperative controller. In each test case (master jets unavailable, all jets available with cost coefficient = 1, master jet costs=1/2, -Z jet costs=3) the cooperative controller planned and executed a two burn trajectory which carried the two spacecraft system from the initial to the commanded final states. In all four test cases the phase space regulator feedback loop maintained the state errors within the specified deadbands during the coast and formationkeeping phases of the test. Table 7.29 summarizes the reaction control jet activity for each test case.

Table 7.29
Summary of jet activity for the V-bar tests.

TEST CASE	OPEN - LOOP		FEEDBACK		COST
	No of Jets	Total Time	No of Jets	Total Time	
Master Jets Unavailable	9	18.96	12	3.84	22.80
All Jets Available; Std Cost	9	14.24	0	0.0	14.24
Master Jet Cost = 1/2	9	18.80	5	2.72	10.76
Both Veh. -Z Jets Cost = 3	15	22.48	25	8.72	31.40

In table 7.29 the fuel savings of the two vehicle cooperative control approach (case 2) over the single pursuit vehicle approach (case 1) is evident. The two vehicle all jets available maneuver used 57% fewer jet firings (9 vs 21) and 37% less fuel (in these cases fuel usage is directly proportional to aggregate firing time; 14.24 vs 22.80). The cooperative controller solution is more efficient as a direct result of the use of more effective master vehicle jets in place of some of the slave vehicle jets employed by the

single vehicle pursuit solution. The increased fuel economy resulting from the incorporation of the actuators on both spacecraft into the maneuver solution is a principle advantage of the cooperative control approach to proximity operations.

In the nominal cooperative control test the cost parameters associated with each jet are unity. Consequently the jets are selected based on the their effective thrust and the geometry of the problem. In the third and fourth test cases the ability of the cooperative controller to blend actuators of dissimilar fuel consumption rates was demonstrated. In test case #3 the cost parameter for all master vehicle jets was set equal to 1/2. Though the aggregate firing time increased (14.24 to 21.52 sec.) as low cost geometrically less efficient master vehicle jets were included into the solution in place of high cost slave vehicle jets, the fuel usage cost decreased (14.24 to 10.76).

In case four the cost parameter for all up (-z) firing reaction control jets was set to 3. In order to avoid the increased fuel costs associated with these jets the cooperative controller substituted geometrically less effective unity cost down (+z) firing jets during both the acceleration and deceleration maneuvers. The resulting cost of the maneuver is of course larger than the cost computed in case 2, but it is lower than the cost of the case 2 jet firing profile with recomputed using the higher cost parameter value.

In addition to verifying the fuel efficiency of the cooperative controller these four tests also demonstrate the controller's versatility. In the third test case (master vehicle jet costs = 1/2) the cooperative control solution reduces to a single active pursuit vehicle approach. Unlike the true single vehicle approach to proximity operations however, the cooperative control approach guarantees that the vehicle performing the pursuit maneuvers is the more efficient of the two vehicles. The relative efficiency of the two vehicles may change drastically due to changes in the availability of the actuators, mass properties, the relative geometry of the vehicles, or the commanded maneuver. The cooperative controller adapts to all these changes in real time.

In the second and fourth test cases, the cooperative controller fires a combination of reaction control jets from each spacecraft in order to implement the two burn trajectory solution. The initial burn in each solution accelerates one of the vehicles to an appropriate approach velocity. To complete the maneuver a second open-loop burn is commanded at the end of the coast period. Rather than decelerating the approaching vehicle, this burn accelerates the second vehicle until the relative velocity of the two spacecraft is nulled and the commanded relative position is attained. This type of coordinated proximity operations

140

maneuver is unique to the cooperative control approach. It cannot be performed using only one active vehicle and would be extremely difficult to perform accurately and efficiently using two independently controlled vehicles

CHAPTER 8

SUMMARY AND CONCLUSIONS

8.0 Conclusions

A new controller capable of controlling the joint maneuvers of two general "active" spacecraft during proximity operations has been developed. This 9 degree of freedom cooperative controller controls the attitude of the master vehicle with respect to an inertial coordinate frame as well as the attitude and position of the slave vehicle with respect to the master. The cooperative control design developed in this thesis is a two-tiered system; an open-loop trajectory solver is used to plan a linearized two burn (accelerate, coast, decelerate) maneuver trajectory and a phase space regulator is used to maintain the system of two vehicles on this trajectory. A simplex algorithm is employed to determine the minimum fuel combination of reaction control jets on both the master and the slave vehicles which satisfies each velocity change request. The cooperative controller has been successfully implemented for a system of two space shuttle spacecraft conducting joint maneuvers in low earth orbit.

Preliminary tests of the cooperative controller using the two shuttle example have verified that cooperative control is a viable alternative to the traditional "pursuit vehicle" approach to proximity operations. The ability of the open-loop trajectory solver to plan a complicated two vehicle maneuver which drives the system to a commanded final state has been demonstrated. The ability of the phase space regulator loop to maintain the system state on the planned nine degree of freedom linearized trajectory and perform formationkeeping functions within specified tolerances and with an acceptable level of reaction control jet activity has also been verified.

The cooperative controller has been shown to be more robust to jet failures than a single vehicle control system. When several reaction control jets on the pursuit spacecraft were designated "unavailable", the vehicle was no longer completely controllable and was unable to perform the commanded approach to the target vehicle. In this same situation the cooperative controller was able to exploit the available control authority of the control jets on both the pursuit vehicle and the "healthy" target vehicle in order to control the two vehicle system and complete the commanded maneuver. Furthermore, in a case where neither the target or the pursuit vehicle was completely controllable, the cooperative

142

controller was able to control the nine degree of freedom system and direct it to the commanded final state. In all cases examined, the additional redundancy achieved by including the target vehicle reaction control jets in the set of usable actuators made the cooperative controller more robust to jet failures than the single pursuit vehicle control system.

Two cooperatively controlled vehicles were also shown to be more efficient than a single pursuit vehicle. During a 100 second v-bar approach maneuver, the cooperatively controlled two-vehicle system performed 57% fewer jet firings and used 37% less fuel than a single pursuit vehicle performing the same maneuver. In addition, during a more complicated 500 second maneuver the cooperatively controlled system was demonstrated to be more efficient than a set of two non-cooperative maneuvering vehicles. In this case the cooperative controller commanded 51% fewer jet firings and used 68% less fuel than the two independently controlled vehicles. Though the savings of the cooperative control approach vary depending on the maneuver and the efficiency of the available reaction control jets, the cooperative controller is never less fuel efficient than either a single pursuit vehicle or pair of maneuvering vehicles.

8.1 Contributions

This thesis has emphasized the extension and integration of several existing approaches to single spacecraft control to the more complex problem of the cooperative control of two spacecraft. The significant contributions of this work are:

(1)   The formulation of the nine degree of freedom, two spacecraft, joint maneuver trajectory solver.

(2)   The formulation of the nine dimensional phase space algorithm for the two vehicle system. This system utilizes a separate phase space representation of each of three 3-dimensional control channels and a single 9-dimensional velocity to be gained vector.

(3)   The development of the proximity operations Cooperative Controller. This controller is a new approach to the solution of the proximity operation control problem; it exploits the maneuverability of both the target and the master spacecraft in order to control the relative position and attitude of the

143

two spacecraft and the attitude of one of the vehicles with respect to an inertial reference frame. The controller is robust to reaction control jet failures and performs fuel efficient proximity operations maneuvers.

(4)   The validation of the cooperative controller design using a software simulation of a two space shuttle system and by comparison to the performance of a single vehicle controller in similar proximity operations scenarios.

8.2 Recommendations for Additional Work

The cooperative controller controls nine degrees of freedom of the two spacecraft system. During various phases of the mission it may be operationally desirable to control the two spacecraft in 12, 6, or even 3 dimensions. (If the two vehicle system is not completely controllable in 9 dimensions it would be desirable to attempt to control just the relative position and relative attitude.) Since the jet selection algorithm is readily formulated for each of these cases it may be desirable to expand the basic cooperative controller to include these specialized control modes.

As currently formulated the jet selection algorithm returns a solution which includes "imaginary jets" when the two vehicle system is not completely controllable (chapter 4). It may be advantageous to incorporate a "controllability alarm" which directs specific action (eg. reduce the order of the controller) when the system is unable to perform a commanded maneuver. (The shuttle OEX autopilot incorporated such an alarm.)

A major cause of state error drift rates observed in the testing performed on the cooperative controller is the minimum impulse and on/off granularity of the reaction control jets. If control actuators with various control granularities could be blended in such a manner as to eliminate a large portion of the drift rates the frequency of corrective jet activity could be drastically reduced and additional fuel savings would result.

The cooperative controller computes a single two burn trajectory to transfer the two spacecraft from the initial state to the commanded final state. In some instances this single maneuver trajectory may be fuel inefficient or even impossible. (In chapter 5 it was shown that the out-of-plane position is not controllable for transfers spanning integer multiples of half an orbit.) A method for planning and optimizing a multi-segment trajectory could be

144

used to provide intermediate state commands to the cooperative controller. Such a system will certainly be required if the cooperative controller is to be applied to the control of a pair of autonomous or semi-autonomous spacecraft.

Finally, in this thesis the cooperative controller was assumed to reside on the "master" spacecraft. While this designation was convenient for the discussion purposes, the algorithm does not have to reside on a particular vehicle. In fact it will be desirable to have the cooperative controller running on both spacecraft simultaneously. In this manner neither vehicle is "surrendering control" to the other spacecraft. Both spacecraft are computing the cooperative solution and then comparing answers. If at any point the separate controllers loose synchronization or disagree, the cooperative maneuver is broken off and the vehicles transition to a single vehicle control mode.. This architecture is especially attractive for operations within the proposed spacestation command and control zone. Spacestation will be required to provide "direct command and control of unmanned vehicles and support monitoring and advising of manned spacecraft operating within the within the command and control zone".[10]

REFERENCES

1. Redding D.C. and N.J. Adams, "An Optimized Rotation Axis Model-Following Controller for STS Orbiter Vernier-Jet Attitude Maneuvers," CSDL-R-1747, Charles Stark Draper Laboratory, Cambridge, MA, November 1984.

2. Bergmann E.V., "A New Spacecraft Autopilot," M.S. Thesis, Department of Aeronautics and Astronautics, M.I.T., Cambridge, MA, May 1976.

3. Paradiso J., "A Highly Adaptable Steering/Selection Procedure for Combined CMG/RCS Spacecraft Control," CSDL-R-1835, Charles Stark Draper Laboratory, Cambridge, MA, March 1986.

4. Hattis P., "A Review of the Space Shuttle Orbital Flight Control System", CSDL-P-1786, Charles Stark Draper Laboratory, Cambridge, MA, October 1983.

5. Bergmann E.V., S.R. Croopnick, J.J. Turkovich, and C.C. Work, "An Advanced Spacecraft Autopilot Concept,"Journal of Guidance and Control, Vol. 2, No.3, Article No. 77-1071, May-June, 1979 , pp. 161-168.

6. Chung A., Linear Programming, Charles E. Merrill Books, Inc., Columbus, Ohio, 1966.

7. Kaplan M.H., Modern Spacecraft Dynamics and Control, John Wiley and Sons, New York, 1976.

8. Hughes P.C. Spacecraft Attitude Dynamics, John Wiley and Sons, New York, 1986.

9. Redding D.C., B.A. Persson, and E.V. Bergmann, "Combined Solution of Spacecraft Rotational and Translational Maneuvers", Paper presented at AIAA/AAS Astrodynamics Conference, Williamsburg, VA, June 1986, 11p.

10. "Space Station Program Definition Requirements Section 3: Space Station System Requirements", JSC31000, Vol. 3, Rev D, NASA, Space Station Program Office, Reston, VA, October 1988.

11. Hollister, W.M. "The Design of a Control System for the Terminal Phase of a Satellite Rendezvous," M.S. Thesis, M.I.T., Cambridge, MA, June 1959.

12. "Flight Data File: Proximity Operations, STS 51-G, SPARTAN", JSC-20035, NASA, Mission Operations Directorate, Operations Division, Lyndon B. Johnson Space Center, Houston Texas, May 10, 1985.

12. "Eyles D., M. Palauszek, and R. Vaughan, "User's Guide to the Space Station Simulator", Rev. 1, CSDL-R-1673, Charles Stark Draper Laboratory, Cambridge, MA, June 1985.

13. Crawford, B.S., "Operational Design of Multi-Jet Spacecraft Control Systems," T-509, Charles Stark Draper Laboratory, Cambridge MA, September 1968.

146

14. Weiler, P., "Initial Exploration of Dynamic Plume Avoidance", CSDL Memo No. CC-88-03, Charles Stark Draper Laboratory, June 1988.

15. Vaughan R., E.V. Bergmann, "Manually Augmented Operations and Docking Control", Charles Stark Draper Laboratory, Cambridge MA

16. Persson B., C. Cooke, "Extended Linear Jet Select", CSDL Memo No. CC-88-04, Charles Stark Draper Laboratory, MA , November 1988.

17. Battin, R.H., _Introduction to the Mathematics and Methods of Astrodynamics_,American Institute of Aeronautics and Astronautics, New York, 1987.

18. Clohessy W.H. and R.S. Wiltshire, "Terminal Guidance System for Satellite Rendezvous", Journal of Aerospace Sciences, Vol. 27, September 1960., pp 653-658, 674.

19. "Automatic Rendezvous and Docking Systems Functional and Performance Requirements", Scientific Systems Inc., Cambridge, MA, March 1985.

20. Ebert W.L., "Kinematics, Dynamics, and Estimation of Rigid-Body Motion Using Euler Parameters (Quaternions)", Applied Physics Laboratory, Johns Hopkins University, Laurel Maryland, November 1981.

21. Jezewski D.J. and J.D. Donaldson, "An Analytic Approach to Optimal Rendezvous Using Clohessy-Wiltshire Equations", Journal of the Astronautical Sciences, Vol. 27, No. 3, pp.293-310, July-September, 1979.

22. Fehse D. W., "Technology Development by the European Space Agency for Autonomous Spacecraft Rendezvous and Docking", Lecture given as part of the M.I.T. / C.S. Draper Seminar Series on Dynamics, Guidance and Control, October 1988.